



**PROGRAMA DE PÓS-GRADUAÇÃO EM ENGENHARIA MECÂNICA
CENTRO TECNOLÓGICO
PRÓ-REITORIA DE PESQUISA E PÓS-GRADUAÇÃO
UNIVERSIDADE FEDERAL DO ESPÍRITO SANTO**

RENAN FÁVARO CALIMAN

**AN EXPERIMENTAL ANALYSIS OF ORIFICE PLATE WET GAS METER BY
THIRD PRESSURE TAPPING FOR LIQUID LOADING ESTIMATION**

VITÓRIA, ES

2022



**PROGRAMA DE PÓS-GRADUAÇÃO EM ENGENHARIA MECÂNICA
CENTRO TECNOLÓGICO
PRÓ-REITORIA DE PESQUISA E PÓS-GRADUAÇÃO
UNIVERSIDADE FEDERAL DO ESPÍRITO SANTO**

RENAN FÁVARO CALIMAN

**AN EXPERIMENTAL ANALYSIS OF ORIFICE PLATE WET GAS METER BY
THIRD PRESSURE TAPPING FOR LIQUID LOADING ESTIMATION**

A dissertation submitted in partial fulfilment of
the requirements for the degree of Master of
Science in Mechanical Engineering.

Advisor: Prof. Rogério Ramos

VITÓRIA, ES

2022

Ficha catalográfica disponibilizada pelo Sistema Integrado de Bibliotecas - SIBI/UFES e elaborada pelo autor

C153a Caliman, Renan Fávaro, 1994-
An experimental analysis of orifice plate wet gas meter by third pressure tapping for liquid loading estimation / Renan Fávaro Caliman. - 2022.
128 f. : il.

Orientador: Rogerio Ramos.
Dissertação (Mestrado em Engenharia Mecânica) -
Universidade Federal do Espírito Santo, Centro Tecnológico.

1. Two phase flow. 2. Flow measurement. I. Ramos, Rogerio. II. Universidade Federal do Espírito Santo. Centro Tecnológico. III. Título.

CDU: 621



PROGRAMA DE PÓS-GRADUAÇÃO EM ENGENHARIA MECÂNICA
CENTRO TECNOLÓGICO
UNIVERSIDADE FEDERAL DO ESPÍRITO SANTO

AN EXPERIMENTAL ANALYSIS OF ORIFICE PLATE WET GAS METER BY THIRD PRESSURE TAPPING FOR LIQUID LOADING ESTIMATION

Renan Fávaro Caliman

COMISSÃO EXAMINADORA

Prof. Dr. Rogério Ramos
Orientador (PPGEM/UFES)

Prof. Dr. Márcio Ferreira Martins
Examinador Interno (PPGEM/UFES)

Prof. Dr. Francisco Júlio do Nascimento
Examinador Externo (UNIFESP)

Dissertação apresentada ao Programa de Pós-Graduação em Engenharia Mecânica da Universidade Federal do Espírito Santo como parte dos requisitos necessários à obtenção do título de Mestre em Engenharia Mecânica

Vitória (ES), 18 julho de 2022.





Aprovação banca Renan Favaro Caliman

Data e Hora de Criação: 18/07/2022 às 19:30:34

Documentos que originaram esse envelope:

- Aprovação banca Renan Favaro Caliman.pdf (Arquivo PDF) - 1 página(s)
- Ata 304 Renan Favaro Caliman.pdf (Arquivo PDF) - 1 página(s)
- Renan Favaro Caliman - questionário CAPES.pdf (Arquivo PDF) - 2 página(s)



Hashs únicas referente à esse envelope de documentos

[SHA256]: 87f56b1d4976f73ffe8fad354d90b9a7cd133b6ba4c079c2b82168a04ee70db9

[SHA512]: 11ab9be4e5bfa107b00f3d011a18f3fadaffa96b155eca2072f0c69a5914c0f340adad9ef25b6123ffaf9b51ba4a80974949ca67ee2857ecfb8472247601e7b1

Lista de assinaturas solicitadas e associadas à esse envelope



ASSINADO - Rogerio Ramos (rogerio.ramos@ufes.br)

Data/Hora: 18/07/2022 - 19:34:28, IP: 187.36.164.54, Geolocalização: [-20.288950, -40.293898]

[SHA256]: a35396abb835f3602f317f8d790af4404083f1a322ca63c27ebbb12d618d486f



ASSINADO - Marcio Ferreira Martins (marcio.martins@ufes.br)

Data/Hora: 18/07/2022 - 19:54:41, IP: 189.94.96.58

[SHA256]: acb65364b4f9e32ebb2eccc24ccaacbd998ce43bb831cd9f7c7adbd3550a5a3e



ASSINADO - Francisco Julio do Nascimento (fjnascimento@unifesp.br)

Data/Hora: 18/07/2022 - 21:58:47, IP: 186.223.213.60, Geolocalização: [-22.014051, -47.902149]

[SHA256]: b8511223b2335060c32093b73ed0ba09afcfba32e525f869075248e1ab829876

Histórico de eventos registrados neste envelope

- 18/07/2022 21:58:47 - Envelope finalizado por fjnascimento@unifesp.br, IP 186.223.213.60
- 18/07/2022 21:58:47 - Assinatura realizada por fjnascimento@unifesp.br, IP 186.223.213.60
- 18/07/2022 21:58:28 - Envelope visualizado por fjnascimento@unifesp.br, IP 186.223.213.60
- 18/07/2022 19:54:41 - Assinatura realizada por marcio.martins@ufes.br, IP 189.94.96.58
- 18/07/2022 19:34:28 - Assinatura realizada por rogerio.ramos@ufes.br, IP 187.36.164.54
- 18/07/2022 19:34:15 - Envelope visualizado por rogerio.ramos@ufes.br, IP 187.36.164.54
- 18/07/2022 19:33:23 - Envelope registrado na Blockchain por rogerio.ramos@ufes.br, IP 187.36.164.54
- 18/07/2022 19:33:20 - Envelope encaminhado para assinaturas por rogerio.ramos@ufes.br, IP 187.36.164.54
- 18/07/2022 19:30:37 - Envelope criado por rogerio.ramos@ufes.br, IP 187.36.164.54

ACKNOWLEDGEMENTS

The search for knowledge is a continuous endless ladder and the master's is an advanced steppingstone that not only brings a better understanding on the concentration area, but a new comprehension of the world and all these were not possible alone.

First, I would like to thank God for guiding me through this step.

I would like to acknowledge my mother Margarida, my guardian angel, my father Valdecir and my brother Marlon for all the support and love that you have given. You are always there for me.

I would like to thank my supervisor Professor Rogério Ramos for his valuable advice, guidance and opportunities given throughout these years and the trust deposited to develop such research. You provided me with the tools that I needed to choose the right direction and successfully complete my dissertation.

I would also like to thank my friends Tiago Guerzet for the huge support from the company in experiments to stimulating discussions in two-phase flow topic, to Ligia Gaigher for valuable tips, to Felipe Paiva for the LabView huge support and finally, but not least to Ullices for the instrumentation expertise.

In addition, my acknowledgement to Petrobras and ANP for financing the NEMOG facilities and the project that originated this work.

ABSTRACT

Wet gas flows are very common in many industrial processes, mainly in oil industries. On those, flow measurement is based in differential pressure devices at least on 40% of the cases, being the orifice plate the most used one, reaching US\$ 21 billion in natural gas measurement at UK industry. However, in case of two-phase flow applications, the liquid loading causes a positive bias on the pressure differential readings, due to phases interactions called over-reading and resulting in an erroneous gas flow rate prediction up to 50%. Through decades apart, many authors proposed correlations to estimate and correct this overestimation for different differential pressure devices, such as orifice plates, venturi tubes and inverted cones, but all needed some liquid content information, which real time estimation is a engineering challenge. To overcome this barrier, industry has been developing an all in one two-phase wet gas flow meters (WGFMs), with liquid loading estimation and over-reading (OR) correction on the same meter. In 2012, ISO TR 11583 (2012) released a methodology to wet gas measurement based on orifice plates or Venturi, using the pressure loss ratio (PLR) technique to liquid content relationship limited by 6D 3rd pressure tap, high pressure levels and low gas wetness. Aiming to investigate this methodology, this work relied on a gas-liquid flow circuit, located at the Research Group for Studies on Oil&Gas Flow and Measurement (NEMOG, in Portuguese), located at Federal University of Espírito Santo, Vitória, Brazil, to promote an air-water flow at 1, 3 and 5 barg pressure line (density ratio (DR) equal to 0.0025, 0.0048 and 0.0071), 360 kg/h air mass flow rate (Gas Froude number (FR_g) equal to 0.74, 0.90 and 1.29) and Lockhart-Martinelli parameter (X_{LM}) equal to 0.15, 0.22 and 0.30 levels. With this data, the most relevant orifice plate OR correlations were tested, considering ISO TR 11583 (2012) proposal and new data fitted equations are proposed for 6D, 20D and 144D third tap distances, resulting in 10%, 10% and 15% accuracy respectively. Finally, a new methodology is proposed by combining ISO TR 11583 (2012) and Petalas and Aziz (1998) two-phase pressure drop model, with a 10% accuracy for 20D tap, but poor results for 144D due to model limitations.

Keywords: Wet gas, orifice plate, over-reading, pressure loss ratio, Lockhart-Martinelli.

LIST OF FIGURES

Figure 1 - Geometrical analysis of a stratified flow (Source: author)	25
Figure 2 - Geometrical analysis of a annular flow (Source: author).....	28
Figure 3 - Flow approximated pressure pattern though orifice plate (Source:adapted from READER-HARRIS, FORSYTH, and BOUSSOUARA (2021)).....	32
Figure 4 - Orifice plate sketch (Source: Author)	32
Figure 5 - Two-phase flow subsets (Source: ISO TR 12748 (2015)).....	35
Figure 6 - Horizontal two-phase wet gas flow regimes (Source: adapted from ISO TR 12748 (2015)).....	36
Figure 7 - Impact of Lockhart-Martinelli definitions on over-reading estimation for a 368 kg/h air mass flow rate and 7 bara line pressure (Source: Author).....	40
Figure 8 - Simplification of an orifice plate DP meter in a single-phase gas flow (Source: author).....	43
Figure 9 - Simplification of an orifice plate DP meter in a two-phase wet gas flow (Source: author)	44
Figure 10 - Water holdup in 4" pipe with a 0.65-beta orifice plate in stratified (left) and annular (right) flows. (Source: adapted from Steven et al. (2011))	45
Figure 11 - Configuration of the third tapping propose by De Leeuw (Source: adapted from ISO TR 12748 (2015)).....	52
Figure 12 - Illustration of pressure profile showing the ΔP_t , ΔP_{PPL} and ΔP_r for an orifice plate meter and a generic third pressure tap (Source: author)	52
Figure 13 - Venturi's PLR to X_{LM} relation at 45 bar. (Source: De Leeuw (1997)).....	53
Figure 14 -The NEMOG's multiphase flow loop sketch (Source: Author)	56
Figure 15 - Storage tanks flowchart (Source: author).....	57
Figure 16 - Separator vessel flowchart (Source: author)	58
Figure 17 - Separator vessel photography (Source: author)	58

Figure 18 - Compressed air supplier schematic flowchart (Source: author)	60
Figure 19 - Single-phase measurement split-range configuration sketch for water and air (Source: author)	61
Figure 20 - Single-phase measurement split-range configuration photography (Source: author)	61
Figure 21 - High and low waterflow rate Coriolis meters in split-range arrangement photography (Source: author)	62
Figure 22 - The high and low mass flow rate orifice plate meters photography (Source: author)	63
Figure 23 - Original mixing arrangement (Source: author)	64
Figure 24 – Final Experimental mixing arrangement (Source: author)	65
Figure 25 - Actual test loop section configuration (dimensions in millimeter) (Source: author)	65
Figure 26 - Test loop section photography (Source: author)	66
Figure 27 - Fitting details of loop section, in perspective (Source: author)	67
Figure 28 - Wet gas measurement pressure taps by ISO TR 12748 (2015) (Source: author)	67
Figure 29 - National Instruments LabVIEW multiphase flow loop supervisory system main page (Source: author)	70
Figure 30 - National Instruments LabVIEW wet gas flow parameters supervisory page (Source: author)	71
Figure 31 - False prediction flow, PDT-3, PDT-4 and PDT-5 histograms illustration (Source: author)	75
Figure 32 - First dry air mass flow rate measurement comparison between reference single-phase meter and test section meter (Source: author)	78
Figure 33 - Single-Phase Meter and the Test Section Meter shift mapping with uncertainty bands (Source: author)	79
Figure 34 - PLR dry test configuration (Source: author)	81

Figure 35 - ISO 5167-2 (2003)'s PLR dry and the new data fit for a 0.68β orifice plate.	82
Figure 36 - ISO 5167-2 (2003)'s PLR dry and the new data fit for a 0.50β orifice plate.	82
Figure 37 - Different configurations for the third downstream pressure tap: (a) 6D, (b) 20D and (c) 144D (Source: author)	84
Figure 38 - Raw data from a 0.50β , 1 barg and 6D 3 rd tap test (Source: author).....	87
Figure 39 - NEMOG's experimental over-reading estimation based on the single-phase air flow measurement with and without the systematic shift correction (OR and X_{LM} relative expanded uncertainties are 2.24% and 1.84% respectively) (Source: author)	88
Figure 40 - Over-reading experimental data points comparison with literature correlations using air-water flow with 0.50 and 0.68 beta and 1 barg line pressure (Source: author)	90
Figure 41 - Over-reading experimental data points comparison with literature correlations for air-water flow with 0.50 and 0.68 beta and 3 barg line pressure (Source: author).....	90
Figure 42 - Over-reading experimental data points comparison with literature correlations for air-water flow with 0.50 and 0.68 beta and 5 barg line pressure (Source: author).....	91
Figure 43 - ISO TR 11583 (2012) X_{LM} and DR limits of applicability with NEMOG's data envelope (Source: author).....	92
Figure 44 - ISO TR 11583 (2012) PLR to X_{LM} extrapolation test with air-water flow (Source: author)	93
Figure 45 - 6D PLR to X_{LM} new data fit results for 0.50β and 0.68β , 1, 3 and 5 barg and 0.15 to 0.31 Lockhart-Martinelli (Source: author)	95
Figure 46 - 20D PLR to X_{LM} new data fit results for 0.50β and 0.68β , 1, 3 and 5 barg and 0.15 to 0.31 Lockhart-Martinelli (Source: author)	97
Figure 47 - 144D PLR to X_{LM} new data fit results for 0.50β and 0.68β , 1, 3 and 5 barg and 0.15 to 0.31 Lockhart-Martinelli (Source: author)	98

Figure 48 - Exemplification of the third pressure tap correction from 20D to 6D using Petalas and Aziz (1998) two phase flow pressure drop model (Source: author)	99
Figure 49 - Experimental configuration in two-phase pressure drop measurement for Petalas and Aziz's (1998) model validation and adjustments (Source: author)	100
Figure 50 - Petalas and Aziz (1998) two-phase pressure drop model experimental validation without pipe roughness adjustment (Source: author)	100
Figure 51 - Petalas and Aziz (1998) two-phase pressure drop model experimental validation with pipe roughness adjustment (Source: author)	101
Figure 52 - Comparison between uncorrected and corrected Lockhart-Martinelli estimation using adjusted PPL by Petalas and Aziz (1998) model in ISO TR 11583 (2012) (Source: author)	102

LIST OF TABLES

Table 1 - Results for different definitions of Lockhart-Martinelli parameter.....	40
Table 2 - Separator vessel technical information.....	59
Table 3 - Water pumping specifications and capabilities.....	59
Table 4 - Compressed air supplier specifications and capabilities	60
Table 5 - The high and low water flow rate Coriolis meters technical information	62
Table 6 - The high and low flow rate orifice plate meters technical information	63
Table 7 - Wet gas measurement pressure transmitters specification	68
Table 8 - Lockhart-Martinelli and GVF ranges for NEMOG's actual configuration.....	69
Table 9 - Normal distribution level of confidence and coverage factors (Source: JCGM (2008)).....	74
Table 10 - The single-phase and test section meters parameters in accordance to ISO 5167-2 (2003).....	77
Table 11 - Water mass flow rate measurement comparison between Coriolis meter and test section meter (Source: author)	78
Table 12 - Single-Phase Meter and the Test Section Meter shift mapping.....	80
Table 13 - Multiple linear regression coefficients ANOVA for the $PLR_{dry,fit}$ data fit	83
Table 14 - Wet gas flow test matrix	85
Table 15 - PLR_{wet} sensitivity in X_{LM} estimation by ISO TR 11583 (2012) correlation .	94
Table 16 - Multiple linear regression coefficients ANOVA for 6D PLR to X_{LM} new data fit	95
Table 17 - Multiple linear regression coefficients ANOVA for 20D PLR to X_{LM} new data fit	96
Table 18 - Multiple linear regression coefficients ANOVA for 144D PLR to X_{LM} new data fit	97

Table 19 - ISO TR 11583 (2012) results using the adjusted Petalas and Aziz (1998) model to correct the 3 rd pressure tap from 20D to 6D	103
Table 20 - ISO TR 11583 (2012) results using the adjusted Petalas and Aziz (1998) model to correct the 3 rd pressure tap from 144D to 6D	104

LIST OF SYMBOLS

ABBREVIATIONS

ANOVA - Analysis of variance

Adj MS - Adjusted mean squares

Adj SS - Adjusted sums of squares

CapEx - Capital expenditure

DP - Differential Pressure

DR - Density ratio

DoF - Degree of freedom, representing the amount of data points

F-value - Function value

GVF - Gas volume fraction

ISO - International Organization for Standardization

IC - Inverted Cone

LHC - Light hydrocarbon

NEMOG - Núcleo de Estudos em Escoamentos de Óleo e Gás (Portuguese)

N/A - Non applicable

OpEx - Operational expenditure

PLR - Pressure loss ratio

P-value - Probability value

UK - United Kingdom

WLR - Water to liquid ratio

WGFM - Wet gas flow meter

LATIN SYMBOLS

A	Pipe cross section area [m^2]
a, b and c	V-cone Over-reading parameter proposed by Steven [–]
Cd	Discharge coefficient in single-phase flow [–]
C	The over-reading parameter [–]
d	Orifice internal diameter [m]
D	Pipe internal diameter [m]
dP/dL	Pressure gradient [Pa/m]
E	Volume fraction [–]
e	Pipe absolute internal roughness [m]
Fr	Densimetric Froude number [–]
f	Friction factor [–]
$\frac{\partial G}{\partial y_i}$	i th variable sensitivity coefficient at G function
g	Gravity acceleration [m/s^2]
h	Liquid height in stratified flow [m]
j	Superficial velocity [m/s]
k	Gas isentropic exponent
K	Coverage factor
L	Pipe length [m]
l	Distances from pressure tapping to downstream orifice plate face [m]
l'	Distances from pressure tapping to upstream plate face [m]

\dot{m}	Mass flow rate [kg/h]
n	Chisholm exponent [–]
N	Number of experimental data points [–]
OR	Over-reading factor [–]
$OR\%$	Percentual Over-reading factor [%]
P	Absolute line pressure [bar]
Q	Volumetric flow rate [m^3/h]
R	The gas constant [$J/kg.K$]
Re	Reynolds number [–]
s	Standard deviation of the measurement
UP	Upstream tap term of Reader-Harris/Gallagher equation [–]
u^A	Type A standard uncertainty
u^B	Type B standard uncertainty
u	Standard uncertainty
U	Expanded uncertainty
V	Flow mean velocity [m/s]
X	The original Lockhart and Martinelli (1949) parameter [–]
x	Quality [–]
X_{LM}	Lockhart-Martinelli parameter [–]

GREEK SYMBOLS

β	Orifice to pipe diameter ratio [–]
ΔP	Differential pressure [Pa]
ε	Expansibility coefficient [–]
μ	Viscosity [$Pa.s$]

ρ	Density [kg/m^3]
ϕ	Traditional to expansion Over-reading ratio [–]
θ	Pipe inclination [<i>degree</i>]
σ	Superficial tension. [N/m]
τ	Shear stress [Pa]
τ_i	Interfacial shear stress [Pa]
ν_i	Degree of freedom of the measurement

SUBSCRIPT

C	Combined uncertainty
c	Core property
$comp$	Compounded uncertainty
Ch	Chisholm equation
D	Pipe internal diameter reference
dry	Dry gas flow, i.e. single phase gas flow
DL	De Leeuw equation for venturi meter
f	Film property
fp	False prediction
fit	Data fitted property
g	Gas property
hl	Head loss reference
I	Interfacial property
IC	Inverted cone meter
i	Ith variable
l	Liquid property

<i>LHC</i>	Light hydrocarbon
<i>m</i>	Meter reference
<i>mix</i>	Mixture property
<i>PPL</i>	Permanent pressure loss
<i>r</i>	Recovered
<i>sl</i>	Based on liquid superficial velocity
<i>St</i>	Steven et al equation for inverted cone
<i>strat</i>	Stratified flow regime
<i>TP</i>	Two-phase
<i>t</i>	Traditional
<i>Venturi</i>	Venturi meter
<i>W</i>	Water
<i>wg</i>	Wall/gas interface
<i>wl</i>	Wall/liquid interface
<i>wet</i>	Wet gas flow, i.e. two phase gas/liquid flow
1	Upstream side reference
2	Downstream side reference

CONTENTS

ACKNOWLEDGEMENTS	III
ABSTRACT	IV
LIST OF FIGURES	V
LIST OF TABLES	IX
LIST OF SYMBOLS	XI
1 INTRODUCTION	18
1.1 MOTIVATION	19
1.2 OBJECTIVES	20
1.3 DISSERTATION OUTLINE.....	21
2 THEORETICAL BACKGROUND	23
2.1 TWO PHASE PRESSURE DROP MODELS	23
2.2 SINGLE PHASE FLOW MEASUREMENT THROUGH DIFFERENTIAL PRESSURE DEVICES.....	31
2.3 WET GAS FLOW MEASUREMENT BY MEANS OF DIFFERENTIAL PRESSURE DEVICES.....	34
2.3.1 What is wet gas flow?	34
2.3.2 Flow regimes in wet gas flows	36
2.3.3 Wet gas parameters	37
2.3.4 The over-reading effect	43
2.3.5 History of Over-reading correction	45
2.3.6 PLR to X_{LM} relationship	51
3 EXPERIMENTAL APPARATUS	56
3.1 SECTION I: FLUID STORAGE	56
3.2 SECTION II: FLUID PUMPING AND SEPARATION	57
3.2.1 Three-phase separator vessel	57
3.2.2 Water circulation pumping	59
3.2.3 Compressed air supplier	59
3.3 SECTION III: SINGLE-PHASE FLOW MEASUREMENT	60
3.4 SECTION IV: FLUIDS MIXING	64

3.5	SECTION V: TEST LOOP	65
3.5.1	Orifice plate wet gas measurement test section.....	66
4	EXPERIMENTAL PROCEDURES, RESULTS AND DISCUSSIONS.....	69
4.1	NEMOG'S WET GAS FLOW TEST ENVELOPE.....	69
4.2	DATA ACQUISITION AND TREATMENT METODOLOGY.....	70
4.2.1	Post processing.....	71
4.2.2	Uncertainty evaluation	72
4.3	DRY AIR FLOW MEASUREMENT COMISSIONING	75
4.4	EVALUATION OF THE ISO 5167-2 (2003) PRESSURE LOSS RATIO FOR DRY FLOW AND A NEW DATA FIT PROPOSAL.....	80
4.5	WET GAS FLOW TESTS	83
4.5.1	Analysis of the main orifice plate over-reading correction correlations available in literature.....	88
4.5.2	ISO TR 11583 (2012) PLR to <i>XLM</i> correlation performance in air-water flow and new data fits correlations considering two extra 3rd tap configurations 92	92
4.5.3	Lockhart-Martinelli estimation using ISO TR 11583 (2012) equation with 3rd tap correction to 6D position using Petalas and Aziz (1998) two phase flow pressure drop model.....	98
5	CONCLUSION	105
5.1	FINAL REMARKS.....	105
5.2	CORRELATIONS SUMMARY	107
5.3	PROPOSAL FOR FUTURE WORK.....	108
	REFERENCES.....	110
	APPENDIX A	114
	APPENDIX B	120
	APPENDIX C	125

1 INTRODUCTION

Measuring is a human need since the dawn of civilizations, arising in favor to make the production management, commercial trades, group work and other tasks as easy and manageable as possible. This thought is summarized in a William Thomson's, Lord Kelvin, famous quote that says "If you cannot measure it, you cannot improve it"

In flow science it is not different. The need for flow measurement arose from piped water supplies management in Rome, mentioning the registers of Julius Frontinus (30 - 103 a.C), a roman engineer, evidencing the beginning of flow measurement knowledge (DELMÉE, 2003).

From the Julius Frontinus studies until today's technology frontier, the knowledge in flow measurement science has undergone great evolutions, mainly after the industrial revolution, by the mid-18th century, with the steam powered machine development, where the complex water-steam flow needed to be controlled. Even nowadays this kind of flow are present in many industrial processes, such as power production plants, food processing and mainly in oil and gas industries and still a big challenge for engineers and researchers to be understood, modeled, and predicted.

A particular case of two-phase flows, like the mid-18th water-steam, are the gas-liquid flows. Present mainly in natural gas production, the so-called wet gas flow, consists of a gas as a continuous phase and a liquid as a dispersed phase combined in the same stream, a common matter that engineering must deal with. This kind of combination occurs especially in oil wells operating on the latter stage of production lives, a stage where the water content of the multiphase flow, increases and the rising of heavier hydrocarbon components condensation, due to the pressure drop in production lines (STEVEN, 2002).

Additionally, depending on its efficiency, separators vessels leave amounts of liquid on the gas outlet. Therefore, to measure the flow rates, expensive two-phase meters are required on those situations.

Measurement of gas flowrate is essential to industry, making possible an appropriated reservoir and well management, production optimization and allocation, flow assurance, property transfer, and legislation matters. However, in most of the gas

production fields, the use of complex multiphase wet gas flow meters (WGFM) is economically unviable due to its high Capital Expenditure (CapEx), as well as high Operational Expenditure (OpEx), e.g the gas measurement requirement in flairs due to legal matters. Given this scenario, the response of differential pressure (DP) meters to wet gas flows becomes an important research topic, mainly because in most of the production's sights in Brazil, single-phase DP meters, such as orifice plates, are already installed to measure dry gas flows. Furthermore, DP meters demand a low installation and operation costs, are based on simple principles, reliable, have repeatable response, many years of operation history and have consensual operation practices consolidated in standards for single phase measurement.

Even though the performance of DP meters in single-phase flows measurement is well known and consolidated in the literature, in case of two-phase applications, the liquid loading causes a positive bias on the pressure differential readings, due to phases interactions called over-reading and resulting in an erroneous gas flow rate prediction up to 50%. Aiming to correct this shift, since 1949, with Lockhart and Martinelli (1949) pioneer empirical work for predicting the pressure drop in a two-phase flow, authors are researching and developing empirical correlations based on experimental data, archiving great progress in recent years, with relatively good wet gas correction performance with a $\pm 2\%$ uncertainty level on over-reading correction (STEVEN, SHUGART and KUTTY, 2018). However, those correlations need a liquid loading input to estimate the over-reading level, but this information is not available in a precise manner, remaining to use outdated information from test separators, adding huge uncertainty on the flow measurement, which turns into a supposition of the actual mass flow rate.

From that need, in the last years authors have been investigating the pressure loss ratio to Lockhart-Martinelli relationship, first observed by De Leeuw (1997) and concretized for venturi and orifice plates in ISO TR 11583 (2012), to develop an all in on wet gas meter with both low CapEx and OpEx.

1.1 MOTIVATION

Flow measurement in industrial facilities is based in DP devices at least on 40% of the cases, being the orifice plate the most used. To illustrate the economic impact of those

devices on flow measurement, the measurement of natural gas in 2006, on the UK gas industry, was estimated in £16 billion (US\$ 21 billion) (READER-HARRIS, FORSYTH, and BOUSSOUARA, 2021).

Furthermore, natural gas flows are often wet gas flows, as exposed on introduction. Consequently, a huge amount of money may be overpaid due to over-reading effect in property transfer, royalties, taxes and other related costs. Although the research and development on over-reading estimation has made great strides, usually over-reading correlations techniques requires a liquid flow rate estimation or some liquid content parameter to predict the bias. However, that information is not available instantly, forcing the meter operators to suppose the liquid content based on old and unprecise data, inducing an extra uncertainty on the gas flow rate prediction process.

To overcome this barrier, industry has been developing an all in on two-phase wet gas flow meters (WGFMs), with liquid loading estimation and over-reading correction on the same meter. Such category of flow meter is very expensive, compared to classical ones, since it requires a set of new technologies associated.

So, in 2012, ISO TR 11583 (2012) released a methodology to wet gas measurement based on orifice plates or Venturi, using the pressure loss ratio (PLR) to liquid content relationship based on a 6D 3rd pressure tap. But according to Steven, Shugart and Kutty (2018) there are some limitations with this methodology, due to very limited data used in development. Furthermore, this 6D 3rd pressure tap fixed location increases the CapEx barrier to new implementations.

In 2018 Steven, Shugart and Kutty (2018) proposed a new equation set to estimate the liquid content by means of PLR for orifice meters, claiming an uncertainty less than $\pm 2\%$ uncertainty for a water to liquid ratio (WLR) = 1 and for all data set tested, a global $\pm 4\%$ uncertainty at a 95% confidence level, but those equations were kept confidential due to proprietary reasons.

1.2 OBJECTIVES

The general objective of this study is to evaluate the PLR to liquid content relationship on different 3rd tap configurations and test the ISO TR 11583 (2012) performance, in an air-water flow by orifice plates at the NEMOG's new gas-liquid flow loop and

propose new correlations and alternatives for the liquid content estimation by means of PLR.

To achieve the main goal, the following specific objectives are defined:

- Commissioning of single phase air flow in the multiphase circuit, evaluating the reference dry air mass flow rate uncertainty and the test meter response to dry air flow (page 75).
- Evaluate the ISO 5167-2 (2003) PLR_{dry} correlation proposing a new data fit (page 80).
- Evaluate the main available orifice plate over-reading correlations performance in NEMOG's installation (page 88).
- Evaluate the ISO TR 11583 (2012) PLR to Lockhart-Martinelli (X_{LM}) correlation performance (page 92).
- Propose three new data fits of PLR vs. X_{LM} using the traditional 6D 3rd tap and two different configuration downstream 3rd tap (page 92).
- Validate the Petalas and Aziz (1998) two phase flow pressure drop model in air-water flow and evaluate the response of PLR vs. X_{LM} and Petalas and Aziz (1998) model together (page 98).

1.3 DISSERTATION OUTLINE

Chapter 1 - Introduction: this chapter provides a brief introduction to multiphase flow and delineates the motivation and research background also the objectives of this dissertation.

Chapter 2 - Theoretical background: this chapter presents the main literature interpretation about two phase flow pressure drop and flow measurement for single and two phase flows, important to understand the dissertation development. Moreover, the main limitations related to correlation proposals are exposed.

Chapter 3 - Experimental apparatus: this chapter exposes the Research Group for Studies on Oil&Gas Flow and Measurement (NEMOG in Portuguese) multiphase flow circuit, where all tests presented in this work were performed.

Chapter 4 - Experimental procedures, results and discussions: this chapter consolidates the experimental procedure result and discussion for each specific objective.

Chapter 5 - Conclusion: this chapter summarizes the principal conclusions of the dissertation, including the new correlations summary with the appropriate range of use. In addition, it is given a series of recommendations for future research.

Appendix A: this appendix brings the calibration certificate for both Coriolis meters used to measure water mass flow rates.

Appendix B: this appendix brings the calibration certificate for the pressure transmitters used to measure the manometric pressure and differential pressures.

Appendix C: this appendix brings the calibration certificate for the temperature transmitter used to measure the flow temperature.

.

2 THEORETICAL BACKGROUND

This chapter brings the theoretical background necessary to understand the two phase flow issue and how to deal with this kind of stream in a flow measurement perspective using differential pressure orifice plate element.

2.1 TWO PHASE PRESSURE DROP MODELS

Throughout history many researchers studied the liquid loading consequences in gas flows. Lockhart and Martinelli (1949) were one of the leading-edge in two-phase flow pressure drop research, suggesting that the dimensionless pressure drop in the gas ($\sqrt{\frac{\Delta P_{TP,hl}}{\Delta P_{g,hl}}}$) or liquid ($\sqrt{\frac{\Delta P_{TP,hl}}{\Delta P_{l,hl}}}$) phase was a unique function of the parameter X , but valid only for stratified flows (TAITEL; DUKLER, 1975).

Taitel and Dukler (1975) studied this dependence, highlighting that in stratified flows it was valid only under the assumption that the gas to interfacial friction factors ratio was constant, i.e. $\frac{f_g}{f_I} \cong \text{constant}$.

In 1985 Mukherjee and Brill (1985) brought an historical review of flow pattern dependent pressure drop models for inclined pipes in addition to a new empirical model for bubble, slug and stratified flows in inclined pipes with field data validation.

Five years later Xiao, Shoham and Brill (1990) published a mechanistic model for gas-liquid two-phase flow in horizontal and near-horizontal pipelines, being able to predict firstly the flow pattern and in sequence estimate the pressure drop based on the flow regime properties for stratified, intermittent, annular, or dispersed bubble flow patterns.

Aiming to synthesize all the two-phase flow modeling available in literature at the time Petalas and Aziz (1998) released a mechanistic model gathering the best of the modellings available, in addition with new empirical correlations for liquid/wall and liquid/gas friction factor in stratified flow and entrained liquid and interfacial friction factors for annular mist flows.

The Petalas and Aziz (1998) mechanistic model

Although the modelling includes other flow patterns like dispersed bubble, bubble and intermittent, this text will focus on the stratified and annular mist regimes in wet gas flow.

In the sequence of Petalas and Aziz (1998) model follows Xiao, Shoham and Brill (1990) publication, where firstly tests the hydrodynamic stabilities of the flow patterns based on the input data such as pipe internal diameter (D), pipe straight length (L), pipe absolute internal roughness (e), fluid properties, line pressure (P), temperature (T) and gas (j_g) and liquid (j_l) superficial velocities, given by equations 1 and 2.

$$j_g = \frac{\dot{m}_g}{\rho_g A} \quad (1)$$

$$j_l = \frac{\dot{m}_l}{\rho_l A} \quad (2)$$

In stratified flows liquid height (h) (Figure 1) plays an important unknown role to verify the stability, , obtained as a solution of both gas and liquid momentum balance shown in equations 3 and 4. These can then be combined eliminating the pressure gradient $\left(\frac{dP}{dL}\right)$.

$$-E_l A \left(\frac{dP}{dL}\right) - \tau_{wl} S_l + \tau_l S_l - \rho_l E_l A g \sin(\theta) = 0 \quad (3)$$

$$-E_g A \left(\frac{dP}{dL}\right) - \tau_{wg} S_g + \tau_l S_l - \rho_g E_g A g \sin(\theta) = 0 \quad (4)$$

Where E_l and E_g are the liquid and gas volume fraction calculated by equations 5 and 6 and S_l , S_l and S_g are the liquid, interfacial and gas perimeters respectively, obtained geometrically in Figure 1.

$$E_l = 1 - E_g \quad (5)$$

$$E_g = \frac{D^2(\alpha - \text{sen}\alpha)}{A} \quad (6)$$

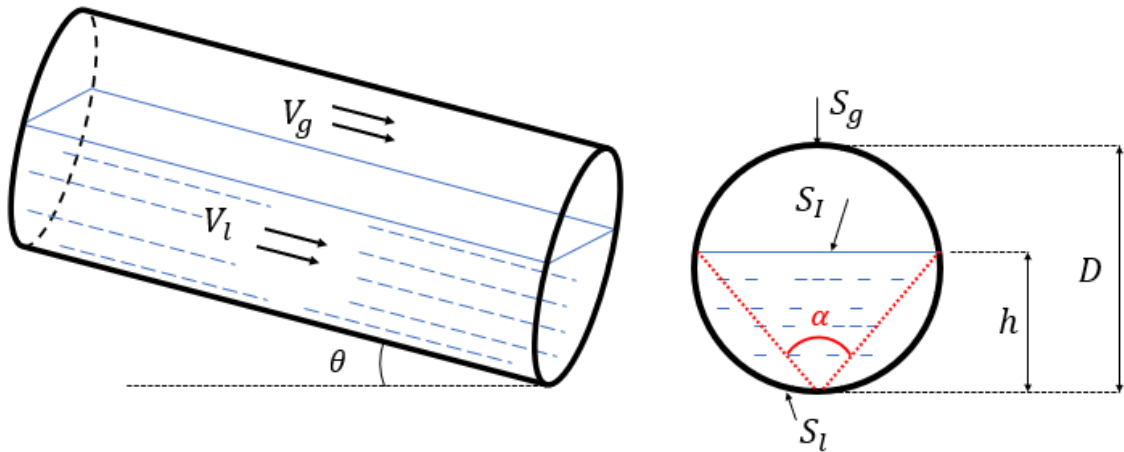


Figure 1 - Geometrical analysis of a stratified flow (Source: author)

The shear stresses (τ_{wl} , τ_{wg} and τ_l) are given by equations 7 to 9, where $V_l = j_l/E_l$, $V_g = j_g/E_g$ and $V_I = V_g - V_l$ are the phases mean velocities (XIAO; SHOHAM; BRILL, 1990).

$$\tau_{wl} = \frac{f_l \rho_l V_l^2}{2} \quad (7)$$

$$\tau_{wg} = \frac{f_g \rho_g V_g^2}{2} \quad (8)$$

$$\tau_l = \frac{f_l \rho_g V_l |V_l|}{2} \quad (9)$$

For the wall/liquid friction factor (f_l) Petalas and Aziz (1998) state that a single-phase approach is not adequate, and instead, they proposed an empirical correlation based on equation 10, where now the f_{sl} is calculated by traditional means using the liquid superficial velocity (j_l) and pipe diameter (D) on Reynolds number (equation 11). Additionally, the friction factor at wall/gas interface (f_g) is calculated by traditional single-phase means, like Colebrook-White equation, differing only on the Reynolds number definition presented in equation 12, where D_g is the hydraulic diameter for the gas phase. Finally, for the interfacial region, the liquid acts like a wall for the gas phase, therefore the shear stress (τ_i) is based on gas properties by an empirical interfacial friction factor (f_i), given by equation 13, where $Fr_l = \frac{V_l}{\sqrt{gh}}$ is the liquid Froude number.

$$f_l = 0.452 \times f_{sl}^{0.731} \quad (10)$$

$$Re_l = \frac{D\rho_l j_l}{\mu_l} \quad (11)$$

$$Re_g = \frac{D_g \rho_g V_g}{\mu_g} \quad (12)$$

$$f_i = (0.004 + 0.5 \times 10^{-6} Re_l) Fr_l^{1.335} \left[\frac{\rho_l D g}{\rho_g V_g^2} \right] \quad (13)$$

After determining the liquid height (h), the stability of stratified flow can be verified using a Taitel and Dukler (1976) approach, based on Kelvin-Helmoholtz wave stability theory, where the wave length is verified to be smaller enough to not bridge the pipe. This is done using a limiting gas velocity, based on equation 14, and limiting liquid velocity exposed in equation 15, as proposed by Barnea (1987).

$$V_g < \left(1 - \frac{h}{D}\right) \sqrt{\frac{(\rho_l - \rho_g)E_g A \cos(\theta)}{\rho_g \sqrt{1 - \left(\frac{2h}{D} - 1\right)^2}}} \quad (14)$$

$$V_l < \sqrt{\frac{gD \left(1 - \frac{h}{D}\right) \cos(\theta)}{f_l}} \quad (15)$$

Once both 14 and 15 criteria are satisfied then the stratified pattern is considered stable and the pressure gradient can be obtained from either equation 3 or 4. If not, the annular mist flow stability is tested.

In annular mist flow pattern, the methodology is based on Taitel and Dukler (1976) and Oliemans, Pots and Trompé (1986) and it is similar to stratified flow test and it. The main assumption is that the film thickness is uniform and the gas core have liquid droplets entrained, but with no slip. The momentum balance equations for liquid film and gas core are given by equations 16 and 17.

$$-A_f \left(\frac{dP}{dL}\right) - \tau_{wl} S_f + \tau_l S_l - \rho_l A_f g \sin(\theta) = 0 \quad (16)$$

$$-A_c \left(\frac{dP}{dL}\right) - \tau_l S_l - \rho_c A_c g \sin(\theta) = 0 \quad (17)$$

Where A_f and A_c are the film and core cross section areas and S_f and S_l are the film, and interfacial perimeters respectively, obtained geometrically in Figure 2

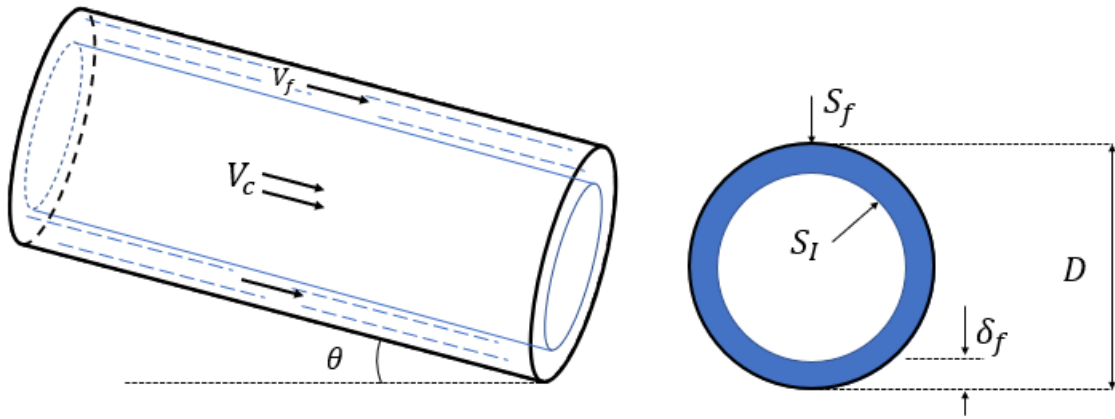


Figure 2 - Geometrical analysis of a annular flow (Source: author)

All geometric parameters can be expressed in terms of dimensionless film thickness $\tilde{\delta}_f = \delta_f/D$ and the liquid fraction entrained on the gas core (FE), as given by the empirical equation 18 (PETALAS; AZIZ, 1998).

$$FE = \frac{0.735 \times \left[\frac{\mu_l^2 j_l^2 \rho_g}{\sigma_l^2 \rho_l} \right]^{0.074} \left(\frac{j_g}{j_l} \right)^{0.2}}{1 + 0.735 \times \left[\frac{\mu_l^2 j_l^2 \rho_g}{\sigma_l^2 \rho_l} \right]^{0.074} \left(\frac{j_g}{j_l} \right)^{0.2}} \quad (18)$$

Where, σ_l is the liquid superficial tension.

The wall/liquid (τ_{wl}) and interfacial (τ_l) shear stresses are given by equations 19 and 20 respectively, where V_f and V_c represents the film and core mean velocities, as shown in equations 21 and 22 respectively, $V_I = V_c - V_f$ is the interfacial velocity and ρ_c is the weighted density for the core calculated as equation 23 (XIAO; SHOHAM; BRILL, 1990).

$$\tau_{wl} = \frac{f_f \rho_l V_f^2}{2} \quad (19)$$

$$\tau_l = \frac{f_l \rho_c V_l |V_l|}{2} \quad (20)$$

$$V_f = \frac{j_l(1 - FE)}{4\tilde{\delta}_f(1 - \tilde{\delta}_f)} \quad (21)$$

$$V_c = \frac{j_g + j_l FE}{(1 - 2\tilde{\delta}_f)^2} \quad (22)$$

$$\rho_c = E_c \rho_l + (1 - E_c) \rho_g \quad (23)$$

Where, E_c is the liquid hold up entrained on core, given by equation 24 (XIAO; SHOHAM; BRILL, 1990).

$$E_c = \frac{j_l FE}{j_g + j_l FE} \quad (24)$$

For the liquid film friction factor (f_f) Petalas and Aziz (1998) state that a single-phase approach is possible using the film Reynold number (Re_f) equation 25 , where D_f is the hydraulic diameter for the liquid film.

$$Re_f = \frac{D_f \rho_l V_f}{\mu_l} \quad (25)$$

For the interfacial friction factor (f_l) Petalas and Aziz (1998) bring an empirical correlation exposed in equation 26 , where D_c is the core internal diameter and f_c is obtained by traditional means.

$$\frac{f_l}{f_c} = 0.24 \times \left[\frac{\sigma_l}{\rho_c V_c^2 D_c} \right]^{0.085} Re_f^{0.305} \quad (26)$$

After determining the liquid film thickness iteratively, two stabilities criteria are tested. The first one is based on Barnea (1987) for upward flows, in which a negative film velocity profile results in instable annular flow, consequently the regime changes to intermittent flow. This transition is based in a minimal interfacial shear stress where the velocity profile changes its direction, calculated with equations 27 and 28 (PETALAS; AZIZ, 1998).

$$\frac{2f_f \rho_l j_l^2 (1 - FE)^2}{\rho_l - \rho_c gD \sin(\theta)} = \frac{E_f^3 \left(1 - \frac{3}{2} E_f\right)}{1 - \frac{3}{2} E_f} \quad (27)$$

$$E_f = \frac{A_f}{A} = 4\tilde{\delta}_f(1 - \tilde{\delta}_f) \quad (28)$$

Solving those equations will result in a minimum film thickness ($\tilde{\delta}_{f,min}$) correspondent to a minimum interfacial shear stress. If $\tilde{\delta}_f > \tilde{\delta}_{f,min}$ the regime becomes instable.

The second criterion assumes that once a limiting liquid volume fraction exceeds the value proposed by equations 29 and 30, the liquid film is unstable, causing blockages of gas core.

$$E_l = 1 - \left(1 - 2\tilde{\delta}_f^2\right) \left(\frac{j_g}{j_g + j_l FE}\right); \quad (29)$$

$$E_l > 0.24 \quad (30)$$

Once both criteria are satisfied, then the annular pattern is considered stable, and the pressure gradient can be obtained from either equation 16 and 17.

According to Petalas and Aziz (1998), this mechanistic model predicted the pressure drop in 59% of the -30° to $+30^\circ$ inclination range data within an 15% accuracy.

2.2 SINGLE PHASE FLOW MEASUREMENT THROUGH DIFFERENTIAL PRESSURE DEVICES

The flow measurement by means of differential pressure devices, for single phase flows, is well known and consolidated in literature, being one of the most simple, reliable and low-cost methods used nowadays. The ISO 5167 (2003) focus on general principles and requirements to develop a low uncertainty DP meter, without requiring external calibration, by five different types of primary devices such as orifice plates, nozzles, Venturi nozzles, Venturi tubes and inverted cones.

The foundation behind those devices is based on Bernoulli's principle (equation 31), where a fluid kinetic energy increasing induces a potential energy decrease, i.e. fluid acceleration causes static pressure drop resulting in differential pressure (ΔP) from upstream to downstream sides of the device, as shown in Figure 3. The acceleration is a result of an area reduction, caused by the primary device inserted on the flow, and requires the continuity equation, considering the following hypothesis: steady state and one dimension flow, incompressible fluid, as equation 32. Therefore, the flow velocity (V) on the primary device can be correlated with the differential pressure (FOX, MCDONALD and MITCHELL, 2020).

$$\frac{P}{\rho} + \frac{V^2}{2} + gz = constant \quad (31)$$

$$\rho VA = constant \quad (32)$$

Reader-harris, Forsyth, and Boussouara (2021) inform that at least 40% of the DP based flow meters are based on orifice plates, which are ruled by ISO 5167-2 (2003). In a simple way, an orifice plate is a device with simple machining process, inserted in

a pipe flange, to create a flow restriction due to area reduction, as presented in Figure 4.

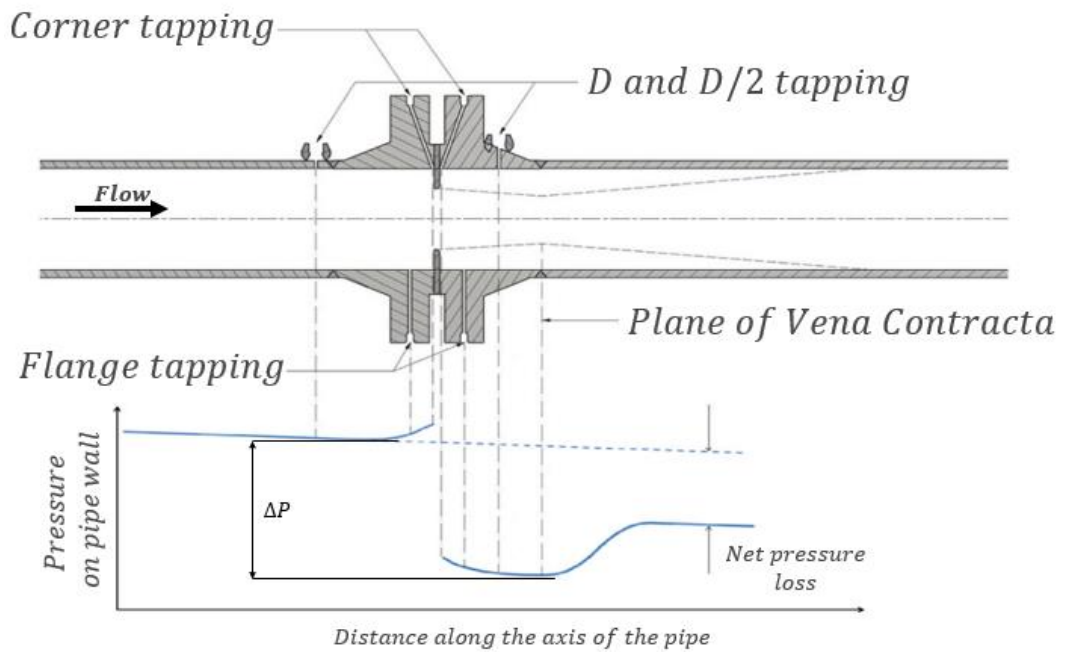


Figure 3 - Flow approximated pressure pattern through orifice plate (Source:adapted from READER-HARRIS, FORSYTH, and BOUSSOUARA (2021))

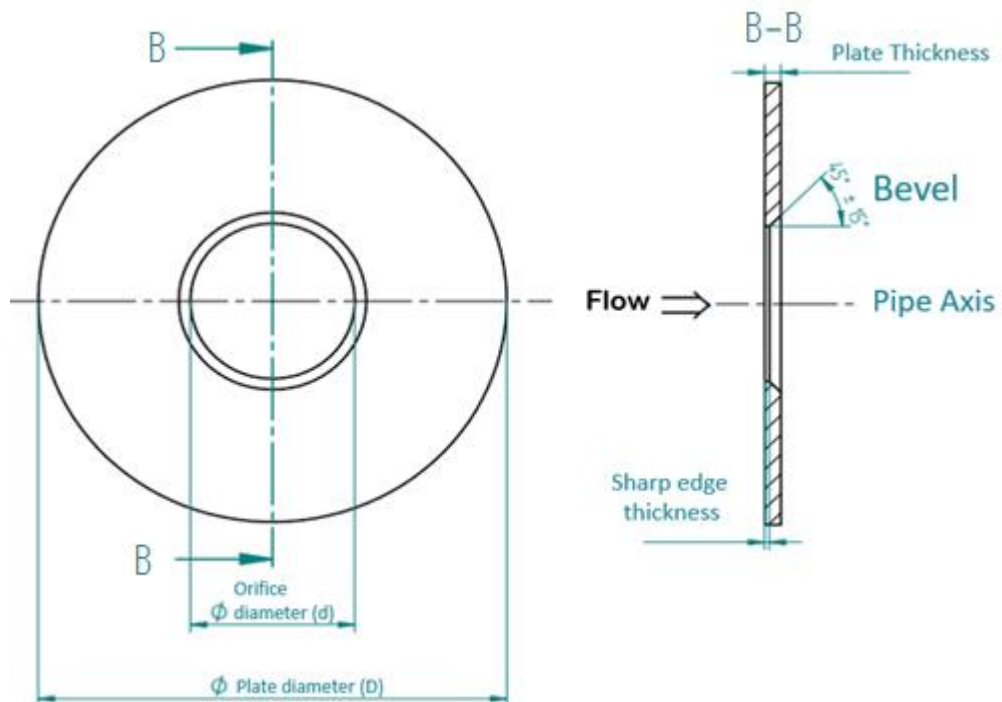


Figure 4 - Orifice plate sketch (Source: Author)

Based on that, ISO 5167-2(2003) brings the mass flow rate \dot{m} equation for orifice plates related to the ΔP (equation 33), where Cd is the discharge coefficient (equation 34), $\beta = d/D$ is the orifice to pipe diameter ratio, ε is the expansibility factor (equation 37), d is the orifice diameter and ρ_1 is the fluid density calculated with upstream static pressure.

$$\dot{m} = \frac{Cd}{\sqrt{1-\beta^4}} \varepsilon \frac{\pi}{4} d^2 \sqrt{2\Delta P \rho_1} \quad (33)$$

$$\begin{aligned} Cd &= 0.5961 + 0.0261\beta^2 - 0.216\beta^8 && \leftarrow C_\infty \text{ term} \\ +0.000521 \left(\frac{10^6 \beta}{Re_D} \right)^{0.7} &+ (0.0188 + 0.0063UP)\beta^{3.5} \left(\frac{10^6}{Re_D} \right)^{0.3} && \leftarrow \text{Slope term} \\ +(0.043 + 0.08e^{-10L_1} - 0.123e^{-7L_1})(1 - 0.11UP) &\left(\frac{\beta^4}{1-\beta^4} \right) && \leftarrow \text{Upstream tapping term} \\ - 0.031(M'_2 - 0.8M'_2{}^{1.1})\beta^{1.3} &&& \leftarrow \text{Downstream tapping term} \\ +0.0011(0.75 - \beta) \left(2.8 - \frac{D}{25.4} \right) &&& \leftarrow \text{For } D < 71.12 \text{ mm} \end{aligned} \quad (34)$$

Where,

$$UP = \left(\frac{19000\beta}{Re_D} \right)^{0.8} \quad (35)$$

$$M'_2 = \frac{2L'_2}{1-\beta} \quad (36)$$

$$\varepsilon = 1 - (0.351 + 0.256\beta^4 + 0.93\beta^8) \left[1 - \left(1 - \frac{\Delta P}{P_1} \right)^{\frac{1}{k}} \right] \quad (37)$$

The Re_D term represents Reynolds dimensionless group, calculated with respect to pipe diameter D , $L_1 = l_1/D$, $L'_2 = l'_2/D$, l_1 and l'_2 are the upstream and downstream tapping distances respectively measured using the respective plate face as reference.

In equation 37, P_1 represents the upstream absolute pressure and k the gas isentropic exponent. For liquid flows, the compressibility is negligible the term ε is equal to the unity.

Although this ISO standard is very useful in a vast range of applications, there are some limitations on its use. Those are:

- The flow must be subsonic through measuring section and not pulsating.
- The fluid must be single-phase.
- The pipe diameter must be within 50 mm to 1000 mm.
- The flow Reynold number must be above 5000.

Recently, aiming to show the Cd equation reliability, Reader-Harris, Forsyth, and Boussouara (2021) publish a meticulous analysis of Cd Reader-Harris/Gallagher equation uncertainty considering all the sources, finding similar results of the ISO 5167-2 original publication. The maximum discharge coefficient uncertainty found, following all the standard requirements, was 0.606% for a 0.67β orifice plate, ratifying that the correlation is very precise.

2.3 WET GAS FLOW MEASUREMENT BY MEANS OF DIFFERENTIAL PRESSURE DEVICES

2.3.1 What is wet gas flow?

Wet gas flow can be classified as a subcategory of two-phase flow, as illustrated on Figure 5 scheme, where a two-phase mixture of a gas and a liquid, flows simultaneously in a pipe. The liquid parcel could be composed by a single substance or be a liquid mixture of two or more components, e.g. water and condensate hydrocarbon (ISO TR 12748, 2015).

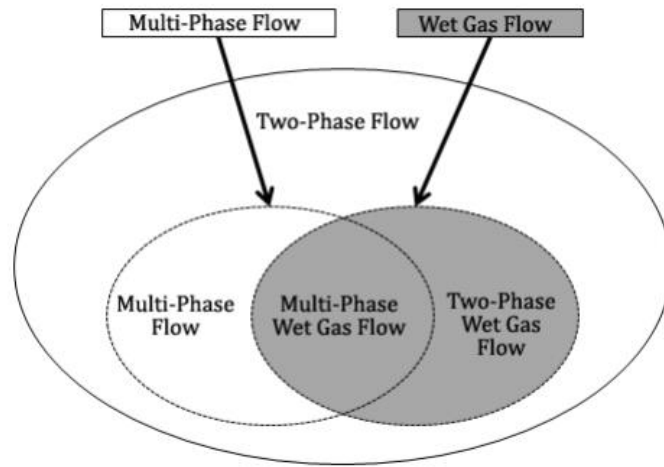


Figure 5 - Two-phase flow subsets (Source: ISO TR 12748 (2015))

To establish a quantitative classification, there are two main definitions of “wet gas” based in parameters that represents the amount of liquid on the mixture. ISO TR 11583 (2012) brings the gas volume fraction (GVF) parameter (equation 38) where Q_g and Q_l are the gas and the liquid volumetric flow rates, respectively, defining wet gas flow as a two-phase mixture with a minimal GVF of 95%.

The other parameter largely referenced to delimit the wet gas flow is the Lockhart-Martinelli parameter (X_{LM}) (equation 39), where \dot{m}_l and \dot{m}_g are the liquid and gas mass flow rates and, ρ_l and ρ_g are the liquid and gas densities respectively. Steven, Shugart and Kutty (2018) state that a wet gas flow is any combination of gas and liquid with X_{LM} less or equal to 0.3, i.e., $X_{LM} \leq 0.3$. Moreover, according to ISO TR 12748 (2015) this boundary value is intended to approximately separate the intermittent to non-intermittent flow regime.

However, this limits for wet gas are not consensual in some regulatory texts, like API (2004) and Corneliussen et al. (2005).

$$GVF = \frac{Q_g}{Q_l + Q_g} \quad (38)$$

$$X_{LM} = \frac{\dot{m}_l}{\dot{m}_g} \sqrt{\frac{\rho_g}{\rho_l}} \quad (39)$$

Even though there are no universal definition of wet gas flow, some industries operators believes that such precise discretion is unnecessary as the meter requires the relative amount of liquid to gas flow rate, no matter how small of large is that ratio. What really matters is the capability of the meter to correct the effect caused by this liquid loading and provide an accurate gas flow rate measurement.

2.3.2 Flow regimes in wet gas flows

Common single-phase characteristics such as boundary layers, turbulence, velocity profile, are not valid for two-phase flows. A proper manner to describe such flows is based on flow pattern, a physical description of the way the liquid and gas phase are interacting, whose accurate characterization depends on several parameters (CORNELIUSSEN et al., 2005).

In addition, ISO TR 12748 (2015) dissert that pipe geometry, fluids properties, line pressure and temperature and phase flow rates all together in a complex phenomenon dictates the flow pattern. For example, in horizontal two-phase wet gas flows, due to inertial forces, the gas velocity is greater than liquid velocity, thus there is a relative velocity between them, called slip velocity. Moreover, the most common flow patterns are: stratified, slug and annular mist flow demonstrated in Figure 6.

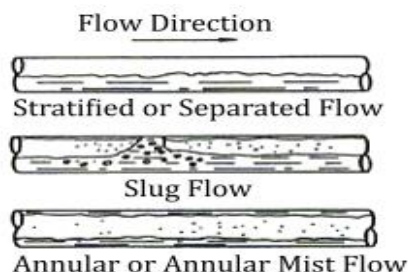


Figure 6 - Horizontal two-phase wet gas flow regimes (Source: adapted from ISO TR 12748 (2015))

The stratified flow regime occurs mainly if the gravitational force is dominant on the liquid phase. This condition develops when the gas is flowing at low velocity, i.e. low gas dynamic pressure and the line pressure is low. The result is a separated flow where the liquid moves on the downside of the pipe and the gas on the upside. The interface could be smooth or wavy depending on the velocity differences.

Slug flow appears when waves in a stratified flow hit the top wall of the tube, intermittently filling the cross section with liquid. This is an unstable flow, undesirable for wet gas metering purposes.

Finally annular mist flows arise at high GVF and high gas dynamic pressure, i.e. high gas velocity and/or density. This pattern is characterized by an asymmetrical ring of liquid and a gas with liquid droplets core. At extreme gas dynamic pressure, the liquid is fully entrained on the gas, dispersed in little droplets, permitting a pseudo-single-phase approach on the modeling (ISO TR 12748, 2015).

All these phenomena play a huge influence on the wet gas flow measurement process, so it is important to establish the flow regime because it will dictate the wet gas meter performance.

2.3.3 Wet gas parameters

As GVF and X_{LM} mentioned above, many parameters are important for a wet gas flow comprehension, so this section will define the most important parameters to a better understanding of this class of flow.

2.3.3.1 The Lockhart-Martinelli parameter (X_{LM})

One of the most used parameters regarding wet gas flows is the Lockhart-Martinelli parameter used to characterize the flow humidity, which was named in honor of R. W. Lockhart and R. C. Martinelli. But during the history some misunderstandings involving this parameter emerged and were published through some works. This section discusses how the misleading interpretation led to the today called Lockhart-Martinelli parameter.

Hall, Griffin and Steven (2007) detail the history of Lockhart-Martinelli parameter, starting with the first definition proposed. They state that Lockhart and Martinelli (1949),

studying the pressure losses in two phase flow, suggested a parameter denoted as X based on generalized Blasius friction factor equation, as defined in equation 40, where $\Delta P_{l,hl}$ and $\Delta P_{g,hl}$ are the head losses of the liquid and gas phases respectively, if flowing alone on the same pipe. This definition was stated for low single phase Reynolds number, unit length, straight smooth pipe. It is clear that the first definition of Lockhart-Martinelli parameter were a pressure loss predictor instead of a liquid loading parameter.

Furthermore, for Reynolds number above 2000, Lockhart and Martinelli (1949) proposed equation 41, where μ_l and μ_g are the liquid and gas viscosity respectively.

$$X = \sqrt{\frac{\Delta P_{l,hl}}{\Delta P_{g,hl}}} \quad (40)$$

$$X = \sqrt{\frac{\Delta P_{l,hl}}{\Delta P_{g,hl}}} = \sqrt{\left(\frac{\dot{m}_l}{\dot{m}_g}\right)^{1.8} \left(\frac{\rho_g}{\rho_l}\right) \left(\frac{\mu_l}{\mu_g}\right)^{0.2}} \quad (41)$$

In sequence Murdock (1962) discussing the behavior of orifice plates in two-phase flows, proposed a parameter expressed by equation 42, where Cd_l and Cd_g represents the liquid and gas single phase discharge coefficient respectively and the subscript m means that the pressure drop is induced by the orifice meter. This equation was unintentionally denoted by the same X parameter and it led to confusions with Lockhart-Martinelli parameter in some derivative works, even though Murdock have never called it in this fashion.

$$X_{Murdock} = \sqrt{\frac{\Delta P_{l,m}}{\Delta P_{g,m}}} = \left(\frac{Cd_g}{Cd_l}\right) \varepsilon \frac{\dot{m}_l}{\dot{m}_g} \sqrt{\frac{\rho_g}{\rho_l}} \quad (42)$$

Lately Chisholm (1977) derived a new parameter as the square root of the ratio of the gas and liquid phase flows inertia, as shown in equation 43, and titled erroneously by him "... the Lockhart-Martinelli correlating group" (*sic*) although it has a completely

different equation. Despite this confusion, this new parameter has no geometrical dependence like the original Lockhart-Martinelli parameter and the Murdock parameter, being a useful non-dimensional tool to compare the liquid loading on different flows.

$$X_{Chisholm} = \frac{\dot{m}_l}{\dot{m}_g} \sqrt{\frac{\rho_g}{\rho_l}} \quad (43)$$

An important discussion brought by Hall, Griffin and Steven (2007) about equation 43, was related to the similar derivation between Murdock's one (equation 42) and the latter, with a difference related to the discharge coefficients. In that, Chisholm (1977) assumed a $Cd_l \approx Cd_g \varepsilon$, which has validity in some circumstances, but not all.

With all that in mind, the use of these different definitions leads to different values of percentual over-reading ($OR\%$), resulting in significant differences on the gas flow correction and in the prediction processes. To illustrate these shifts, let's consider an air-water flow with a 368 kg/h air flow rate and varying only the water mass flow rate. The water mass flow rate increase results in a liquid load increase, in other words the Lockhart-Martinelli parameter increases. Considering the Chisholm (1977) equation 43 as base value for the Lockhart-Martinelli parameter, the use of different definitions as Lockhart and Martinelli (1949) - Low Re (equation 40), Lockhart and Martinelli (1949) - High Re (equation 41) and Murdock (1962) (equation 42) results in 31 to 58% of relative shift on the over-reading estimation comparing the extremes values, as shown in Figure 7 and in Table 1. This result concretizes the importance of an adequate choice of the procedure to estimate the gas wetness parameter.

Thirty years after Chisholm's publication, Hall, Griffin and Steven (2007) deducted the Lockhart-Martinelli parameter based on the square root of the gas (Fr_g) to liquid (Fr_l) densiometric Froude number ratio, as shown in equation 44, been one of the milestones towards the consecration of X_{LM} equation.

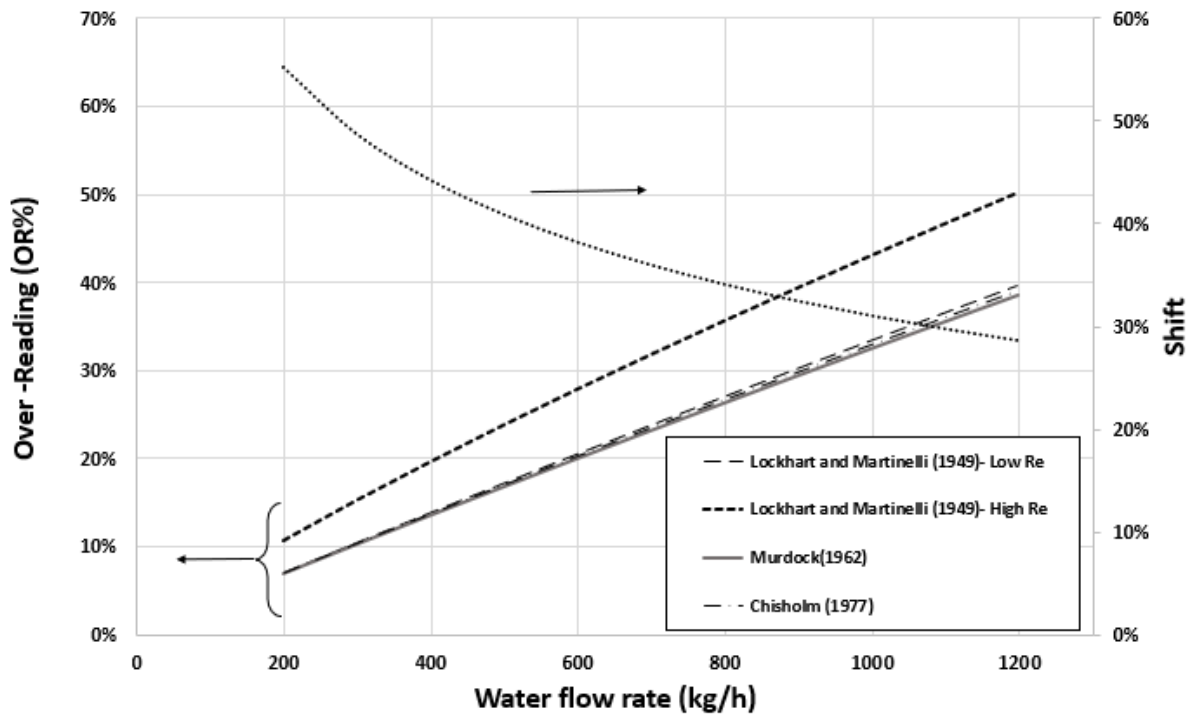


Figure 7 - Impact of Lockhart-Martinelli definitions on over-reading estimation for a 368 kg/h air mass flow rate and 7 bara line pressure (Source: Author)

Table 1 - Results for different definitions of Lockhart-Martinelli parameter

\dot{m}_l (kg/h)	Equation 40		Equation 41		Equation 42		Equation 43		OR% Highest Shift ¹
	Value	OR%	Value	OR%	Value	OR%	Value	OR%	
200	0.050	7.0%	0.077	10.9%	0.048	6.8%	0.049	6.9%	58%
598	0.149	20%	0.207	28%	0.145	20%	0.147	20%	38%
798	0.199	27%	0.268	36%	0.194	26%	0.196	27%	34%
1197	0.298	40%	0.386	50%	0.291	39%	0.294	39%	29%

1 – Calculated with equation 43 OR% value as reference

$$\frac{Fr_l}{Fr_g} = \frac{\frac{\dot{m}_l}{A\sqrt{gD}} \sqrt{\frac{1}{\rho_l(\rho_l - \rho_g)}}}{\frac{\dot{m}_g}{A\sqrt{gD}} \sqrt{\frac{1}{\rho_g(\rho_l - \rho_g)}}} = \frac{\dot{m}_l}{\dot{m}_g} \sqrt{\frac{\rho_g}{\rho_l}} = X_{LM} \quad (44)$$

Another important milestone was published by Steven (2008), where in an inspired text of dimensionless analysis of a horizontal Venturi meter operating in two-phase flow, found the equation 44 parameter as one of dimensionless group generated by Buncckinghan-Pi Theorem. This constation cement the parameter importance for two-phase flows, so said that, in this dissertation the parameter X_{LM} (equation 43 or 44) will be called Lockhart-Martinelli parameter.

Finally, to facilitate the interpretation of the X_{LM} parameter is important to establish the conversion from/to other alternative wet gas parameters like GVF and quality $x = \frac{\dot{m}_g}{(\dot{m}_g + \dot{m}_l)}$, shown by equation 45.

$$GVF = \frac{1}{1 + X_{LM} \sqrt{\frac{\rho_g}{\rho_l}}} = \frac{1}{1 + \left(\frac{1-x}{x}\right) \frac{\rho_g}{\rho_l}} \quad (45)$$

2.3.3.2 Density ratio (DR)

The density ratio, expressed by equation 46 , is an important dimensionless parameter to carry the influence of line pressure on the over-reading estimation. Assuming a perfect gas model, represented by equation 47, it is possible to demonstrate that DR is a direct function of the absolute pipe internal pressure, for other parameters held constant, as liquids density, due to its negligible change for a wide range of absolute pressure.

$$DR = \frac{\rho_g}{\rho_l} \quad (46)$$

$$\rho_g = \frac{P}{R_g T} \quad (47)$$

2.3.3.3 Gas densiometric Froude number (Fr_g)

The gas densiometric Froude number, as equation 48, is a dimensionless parameter of the gas flow rate, representing the ratio of inertial to gravity forces, important to

evaluate the flow pattern in two-phase flows as exposed by De Leeuw (1997), where A is the pipe cross section area, g the gravity acceleration and D the pipe internal diameter.

$$Fr_g = \sqrt{\frac{\text{Superficial Gas Inertia}}{\text{Liquid Gravity Force}}} = \frac{\dot{m}_g}{A\sqrt{gD}} \sqrt{\frac{1}{\rho_g(\rho_l - \rho_g)}} \quad (48)$$

2.3.3.4 Water to liquid ratio (WLR)

Until now, every definition was based only in one liquid specie and one gas specie, however there are situations where the liquid content is a mix of two or more liquids, like water and light hydrocarbon (LHC). So, on these situations the liquid density is a mixture density. Considering that, the liquid compounds behave as a homogeneous mixture, Steven, Shugart and Kutty (2018) say that the liquid mix density ($\rho_{l,mix}$) is defined by equation 49, where WLR is the water to liquid ratio, defined in equation 50 (\dot{m}_{LHC} and \dot{m}_W are the light hydrocarbon and water mass flow rates), ρ_{LHC} and ρ_W are the light hydrocarbon and water density, respectively.

$$\rho_{l,mix} = \frac{\rho_W \times \rho_{LHC}}{\rho_{LHC} \times WLR + \rho_W \times (1 - WLR)} \quad (49)$$

$$WLR = \frac{\dot{m}_W}{\dot{m}_W + \dot{m}_{LHC}} \quad (50)$$

2.3.3.5 The over-reading parameter (OR)

The most important parameter in wet gas flow measurement by DP meters is the over-reading (OR), representing the positive bias caused by the presence of liquid mixed in the gas flow. It is defined as the false prediction of total gas mass flow rate (\dot{m}_{fp}) to real dry gas mass flow rate (\dot{m}_g) ratio, as equation 51 . An approximated practical way

to calculate the OR is given by the square root of the two-phase differential pressure ($\Delta P_{TP,m}$) to gas differential pressure ($\Delta P_{g,m}$) ratio, as in many flow conditions the simplification $\varepsilon C_d \approx \varepsilon_{TP} C_{d,TP}$ can be applied on the mass flow rates equations ratio equation 51. Often in literature the OR is described as a percentage, as equation 52.

$$OR = \frac{\dot{m}_{fp}}{\dot{m}_g} \cong \sqrt{\frac{\Delta P_{TP,m}}{\Delta P_{g,m}}} \quad (51)$$

$$OR\% = (OR - 1) \times 100\% \quad (52)$$

2.3.4 The over-reading effect

In single-phase gas applications, a DP meter primary device causes a certain differential pressure $\Delta P_{g,m}$ as illustrated in Figure 8.

The presence of considerable liquid loading in a gas stream causes a positive bias called over-reading (OR), i.e the $\Delta P_{TP,m}$ in a wet gas flow is higher than the dry gas $\Delta P_{g,m}$. as presented in Figure 9.

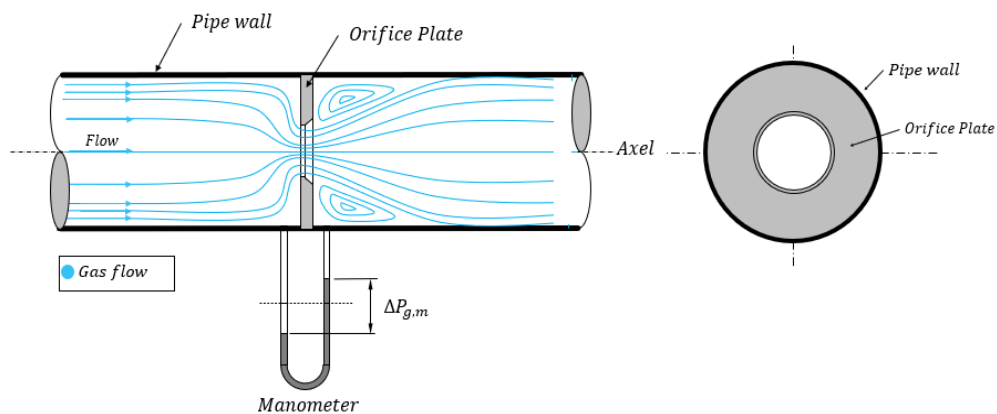


Figure 8 - Simplification of an orifice plate DP meter in a single-phase gas flow (Source: author)

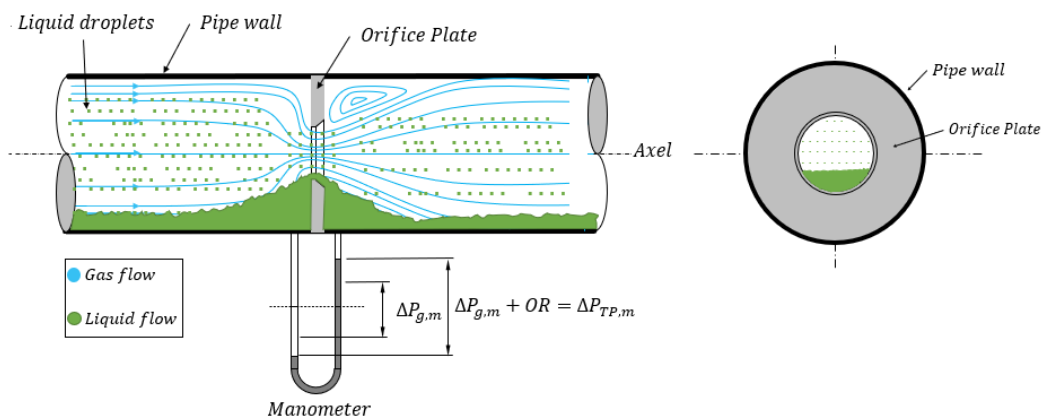


Figure 9 - Simplification of an orifice plate DP meter in a two-phase wet gas flow (Source: author)

This phenomenon is a consequence of four main flow dynamic changes from a dry gas flow to a wet gas flow:

- **Phase interfacial interaction:** in a single-phase flow only the fluid interacts with the pipe wall. On the other hand, when a second phase is present on the flow, a interfacial region appears, which in liquid and the gas different velocities develops a shear stress that consumes flow energy (WALLIS, 1969).
- **Liquid acceleration:** In the acceleration process on the meter restriction, more kinetic energy is dispended on liquid acceleration than on gas phase. This is a consequence of a higher density in liquids than in gases, resulting in more energy dissipation.
- **Area reduction:** Looking at Figure 8 and Figure 9, it is clear that the orifice area from a gas phase perspective, is reduced by the presence of a liquid phase. In such manner from equation 32 the gas velocity will be higher than if it were flowing alone, i.e more energy consumption.
- **Flow geometry change:** in orifice-plate-based meters the plate acts like a barrier for the liquid movement, accumulating on the upstream side, causing a significant change on the flow geometry, resulting in flow dynamic changes. This phenomenon is demonstrated on Figure 10, taken in a view port of a 20-minute steady flow.

Adding these four main effects, the presence of liquid leads to higher pressure drop in the meter's primary device, such as the orifice plate, than in single phase gas flow, resulting in a false prediction of total gas mass flow rate (\dot{m}_{fp}).

However, it is important to call attention to low wetness (typically $X_{LM} < 0.02$ (ISO TR 12748, 2015)) phenomenon denominated under-reading, as described by Ting (1993), diverging from the expected behavior of wet gas flows. In that work, it was postulated that the pipe wetted internal surface decrease the wall friction, reducing the pressure drop.

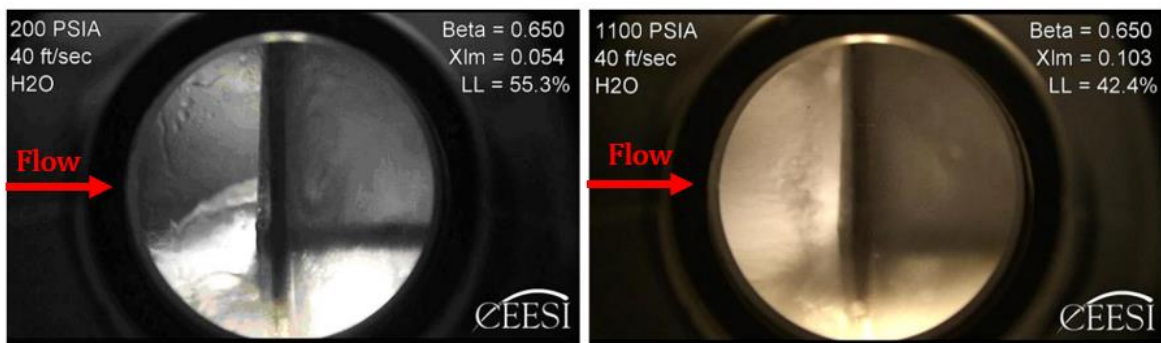


Figure 10 - Water holdup in 4" pipe with a 0.65-beta orifice plate in stratified (left) and annular (right) flows. (Source: adapted from Steven et al. (2011))

2.3.5 History of Over-reading correction

The first important contribution on the wet gas flow measurement field was driven by Murdock (1962), the Associated Technical Director for Applied Physics at the Naval Boiler and Turbine Laboratory, Philadelphia. Murdock published an extensive wet gas meter correlation for orifice plates based on experimental data of air-water, steam-water, natural gas-water, and natural gas-distillate flows. The correlation proposed exhibits linear behavior of liquid loading, as shown in equation 53 with a reported uncertainty of $\pm 1.5\%$. Murdock recognized the significance of the term $\sqrt{\frac{\Delta P_{l,m}}{\Delta P_{g,m}}}$ to describe the relative amount of liquid in gas flow, which lately was called Lockhart-Martinelli parameter, by other authors.

$$\sqrt{\frac{\Delta P_{TP,m}}{\Delta P_{g,m}}} = 1.26 \sqrt{\frac{\Delta P_{L,m}}{\Delta P_{g,m}}} + 1 \quad (53)$$

The huge relevance on Murdock's work is based in the publication of 90 experimental data points with a 2.5 to 4 inches pipe diameter range, a 0.26 to 0.5 orifice plate beta range and a liquid loading range, expressed in terms of X_{LM} , from 0.041 to 0.25. Despite the significance of his work in wet gas knowledge, Steven et al. (2011) states that Murdock assumed a separated flow, although some of data set had other flow patterns based on the flow rates. Additionally, he did not take to account important parameters for a two-phase flow, like line pressure and slip ratio, resulting in a limited over-reading correlation, depending only on gas wetness.

Chisholm (1977) continuing the 1974's two-phase flow investigation and, motivated by the limitations of Murdock's work, studied the pressure line influence and the slip ratio on the orifice plate over-reading in wet gas flows. According to Collins and Clark (2013), Chisholm was a National Engineering Laboratory (NEL) member, where he developed his experiments using water-vapor combinations with 10, 30, 50 and 70 bar of pressure in 21, 32 and 44mm pipe diameter. His paper introduced a new liquid loading parameter for orifice plates, called by him as Lockhart-Martinelli parameter, as defined in equation 43. Such definition was applied to develop a new over-reading correction correlation, represented by equations 54 and 55, where the pressure influence on the over-reading was implicit on the gas to liquid density ratio (DR), characterized by the C_{Ch} term. He claimed a $\pm 2\%$ uncertainty performance comparing to experimental data.

$$OR_{Chisholm} = \sqrt{1 + C_{Ch} X_{LM} + X_{LM}^2} \quad (54)$$

$$C_{Ch} = \left(\frac{\rho_g}{\rho_l}\right)^{\frac{1}{4}} + \left(\frac{\rho_l}{\rho_g}\right)^{\frac{1}{4}} = (DR)^{\frac{1}{4}} + \left(\frac{1}{DR}\right)^{\frac{1}{4}} \quad (55)$$

Steven et al. (2011) states that Chisholm's considerations to develop the correlation were an incompressible and stratified flow, with a constant phase velocity ratio (or slip ratio) and a dependence on the gas to liquid density ratio (DR). These assumptions limited the correlation for a low densitometric Froude number, where the flow pattern is predominantly stratified i.e., limited in a low gas flow rate. Chisholm related the over reading as being dependent on the split ratio rather than the flow pattern.

After Chisholm's publication, a small amount of research was done on the wet gas metering by differential pressure meters field. However, with the rising interest on natural gas flows by the industry, De Leeuw (1997), a Shell International Exploration and Production employee, released research on wet gas metering with a 4", 0.4 beta ratio Venturi, showing that the flow pattern governed the Venturi's over-reading in addition with Lockhart-Martinelli parameter and DR relation. According to De Leeuw, the flow pattern was a gas densitometric Froude number function and hence the over-reading, with a directly proportional relation, i.e. as gas densitometric Froude number rises the over-reading rises, if all other parameters are kept unchanged. Another constation was that Venturi's over-reading is higher than orifice meter over-reading, demanding so, higher correction factor. A new data set was acquired from the SINTEF Multiphase Flow laboratory to a 4" diameter, 0.4 beta ratio Venturi in a Nitrogen- Diesel oil flow, covering a 15 to 90 bar pressure range, gas velocities up to 17 m/s, $1.5 \leq Fr_g \leq 4.8$ and $0 \leq X_{LM} \leq 0.3$. With these combinations the minimal gas density tested was 17 kg/m³, becoming a limitation of the algorithm. The Venturi meter correlation proposed is shown as equation set 56 to 58 with a stated uncertainty of $\pm 2\%$.

$$OR_{DL,venturi} = \sqrt{1 + C_{DL}X_{LM} + X_{LM}^2} \quad (56)$$

$$C_{DL} = (DR)^n + \left(\frac{1}{DR}\right)^n \quad (57)$$

$$\begin{cases} n = 0.41 \text{ for } Fr_g \leq 1.5 \\ n = 0.606[1 - \exp(-0.746Fr_g)] \text{ for } Fr_g > 1.5 \end{cases} \quad (58)$$

Following up the development of differential pressure technology, Stewart et al. (2002), members of NEL 1999-2002 Flow Programme, investigated the inverted cone (IC) meters performance on wet gas flows. Two IC meters, with 0.55 and 0.75 beta ratio, were used to collect new experimental data in three pressure levels 15, 30 and 60 bar, at a range of Nitrogen and Kerozene flowrates, resulting in a 0.4 to 4.0 gas densiometric Froude number range. The results indicated a strong over-reading dependence on Lockhart-Martinelli parameter, a pressure and a gas densiometric Froude number effect similar to that occurred in Venturi meters. To develop a new correlation applied to IC meters, the authors firstly tested the available data with existing Venturi correction correlations, noting that Venturi meters over-reading were higher than in IC, hence the gas flow rate error was over corrected. Based on this results, new correlations were proposed, one for each beta ratio.

In 2005, Steven, Kegel and Britton (2005) unified all the IC data available at that time and slight improved the Stewart et al. (2002) correlation as shown in equations 59 to 61 resulting in a gas flow rate prediction to $\pm 2\%$ uncertainty.

$$OR_{St,IC} = \frac{1 + aX_{LM} + bFr_g}{1 + aX_{LM} + bFr_g} \quad (59)$$

$$\begin{cases} a = 2.431 \\ b = -0.151 \text{ for } DR < 0.027 \\ c = 1 \end{cases} \quad (60)$$

$$\begin{cases} a = -0.0013 + \left(\frac{0.3997}{\sqrt{DR}}\right) \\ b = 0.0420 - \left(\frac{0.0317}{\sqrt{DR}}\right) \text{ for } DR \geq 0.027 \\ c = -0.7157 + \left(\frac{0.2819}{\sqrt{DR}}\right) \end{cases} \quad (61)$$

Steven, Ting and Stobie (2007), motivated by earlier observations about beta ratio to over-reading inverse relationship on Venturi's, studied this behavior in orifice plates. Conclusions showed that in orifice plates this effect is far less sensitive than in Venturi,

smaller enough to be negligible. On the other hand, Chisholm did not report similar beta effect on his publication and De Leeuw said it is irrelevant in Venturis.

Steven (2006) proceeded a theoretical derivation of Chisholm's model for a homogeneous flow developing a correction correlation, which equations set is similar to Chisholm's publication, but changing only the exponent from $\frac{1}{4}$ to $\frac{1}{2}$. Such homogeneous model works for different types of differential pressure meters, being dependent only on Lockhart-Martinelli parameter and on gas to liquid density ratio (DR), regarding the fact that the flow needs to have a negligible slip.

Reader-Harris, Nel and Graham (2009) continuing the de Leeuw's studies, proposed a new correction correlation for Venturis, taking in account the Froude and beta effect. They collected new wet gas data from National Engineering Laboratory 4" loop using Nitrogen-Exxsol 80, Argon-Exxsol 80 and Nitrogen-water as two-phase fluid with 0,4 to 0.75 beta range, 15 to 60 pressure range and $0 \leq X_{LM} \leq 0.3$. The resulting correlation is similar to De Leeuw's correlation, substituting only the n exponent to equation 62, where β is the diameter ratio (beta ratio) and H is a function of the surface tension i.e., a fluid function being 1 for hydrocarbon fluids, 1.35 for ambient temperature water and 0.79 for hot water (in a wet-steam flow).

$$n = \max \left[0.583 - 0.18 \times \beta^2 - 0.578 \times \exp \left(-0.8 \frac{Fr_g}{H} \right); 0.392 - 0.18 \times \beta^2 \right] \quad (62)$$

Another important observation made by Reader-Harris and Graham, is the fact that the discharge coefficient for wet gas flows is different from dry gas flows. The wetness results in a Cd decrease. So, they proposed an appropriated empirical way to estimate the Cd for wet gas flows, given by equations 63 and 64.

$$Cd_{TP} = \left[1 - 0.0463 \times \exp(-0.05 Fr_{g,th}) \right] \quad (63)$$

$$Fr_{g,th} = \frac{Fr_g}{\beta^{2.5}} \quad (64)$$

Within the data set range, Reader-Harris and Graham stated a $\pm 3\%$ uncertainty for $X_{LM} \leq 0.15$ and $\pm 2.5\%$ uncertainty for $0.15 < X_{LM} \leq 0.3$.

Back to orifice meters studies, Steven and Hall (2009) evaluating natural gas flows with liquid loading noticed that orifice plates had the same Fr_g and DR effect observed in Venturis i.e., an Fr_g increase resulted in a OR increase and a DR increase resulted in a OR decrease. To improve the data set range, new experiments were done in CEESI and NEL laboratories with natural gas and nitrogen as gas phases and Stoddard solvent, Exxsol 80 and Decane as liquid phases. The geometry and properties ranges were 2" to 4" pipe diameter, 6.7 to 79 bar pressure, 0.25 to 0.73 β , 1.5 to 4.8 Fr_g and $0 \leq X_{LM} \leq 0.55$. This new data set together with the former data set available resulted in the following correlation, similar to Chisholm's changing the n exponent to equation 65 . Steven and Hall state a $\pm 2\%$ uncertainty at a 95% confidence level.

$$\left\{ \begin{array}{l} n = 0.214 \text{ for } Fr_g \leq 1.5 \\ n = \left[\left(\frac{1}{\sqrt{2}} \right) - \left(\frac{0.3}{\sqrt{Fr_g}} \right) \right]^2 \text{ for } Fr_g > 1.5 \end{array} \right. \quad (65)$$

Testing this correlation with a 0 to 100% WLR data, which was not used to develop the correlation, Steven and Hall (2009) found a slight shift on the correction up to -3%, a over-correction result.

Steven et al. (2011) with more two-compound liquid loading (water + hydrocarbon) data observed that the water content on liquid mixture reduced the OR , in an almost linear manner. It was a result of transition gas densiometric Froude number increase from stratified to annular mist flow pattern. As the WLR increases i.e., the water content on the liquid loading increases, the mixture surface tension increases, tending the flow pattern to separated flow. After this finding Steven et al. (2011) included the WLR effect in the previously orifice plate correlation changing only de Chisholm exponent as shown in equations 66 and 67 , where $Fr_{g, strat}$ is the transitional gas densiometric Froude number between stratified to annular mist flow.

$$\begin{cases} n = \left[\left(\frac{1}{\sqrt{2}} \right) - \left(\frac{0.4 - 0.1 \times \exp(-WLR)}{\sqrt{Fr_{g, strat}}} \right) \right]^2 & \text{for } Fr_g \leq Fr_{g, strat} \\ n = \left[\left(\frac{1}{\sqrt{2}} \right) - \left(\frac{0.4 - 0.1 \times \exp(-WLR)}{\sqrt{Fr_g}} \right) \right]^2 & \text{for } Fr_g > Fr_{g, strat} \end{cases} \quad (66)$$

$$Fr_{g, strat} = 1.5 + (0.2 \times WLR) \quad (67)$$

As reported by Steven et al. (2011) this algorithm corrected the data within a $\pm 2\%$ uncertainty at a 95% confidence level.

Is important to highlight that all these empirical correlations are based on data fitting, therefore being in some level dependent on the data set installations, where extrapolations tend to increase uncertainty.

2.3.6 PLR to X_{LM} relationship

As seen on the previous section, usually the over-reading correction correlations demand a liquid flow rate or a liquid content parameter previous knowledge, to predict the over-reading. Nonetheless this information is not available since the traditional meters were developed to measure single-phase flows. Consequently, this liquid loading info needs to be gathered from an external source like test separator, historical data, trace dilution methods or equation of state predictions, which bring high uncertainty to the measurement process, resulting in an inaccurate gas flow rate prediction (STEVEN, 2007).

Aiming to mitigate this limitation De Leeuw (1997) published an important *PLR* to X_{LM} relation. The pressure loss ratio (*PLR*) is defined as the ratio between the permanent pressure loss (ΔP_{PPL}), measured by an extra third pressure tapping, operating in conjunction with the traditional pressure differential (ΔP_t), as exemplified in Figure 11 (Venturi tube application) and Figure 12 (Orifice plate application). According to De Leeuw, the *PLR* in Venturi tube is affected by the liquid presence, increasing with it. Consequently, this relation could potentially be used to predict the liquid loading without external methods, i.e. being directly related to X_{LM} as exposed in Figure 13. However, the sensitivity of *PLR* with the amount of liquid is variable, being wetness and

pressure dependent, decreasing with these parameters increasing. For Venturi tube, De Leeuw states that the use would be suitable for Lockhart-Martinelli values below 0.15 ($X_{LM} < 0.15$, i.e. a GVF of 98.97% at 3 barg). Despite these significant observations, no acceptable correlation formula was proposed in that work.

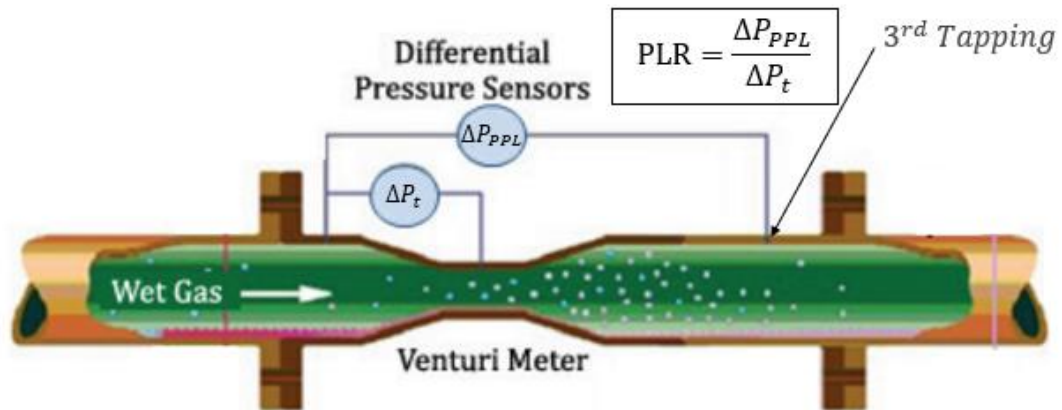


Figure 11 - Configuration of the third tapping propose by De Leeuw (Source: adapted from ISO TR 12748 (2015))

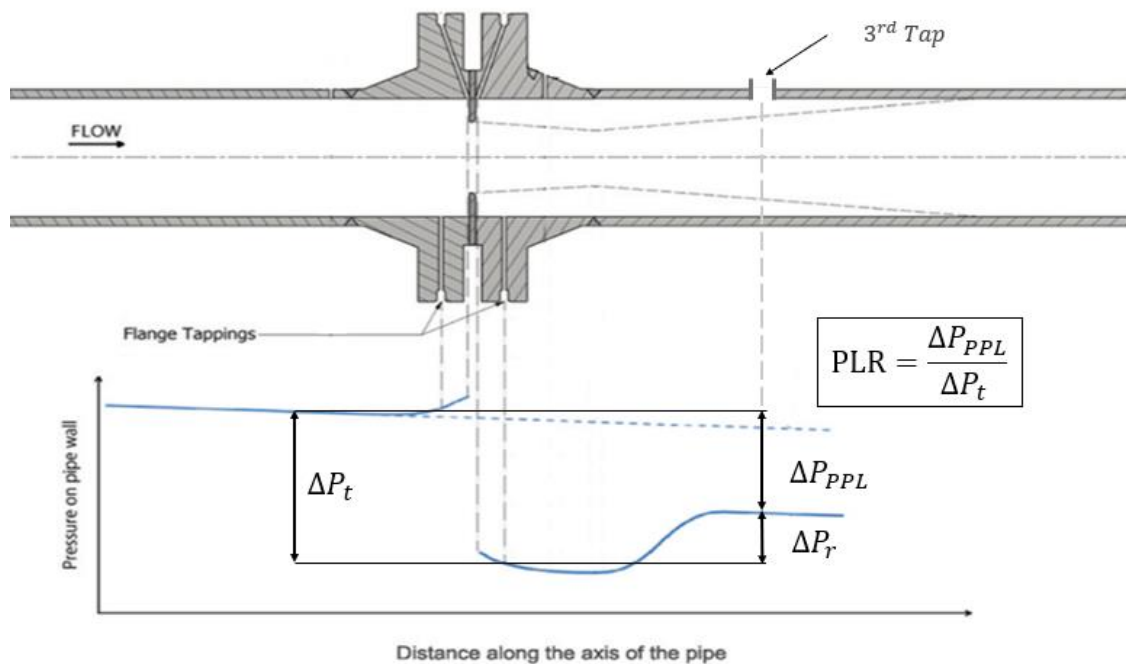


Figure 12 - Illustration of pressure profile showing the ΔP_t , ΔP_{PPL} and ΔP_r for an orifice plate meter and a generic third pressure tap (Source: author)

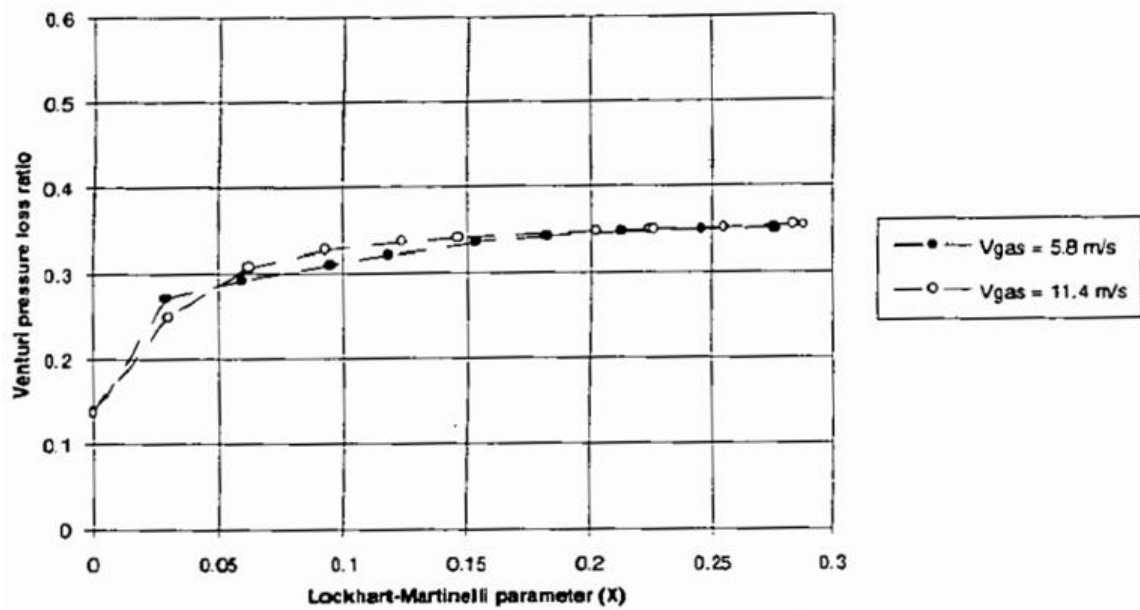


Figure 13 - Venturi's PLR to X_{LM} relation at 45 bar. (Source: De Leeuw (1997))

From 2001 to 2005, many reported attempts to use this method, applied to the inverted cone, have had poor results and additional methods using a second DP meter in series with inverted cone, in the expansion region tested exhaustively, had no farther results. However, in 2005 Steven, Kegel and Britton (2005) released an IC wet gas meter using the third tap to create a V-cone expansion meter correlations, which combined with the traditional V-cone correlations (equations 59 to 61) resulted in a Lockhart-Martinelli estimation based on the ratio between the traditional meter OR and the expansion meter OR , as equations 68 and 69, where the subscripts TM and EM means traditional meter and expansion meter respectively. The authors stated uncertainty of $\pm 5\%$ for the gas mass flow rate (STEVEN, 2007).

$$\phi = \frac{OR_{TM}}{OR_{EM}} = \frac{(\dot{m}_{fp})_{TM}}{(\dot{m}_{fp})_{EM}} \quad (68)$$

$$X_{LM} = \frac{(\phi - 1)^2}{4 \times \exp \left[-2.74 - 22.3 \times DR - \frac{1.27}{Fr_g} \right]} \quad (69)$$

Back to orifice plates, Steven et al. (2011) brought back the ISO 5167-2 (2003) PLR_{dry} correlation for a single-phase flow as a baseline, as shown in equation 70, explaining that the discharge coefficient and consequently the pressure loss ratio have a relatively low sensitivity to Reynolds, remaining almost invariant for a given beta. Hence it could be used to predict the Lockhart-Martinelli parameter in wet gas flows. They state that PLR_{wet} is sensitive to X_{LM} only in orifice plates to beta larger or equal to 0.5 ($\beta \geq 0.5$), due to PLR_{dry} proximity to unit at lower betas, and an extremely DR dependence. However, ISO 5167-2 (2003) stated that the PLR_{dry} equation is an approximation with a D upstream and $6D$ downstream taps for the pressure loss and no uncertainty is mentioned.

$$PLR_{dry} = \frac{\sqrt{1 - [\beta^4(1 - Cd^2)]} - Cd\beta^2}{\sqrt{1 - [\beta^4(1 - Cd^2)]} + Cd\beta^2} \quad (70)$$

In face of such finding and considering the Steven and Hall (2009) and Reader-Harris, Nel and Graham (2009) correction correlations for orifice plates and Venturis respectively, the International Organization for Standardization (ISO) released the ISO TR 11583 (2012), recommending a wet gas measurement methodology based on the traditional DP meters methodology in addition to a Lockhart-Martinelli parameter estimation by means of the difference between PLR_{dry} and PLR_{wet} , showed in equations 70, 71 and 72, limited by $0.5 \leq \beta \leq 0.68$, $X_{LM} < 0.45DR^{0.46}$ and $DR \leq 0.21\beta - 0.09$. No limitations to the pressure tapping were recommended.

$$Y = PLR_{wet} - PLR_{dry} \quad (71)$$

$$X_{LM} = \frac{6.41Y}{\beta^{4.9}} (DR)^{0.92} \quad (72)$$

Steven, Shugart and Kutty (2018) argued that the PLR_{dry} equation (equation 70) had some shifts from the experimental data available and the X_{LM} equation (equation 72)

did not behave well for $\beta > 0.55$ and was developed only for hydrocarbon liquid loading, not for water content. Other limitations exposed was about the X_{LM} and DR parameters, resulting in a narrow range of applicability due to the reduced database used to develop this correlation. To improve these limitations Steven, Shugart and Kutty (2018) proposed a new equation set including an improving PLR_{dry} equation. Unfortunately, for confidentiality matters, they did not expose their algorithm, but stated less than $\pm 2\%$ uncertainty for a WLR = 1 and for all data set tested, a global $\pm 4\%$ uncertainty at a 95% confidence level.

3 EXPERIMENTAL APPARATUS

The Research Group for Studies on Oil&Gas Flow and Measurement (NEMOG in Portuguese) is located at Federal University of Espírito Santo, Vitória, Brazil to realize research on flow measurement field. One of the research lines is the multiphase flow measurement and characterization, relying with a new and up to date multiphase flow loop operating with air, water and mineral oil, as shown in Figure 14, pressure class #150psi (10 barG).

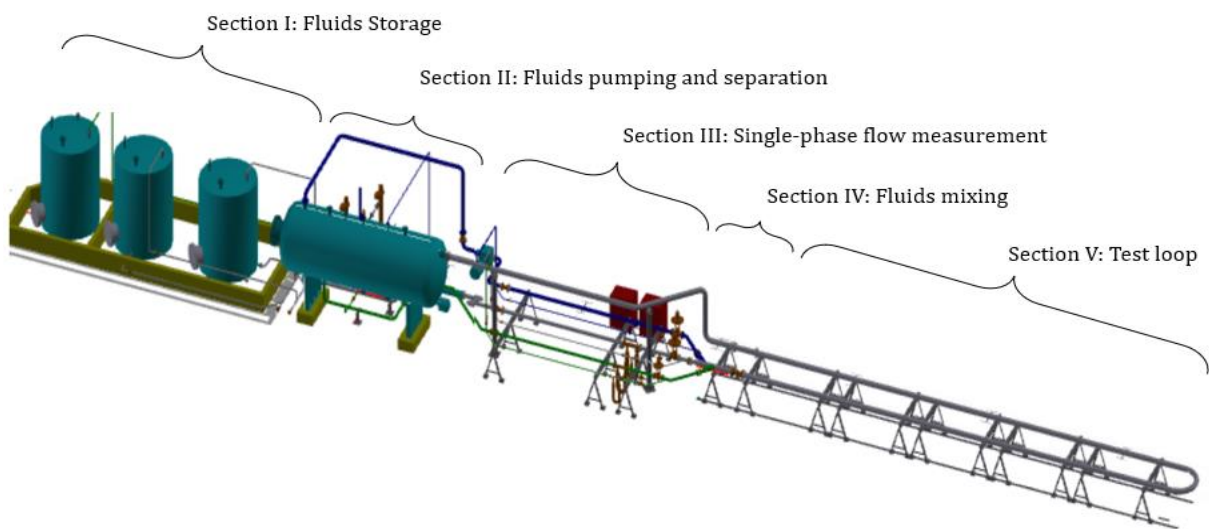


Figure 14 -The NEMOG's multiphase flow loop sketch (Source: Author)

3.1 SECTION I: FLUID STORAGE

The fluid storage counts with three steel tanks designed to store tap water, mineral oil and emulsified fluids from the separator vessel. With an 3 m³ volumetric capacity each, the tanks operate under atmospheric pressure. Figure 15 shows a schematic view of the tanks.

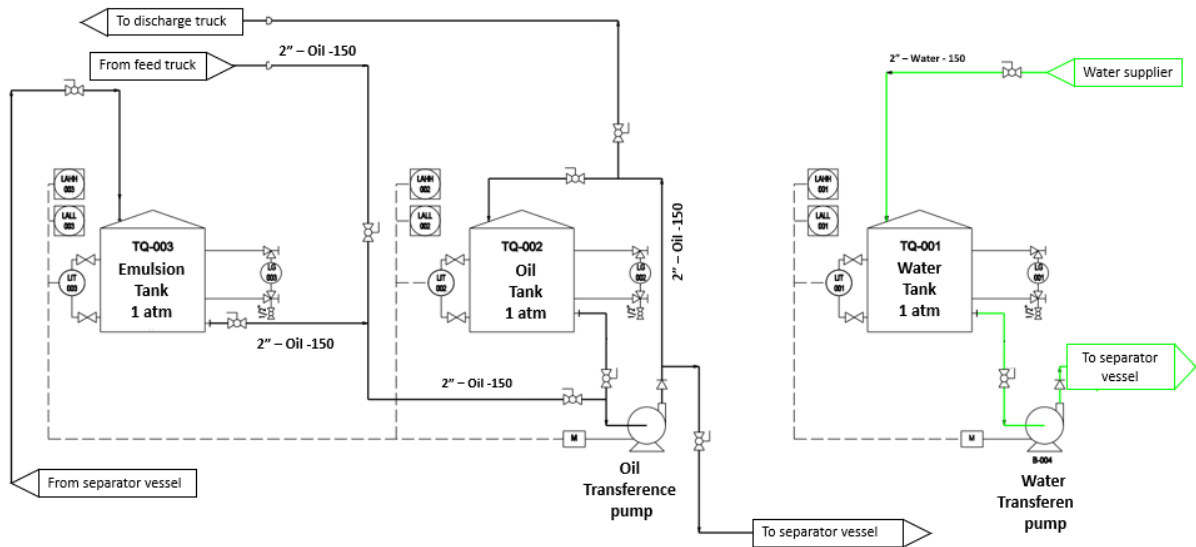


Figure 15 - Storage tanks flowchart (Source: author)

3.2 SECTION II: FLUID PUMPING AND SEPARATION

This section is divided in four subsections, the three-phase separator vessel, the oil pumping, the water pumping, and the compressed air supplier.

3.2.1 Three-phase separator vessel

The three-phase separator vessel, shown in Figure 16, is responsible to pre storage the water and oil before the single-phase measurement and to separate the fluid emulsion formed after the circulation on the test loop, where a schematic flowchart of the fluids before and after separation process. Figure 17 shows a separator vessel photography, and the technical information are exposed in Table 2.

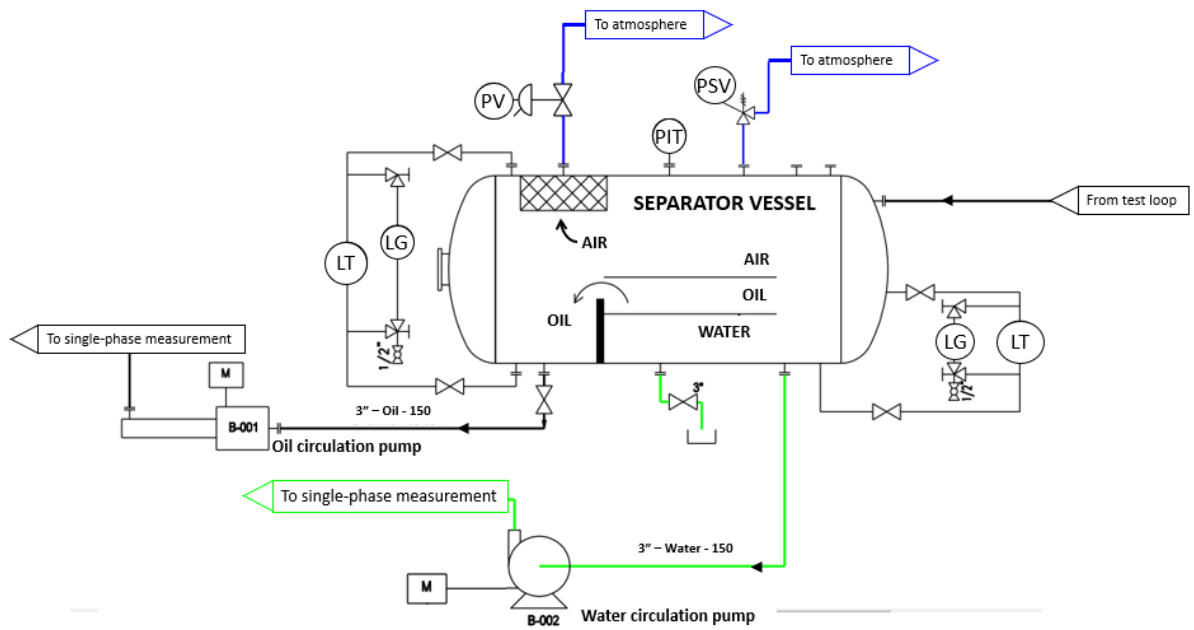


Figure 16 - Separator vessel flowchart (Source: author)



Figure 17 - Separator vessel photography (Source: author)

Table 2 - Separator vessel technical information

Volumetric Capacity	6,7 m ³
Operational Temperature	25 °C
Operational Pressure	10 barg
Project Limit Temperature	50 °C
Project Pressure	13 barg
Hydrostatic Pressure Test	20 barg
Material	Steel
Full load weight	9300 kg

3.2.2 Water circulation pumping

The water used in the flow circuit is supplied from the separator vessel and pumped by a centrifugal water pump coupled to a Weg induction electric motor controlled by a variable-frequency driver. This configuration results in the following capabilities, with operational data, shown in Table 3.

Table 3 - Water pumping specifications and capabilities

Water pump	KSB Meganorm 80-50-125
Electric motor	WEG W22 7.5 HP
Driver	Schneider ATV600
Maximum Pressure¹	3.33 barg
Maximum Mass Flow Rate²	42000 kg/h

1 - With no flow rate and the separator vessel, i.e. the suction line at atmospheric pressure

2 - For the actual test loop configuration, i.e. actual installed pressure drop

3.2.3 Compressed air supplier

The compressed air is supplied by an Kaeser ASD 40 volumetric screw compressor that feeds an intermediary pressure vessel and goes to an air dryer, before entering the single-phase measurement, as shown in Figure 18. Since the compressor uses a

fixed volume screw to compress the air, the maximum air mass flow rate becomes dependent on the local air density, i.e. on the laboratory atmospheric pressure and temperature. Table 4 brings the system configuration and capability.

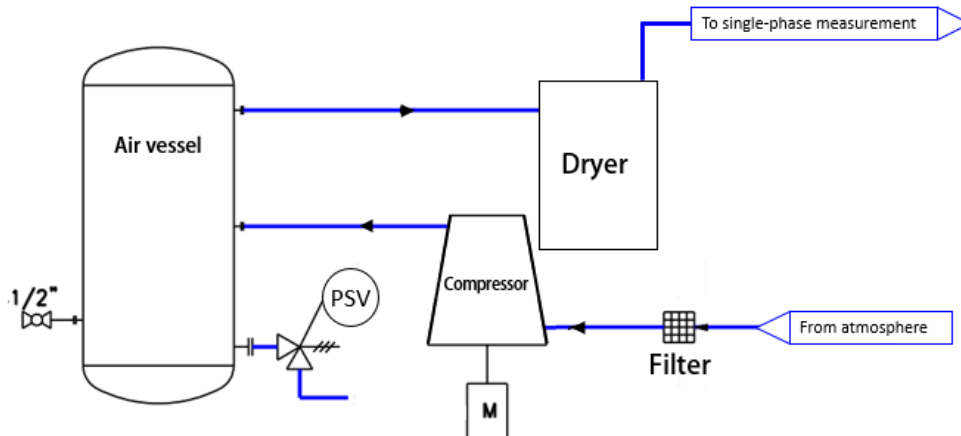


Figure 18 - Compressed air supplier schematic flowchart (Source: author)

Table 4 - Compressed air supplier specifications and capabilities

Compressor	Kaeser ASD 40
Maximum Pressure	8.62 barg
Maximum Mass Flow Rate @ 23 °C	387 kg/h ¹
Maximum Mass Flow Rate @ 30 °C	351 kg/h ^{1, 2}
Air Vessel	13 barg, 1m ³

1 - Based on a 5 barg test loop back pressure

2 - This mass flow rate reduction occurs due to the air specific volume increase in the suction line, resulting in a volumetric efficiency reduction

3.3 SECTION III: SINGLE-PHASE FLOW MEASUREMENT

The flow rate measurement of each phase is configured in a split-range way to amplify the circuit measurement capability, as sketched in Figure 19 and Figure 20, where high flow rates and low flow rates are separated. For the water side, two different

flow range Coriolis flowmeters are used with technical information exposed in Table 5 and shown in Figure 21, providing both mass and volumetric flow rates.

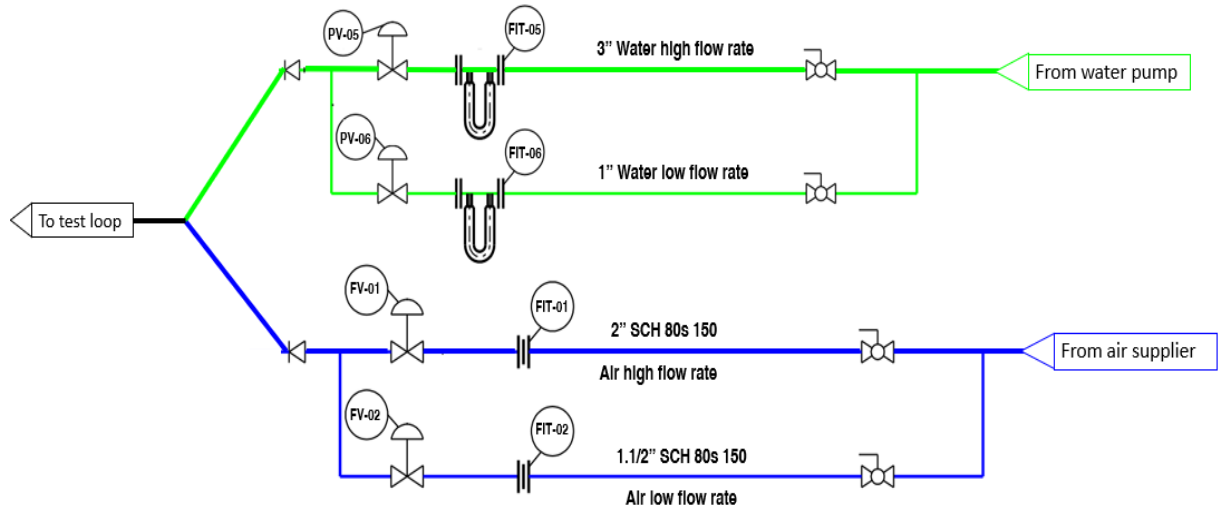


Figure 19 - Single-phase measurement split-range configuration sketch for water and air (Source: author)



Figure 20 - Single-phase measurement split-range configuration photography (Source: author)



Figure 21 - High and low waterflow rate Coriolis meters in split-range arrangement photography (Source: author)

Table 5 - The high and low water flow rate Coriolis meters technical information

	High flow rate	Low flow rate
Manufacturer	Metroval	Metroval
Model	SMT-100	SMT-50
Identifier Code	FIT-05	FIT-06
Mode	Totalizing	Totalizing
Maximum Calibrated Flow Rate	80 m ³ /h	20 m ³ /h
Minimum Calibrated Flow Rate	8 m ³ /h	2 m ³ /h ¹
Calibration Certificate	Appendix A	Appendix A

1 - Although the calibration process was performed at this minimal value, the manufacturer informed that this flow meter could measure at least 0,65 m³/h, increasing to 0,5% the measurement uncertainty.

For the air side, the mass flow rate measurement are done by two different orifice plates, configured as exposed in Table 6 and shown in Figure 22.



Figure 22 - The high and low mass flow rate orifice plate meters photography (Source: author)

Table 6 - The high and low flow rate orifice plate meters technical information

	High flow rate	Low flow rate
Manufacturer	Ituflux	Ituflux
Identifier code	FIT-01	FIT-02
Material	AISI 316	AISI 316
Tap	Flange	Corner
Upstream/Downstream tap distance	26/26 mm	3/3 mm
Pipe diameter	50.10 mm	39.10 mm
Orifice diameter	25.02 mm	14.67 mm
Beta ratio	0.4994	0.3752
Upstream straight pipe length	22 D	22 D
Downstream straight pipe length	8 D	8 D
Maximum Project Mass Flow Rate	1180 kg/h	236 kg/h
Minimum Project Mass Flow Rate	236 kg/h	59 kg/h
Calibration certificate	N/A ¹	N/A ¹

1 - The measurement uncertainty is given by ISO 5167-2

3.4 SECTION IV: FLUIDS MIXING

The mixing section is one of the most important parts of the multiphase flow loop due to the influence on the downstream flow pattern. Considering only water and air flow, the original mixing configuration of the installation is located after the single-phase measurement and consists of two 45° Y fits, 6" pipes converging to a single 6" pipe leading to the teste loop, as shown in Figure 19 and Figure 23.

Nonetheless, preliminary tests showed that the mixing upstream of the 6" to 2" reduction was resulting in an intermittent flow pattern even in low water mass flow rate, causing high range fluctuations on the test section pressure measurements downstream, leading to an inconclusive data.

Following up, a new mixing section was developed and installed downstream of the pipe reduction, illustrated in Figure 24. This configuration led to a more stable two-phase flow with flow patterns from stratified to annular mist.



Figure 23 - Original mixing arrangement (Source: author)

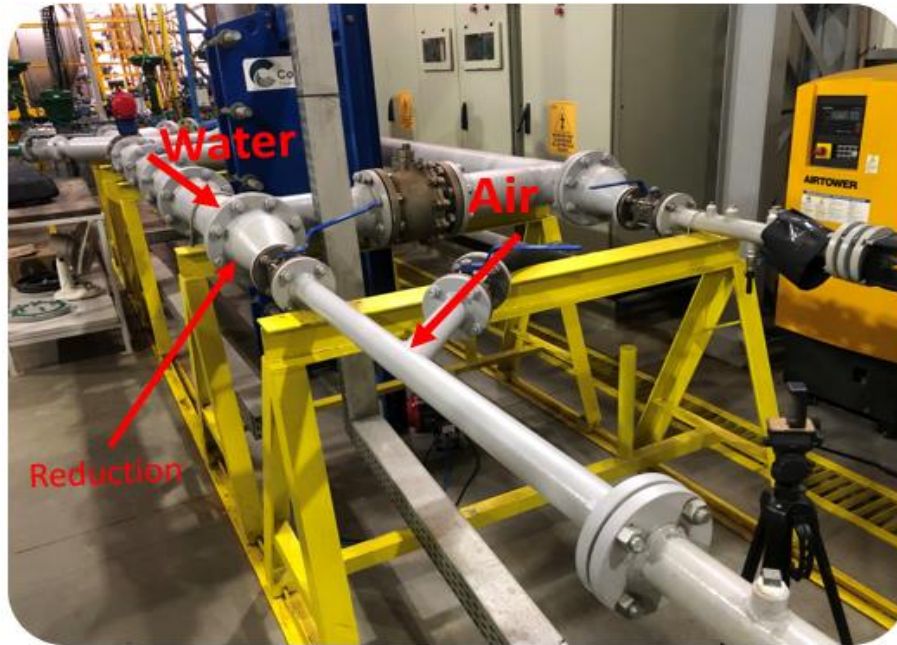


Figure 24 – Final Experimental mixing arrangement (Source: author)

3.5 SECTION V: TEST LOOP

The experiments are performed in test loop section. It counts on interchangeable 2" sch 40 pipe spools of different lengths from 600 mm to 3000 mm, two flexible stretches and two 600 mm borosilicate pipe spools providing a set of loop configurations and inclinations. The actual installation is composed by two branches of horizontal 2" sch 40 pipes, one inlet and one in return with 6776 mm each, connected by a section with two 90° bends as shown in Figure 25 and Figure 26.

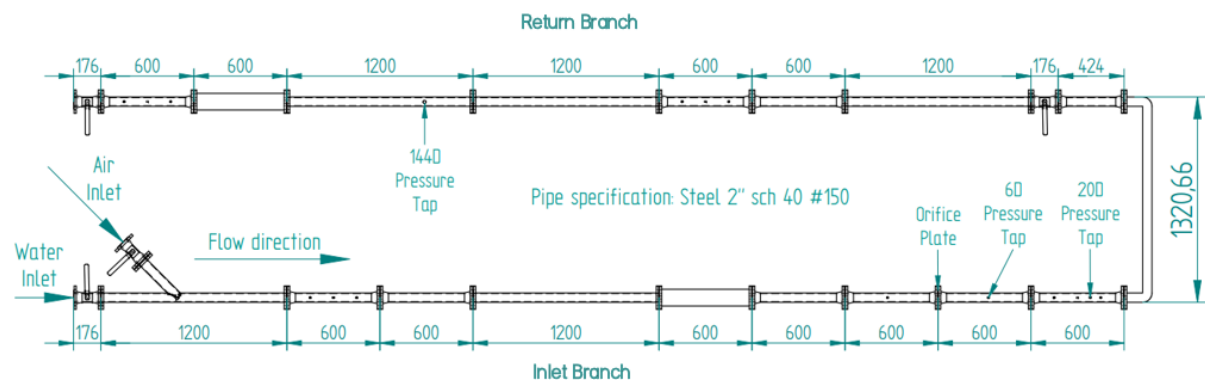


Figure 25 - Actual test loop section configuration (dimensions in millimeter) (Source: author)



Figure 26 - Test loop section photography (Source: author)

3.5.1 Orifice plate wet gas measurement test section

This section, located in the end of inlet branch, is composed by two 600 mm spools with an additional 6D ½" BSP pressure tap, measured from the orifice plate flange (flange taps). The orifice plate is fixed in-between the spools flanges, each equipped with a 25,4 mm flange pressure tap., resulting in an installation with 93D upstream and 26D downstream straight pipe length. Additionally, two extra pressure taps are provided along the test loop to enable supplementary 3rd pressure tap configurations, one located 20D and other 144D from the orifice plate downstream face as seen in Figure 25 and Figure 27. Moreover, two borosilicate translucent pipe sections are mounted to visually inspect the flow pattern behavior.

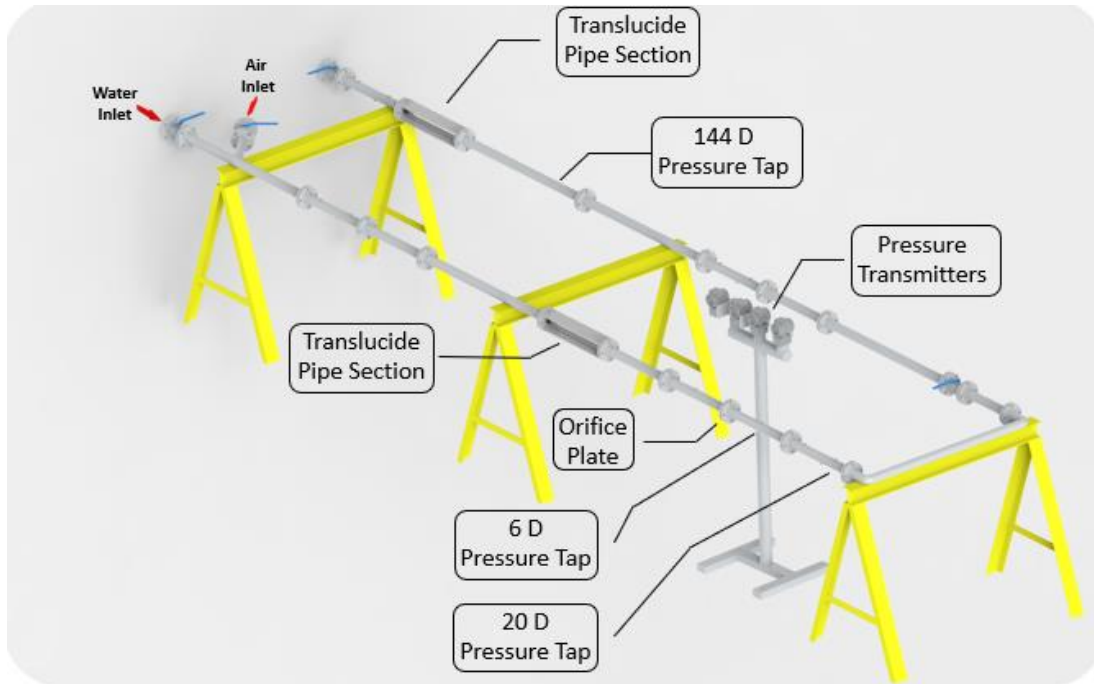


Figure 27 - Fitting details of loop section, in perspective (Source: author)

Figure 28 exhibits the pressure transmitters taps primary configuration and Table 7 exposes the transmitters specifications. In addition, to complete the wet gas flow meter sensors, a low perturbation temperature transmitter (appendix C) is installed 14D downstream of the orifice plate. Further tests will change the Figure 28 6D 3rd tap for the 20D and 144D configuration, with more details in section 4.5.

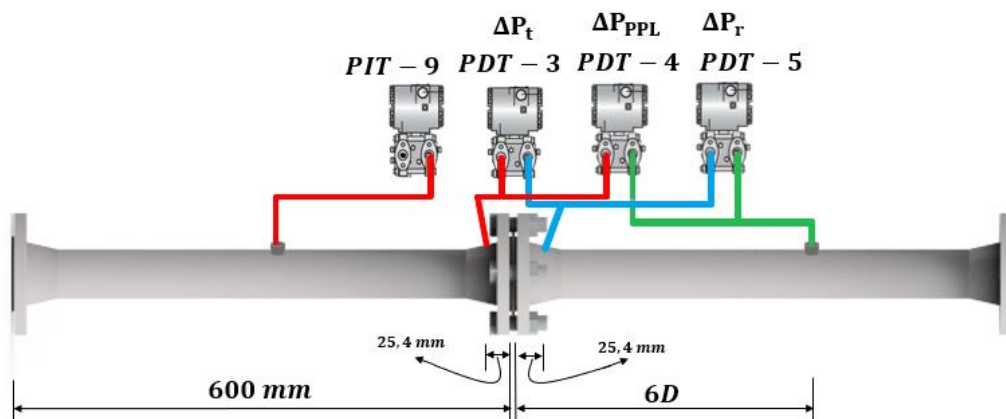


Figure 28 - Wet gas measurement pressure taps by ISO TR 12748 (2015) (Source: author)

Table 7 - Wet gas measurement pressure transmitters specification

	Identifier TAG			
	PIT-9	PDT-3	PDT-4	PDT-5
Manufacturer	Smar			
Code	LD301- M41I- TU11-011	LD301- D31I- TU11-011	LD301- D21I- TU11-011	LD301- D21I- TU11-011
Application	Manometric	Differential	Differential	Differential
Lower Range Limit (kPa)	-100	-250	-50	-50
Upper Range Limit (kPa)	2500	250	50	50
Sensor type	Capacitive			
Diaphragm	316L Stainless Steel			
Lower Range Calibration (kPa)	0	0	0	0
Upper Range Calibration (kPa)	1000	68.5	49.4	24.5
Calibration certificate	Appendix B			

4 EXPERIMENTAL PROCEDURES, RESULTS AND DISCUSSIONS

4.1 NEMOG'S WET GAS FLOW TEST ENVELOPE

The previous chapter exposes multiphase flow circuit equipment's ranges and with this mapping it could establish the actual configuration wet gas parameters limits for NEMOG's circuit. It is important to call attention to the air mass flow rate maximum values exposed in Table 4, which considers a back pressure of 5 barg at the test loop. So as the pressure at the test loop increases towards the 8.62 barg compressor maximum pressure, the maximum air mass flow rate decreases. Therefore, it is decided to limit tests campaign at 5 barg pressure, starting at 1 barg in addition with a 3 barg level. That said, along with water circulation pump (Table 3) and single-phase measurements capacities (Table 5 and Table 6), Table 8 exhibit the Lockhart-Martinelli and GVF limits, as the main wet gas parameters, considering three different pressure levels and a mean air mass flow rate of 360 kg/h.

Table 8 - Lockhart-Martinelli and GVF ranges for NEMOG's actual configuration

Pressure (barg)	Water mass flow rate (kg/h)					
	645 ¹		945		1286	
	X_{LM}	GVF ²	X_{LM}	GVF ²	X_{LM}	GVF ²
1	0.087	99.58%	0.128	99.38%	0.174	99.16%
3	0.123	99.16%	0.180	98.78%	0.245	98.35%
5	0.150	98.75%	0.220	98.18%	0.300	97.54%

1 - Represents the minimum measurement capability of water mass flow rate by Coriolis meter

2 - Conversion as Equation 45

Analyzing Table 8 together with the forementioned pressure limitations towards the air flow, it is possible to notice that the lower limitation for Lockhart-Martinelli parameter relies on the minimal measurable water flow rate by the Coriolis meter. Thus, to establish equal levels of gas wetness for test points, it's decided to use three X_{LM} points at 5 barg row as base values, to cover the maximum wet gas flow range considered in literature, as mentioned in section 2.3.1. To summarize, the experimental envelope for the wet gas experiments is $\dot{m}_{air} = 360$ kg/h mean air mass flow rate as a fixed

value, pressures line set at 1,3 and 5 barg and Lockhart-Martinelli ranging at $X_{LM} = 0.15, 0.22$ and 0.30 .

Another important variable to determine is the beta ratios for orifice plates to be tested. The experiments aim to be validated with the Steven et al. (2011) work, where they present a relevant relation between pressure loss ratio and Lockhart-Martinelli only for $\beta = 0.5$ or higher. Along this, an orifice plate with $\beta = 0.5$ and $\beta = 0.68$ are manufactured.

4.2 DATA ACQUISITION AND TREATMENT METHODOLOGY

The multiphase flow loop supervisory and control system is developed in the National Instruments LabVIEW platform, where the process variables are received by a 4 - 20 mA protocol for the pressure and temperature transmitters and by Modbus for the control valves, Coriolis metres, variable-frequency driver and other secondary equipment. Those variables are converted, according to the range set on the transmitter, to the respective unit selected by the user, processed on the supervisory program to result in mass flow rates (for air flow) and then recorded in a log sheet, in an approximately 0,2 second cycle period (frequency = 5Hz). Figure 29 shows the multiphase flow loop supervisory main page where the single-phase parameters are monitored and Figure 30 the wet gas parameters page view, where the main parameters involved in a wet gas flow are monitored.

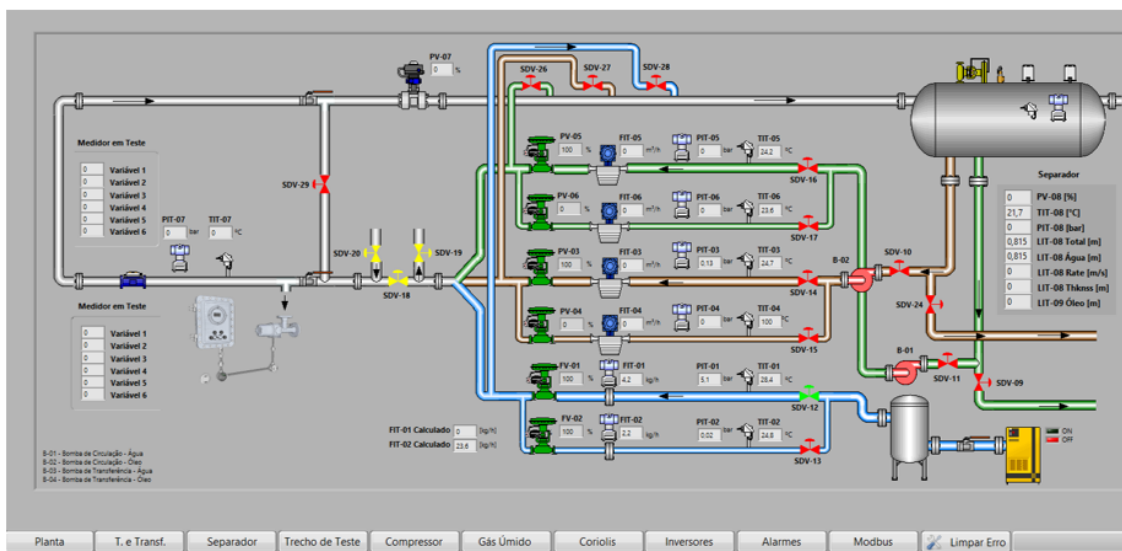


Figure 29 - National Instruments LabVIEW multiphase flow loop supervisory system main page (Source: author)

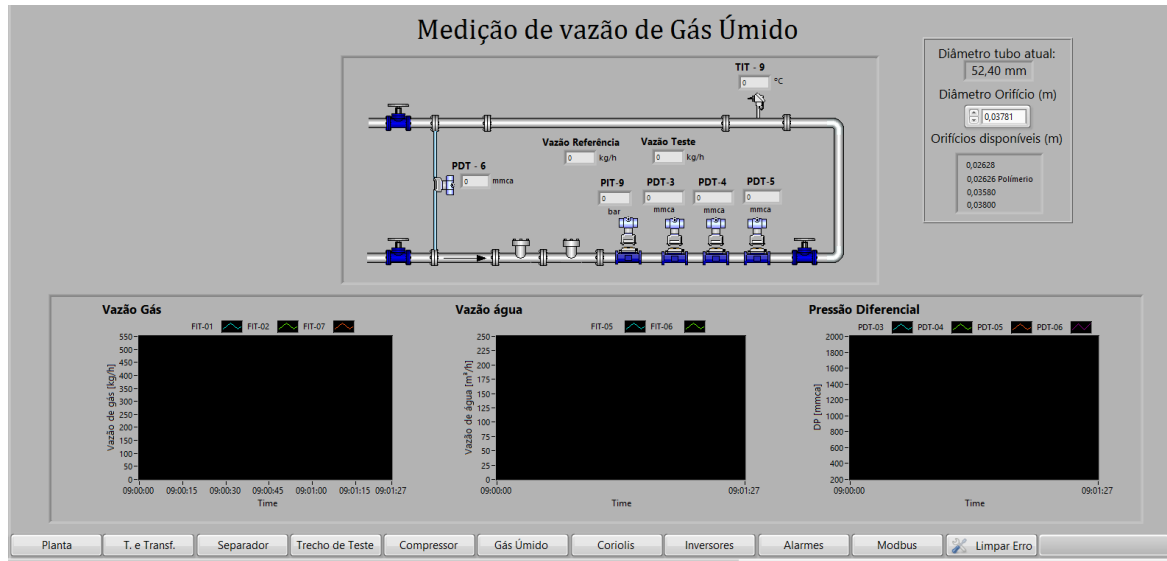


Figure 30 - National Instruments LabVIEW wet gas flow parameters supervisory page (Source: author)

An important task regarding the pressure transmitters is related to the water draining from the pressure tapping tubes before each test battery. The presence of liquid in those tubes interfere in pressure measurement procedure, resulting in invalid data.

4.2.1 Post processing

The data post processing procedure is an important part of the experimental research, owing to statistically extract the significant data intervals and eliminate noises and outliers.

So, in this work, after the ending of an experimental campaign, the log is saved and post processed using all primary variables, such as pressure and temperature to double check the air mass flow rates results, as calculated by the supervisory system, for both the single-phase meter, located at the single-phase flow measurement section, and the test meter, located at the test loop section. This task is performed using a Mathworks Matlab® algorithm performing the ISO 5167-2 (2003) recommendations, in addition with the uncertainty evaluation of each property, as explained in the next subsection. Further, data is transferred for a Microsoft Excel® sheet, where the statistical analysis is developed. Due to different procedures used in each experimental step, the further individual methodology executed is explained on respective chapter.

4.2.2 Uncertainty evaluation

The uncertainty evaluation of each experimental measured variable follows the JCGM (2008) in addition with ISO 5167-2 (2003) considerations for air mass flow rate uncertainty.

JCGM (2008) exposes that an uncertainty reporting is extremely important in experimental works, making possible the comparison between previously and future works, being a reliable source of data. The experimental standard uncertainty is a result of several components contributions, which can be grouped into two main categories: A and B. The first one is based on statistical evaluation of the estimated standard deviation (s_i) and the degree of freedom (ν_i) of the measurement, calculated by equation 73 where N is the number of experimental data points. The latter is defined by other means, like calibration certificates and other methods, calculated by equation 74 where U_i is the expanded uncertainty and K is the coverage factor.

$$u_i^A = \frac{s_i}{\sqrt{N}} \quad (73)$$

$$u_i^B = \frac{U_i}{K} \quad (74)$$

Although some measured variables, such as water mass flow rate and pressure, there is a type B standard uncertainty available via calibration certificate, a type A standard uncertainty estimation is performed to each flow property cited in this dissertation, which is then associated to type B, as the equation 75, avoiding misleading uncertainty estimation.

$$u_{i,comp} = \sqrt{u_i^A + u_i^B} \quad (75)$$

4.2.2.1 Combined standard uncertainty (u_C)

After determining all the individual flow properties standard uncertainty, is necessary to combine them to propagate the uncertainty through the used equations, appraising the final properties standard uncertainty. To implement it, JCGM (2008) recommends equation 76 for independent quantities, where $\frac{\partial G}{\partial y_i}$ is the sensitivity coefficient of each involved variable and $u_{i,comp}$ is the respective compounded standard uncertainty.

$$u_C(y_i) = \sqrt{\sum_{i=1}^z \left(\frac{\partial G}{\partial y_i}\right)^2 u_{i,comp}^2} \quad (76)$$

For the air mass flow rate ISO 5167-2 (2003) gives a practical working formula for the relative combined standard uncertainty, given by equation 77. Additionally, ISO 5167-2 (2003) provides the discharge coefficient and expansion factor relative standard uncertainty. The pipe internal diameter (D) and the orifice diameters (d) is carried by equation 73 with eight measures procedure using a 0,002 mm caliper, resulting in a equal 0,005 standard uncertainty for the pipe and the orifices diameters. Further the differential pressure (ΔP) uncertainty is managed by equation 75 using the Excel sheet statistical results for type A standard uncertainty and the calibration certificate mentioned in section 3.5.1 for type B standard uncertainty. Moreover, the air density (ρ_g) uncertainty is obtained by equation 76, considering perfect gas equation 47, (gas constant R_g uncertainty is considered negligible here).

$$\frac{u_C(q_m)}{q_m} = \sqrt{\left(\frac{u(Cd)}{Cd}\right)^2 + \left(\frac{u(\varepsilon)}{\varepsilon}\right)^2 + \left(\frac{2\beta^4}{1-\beta^4}\right)^2 \left(\frac{u(D)}{D}\right)^2 + \left(\frac{2}{1-\beta^4}\right)^2 \left(\frac{u(d)}{d}\right)^2 + \frac{1}{4}\left(\frac{u(\Delta p)}{\Delta p}\right)^2 + \frac{1}{4}\left(\frac{u(\rho_g)}{\rho_g}\right)^2} \quad (77)$$

Finally, for the other wet gas parameters mentioned in section 2.3.3 the combined uncertainty is performed as equation 76.

4.2.2.2 Expanded uncertainty (U_i)

To express the expanded uncertainty, given by equation 78, a function of combined standard uncertainty (u_c), obtained as aforementioned, and a coverage factor (K), to statistically ensure a confidence level for the property measurement. JCGM (2008) describe the methodology to evaluate the coverage factor based on the measurement's probabilistic distribution and degree of freedom. However, it gives a practical way to determine this coverage factor assuming a data normal distribution and using Table 9. Figure 31 shows four properties distribution histograms, where false prediction flow is the mass flow rate measured by the test section orifice plate wet gas meter and PDT-3, PDT-4 and PDT-5 are the respective pressure differential transmitters. It could be seen that the histograms adequately meet the requirements for a normal distribution, enabling the use of Table 9 coverage factors. For this research is adopted a 95% confidence level with a 1.960 coverage factor.

$$U_i = K u_c(y_i) \quad (78)$$

Table 9 - Normal distribution level of confidence and coverage factors (Source: JCGM (2008))

Level of confidence (%)	Coverage factor (K)
68.27	1
90	1.645
95	1.960
95.45	2
99	2.576
99.73	3

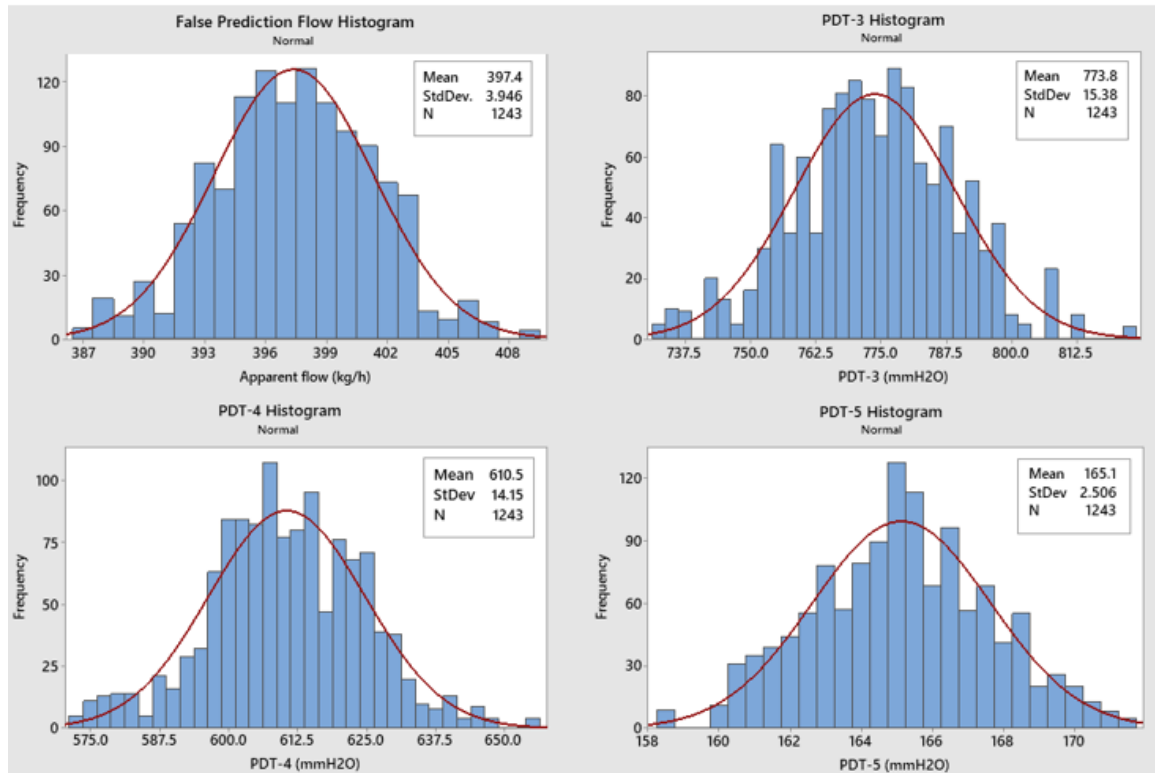


Figure 31 - False prediction flow, PDT-3, PDT-4 and PDT-5 histograms illustration (Source: author)

4.3 DRY AIR FLOW MEASUREMENT COMMISSIONING

In order to commissioning the single-phase air flow measurement ISO 5167-2 (2003) requirements may be checked for installations criteria to validate both section III single-phase flow measurement and teste section measurement. The ISO 5167-2 (2003) main criteria are:

- Pressure taps:
 - Flange taps:
 - Upstream tap distance: $25,4 \pm 1 \text{ mm}$
 - Downstream tap distance: $25,4 \pm 1 \text{ mm}$
 - Corner taps:
 - Upstream tap distance: 1 to 10 mm
 - Downstream tap distance: 1 to 10 mm

- Limits of use
 - $d \geq 12.5 \text{ mm}$
 - $50 \leq D \leq 1000 \text{ mm}$
 - $0.1 \leq \beta \leq 0.75$
 - $Re_D \geq 5000$
 - $P_2/P_1 \geq 0.75$

- Installation requirements
 - Upstream straight pipe length from a full-bore valve fully open for a $0,5\beta$ orifice plate: 12 D (for the single-phase measurement installation)
 - Upstream straight pipe length from a single 45° bend (air inlet on the mixer) to orifice plate, considering zero additional uncertainty on the discharge coefficient: 44 D (for the test section measurement installation)
 - Downstream straight pipe length: 8 D

Table 10 summarize the ISO 5167-2 (2003) points followed by section III single-phase meter and teste section meter information, where it can be concluded that all above-mentioned criteria are met.

After the installations requirements analyses, an air flow measurement test is performed to compare the two meters measurement results, consisting of different control valve opening to observe the system response.

Table 10 - The single-phase and test section meters parameters in accordance to ISO 5167-2 (2003)

	ISO 5167-2 (2003)	Single-phase Meter	Test Section Meter
Tap type	Flange	Flange	Flange
Upstream/Downstream tap distance	25,4 ± 1 mm	26/26 mm	25,4/25,4 mm
Pipe diameter	50 to 1000 mm	50.10 mm	52.40 mm
Orifice diameters	$d \geq 12.5\text{mm}$	25.02 mm	26.28 and 35.80 mm
Beta ratios	0.1 to 0.75	0.4994	0.5015 and 0.6833
Upstream straight length	12 D/ 44D	22 D	93 D
Downstream straight length	8 D	8 D	26 D
Reynolds Number	≥ 5000	8543	7398
Pressure ratio (P_2/P_1)	≥ 0.75	0.98	0.79

Figure 32 shows the results revealing an average 10% shift between the two meters. Another important realization is the compressor maximum supply capacity evidenced if control valve is 50% opened and the air mass flow rate could not be kept constant, dropping to 360 kg/h. It becomes clearly to valve 60% opening level. In this case, the flow rate curve slope decreases fast, as a consequence of vessel's pressure drop. The last part of the graphic (t=420s) shows a pressure recovery, due to return of compressor operation.

This bias recognition led to a deep investigation, aiming to reduce or eliminate this difference. The pressure transmitters were rechecked, the signal treatment by the supervisory system was checked, a leaking search was done, a compressible flow analysis was accomplished and finally a parallel configuration test was performed, where the test section meter was installed on the single-phase measurement orifice plate, in parallel with the reference meter, resulting in accordingly measurements.

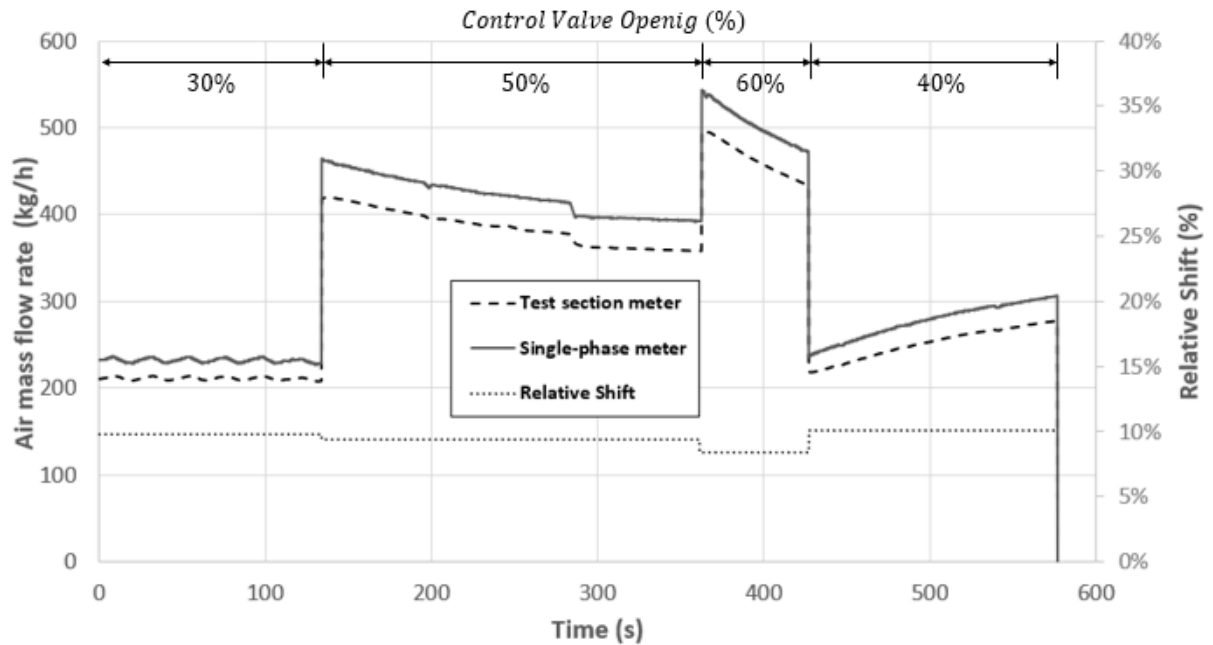


Figure 32 - First dry air mass flow rate measurement comparison between reference single-phase meter and test section meter (Source: author)

In sequence, a water measurement comparison was executed, using the calibrated low-rate Coriolis meter as reference to the test section orifice meter. Table 11 brings the results, in which each water mass flow rate is an average value of 2-minute data acquisition. Both meters were considered in accordance, since the expanded uncertainty for the metering section reach approximately 1.5% and the maximum shift was 2.29%, resulting in a 0.79% effective shift. Hence, the test section orifice meter was considered reliable.

Table 11 - Water mass flow rate measurement comparison between Coriolis meter and test section meter (Source: author)

Test Section Meter (kg/h)	Expanded Uncertainty (\pm kg/h) ¹	Coriolis Meter (kg/h)	Expanded Uncertainty (\pm kg/h) ¹	Relative Shift
1544.34	23.17	1580.52	7.90	-2.29%
3124.93	46.87	3184.08	15.92	-1.86%
5095.99	76.44	5190.34	25.95	-1.82%

¹ - Based on section 4.2.2.2

To characterize and adjust the deviation observed between the single-phase meter and the test section meter for dry air flow, extensive readings were executed, in order to verify the repetitive behavior of the meter. Each one was composed by a 5-minute steady state air flow (considered as a variability lower than 0.5%) data acquisition after a 2-minute flow stabilization. Table 12 presents the behavior of this experimental campaign, where each experimental point is 5-minute mean value. It is important to clarify that these points were gathered in different days, which explains the different values of maximum air single-phase measurement, due to different environmental conditions leading to distinct compressor volumetric efficiency.

Figure 33 exhibit the Table 12 data and the uncertainty bars, indicating that the difference between the two meters is a systematic error, which could be corrected by a factor computed from the average deviation value. So, for further analysis, in each experimental campaign, a previous data acquisition in dry air flow is performed, which the test section meter is considered the base value and the single-phase meter is corrected by the day-shift value. After this procedure the main experimental analysis is executed.

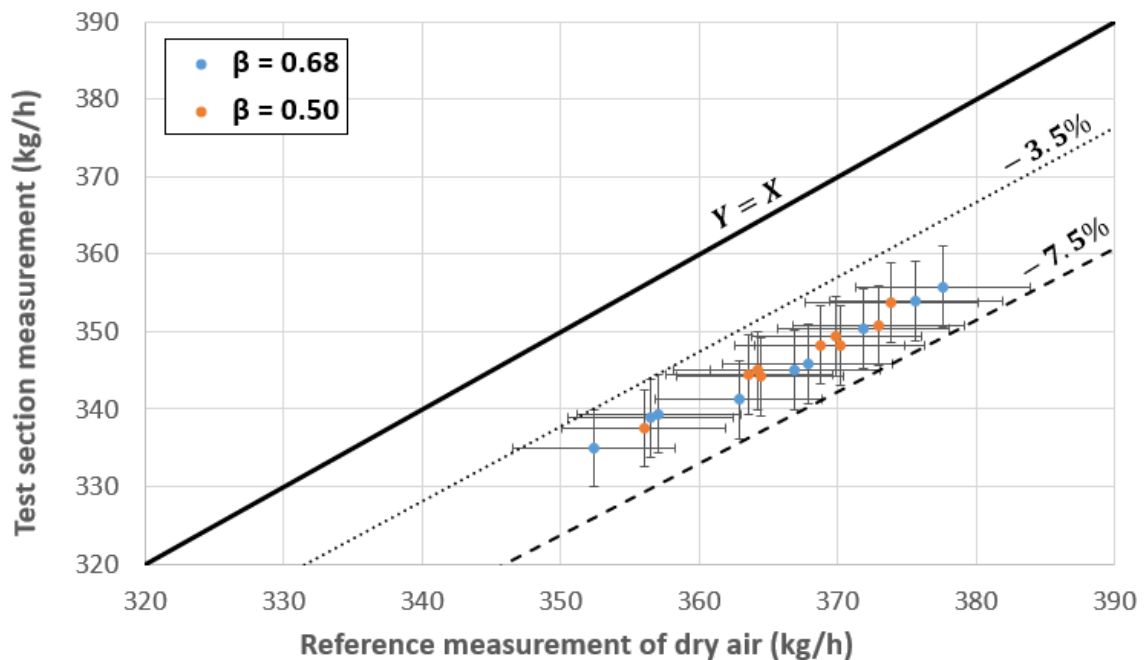


Figure 33 - Single-Phase Meter and the Test Section Meter shift mapping with uncertainty bands (Source: author)

Table 12 - Single-Phase Meter and the Test Section Meter shift mapping

Beta	Pressure (barg)	Air single-phase measurement (kg/h)	Expanded Uncertainty (\pm kg/h) ¹	Air test section measurement (kg/h)	Expanded Uncertainty (\pm kg/h) ¹	Shift
0.68	1.08	357.09	5.93	339.39	4.99	4.95%
	3.04	356.50	5.92	338.84	4.98	4.95%
	5.11	352.39	5.85	334.93	4.92	4.95%
	1.10	367.84	6.11	345.86	5.08	5.98%
	3.00	366.95	6.09	345.02	5.07	5.98%
	5.05	362.89	6.02	341.21	5.02	5.98%
	1.12	377.61	6.27	355.79	5.23	5.78%
	3.10	375.65	6.24	353.94	5.20	5.78%
	5.07	371.84	6.17	350.34	5.15	5.78%
0.50	1.10	373.91	6.21	353.74	5.20	5.39%
	3.01	363.61	6.04	344.44	5.06	5.27%
	4.97	356.03	5.91	337.53	4.96	5.20%
	1.06	369.92	6.14	349.39	5.14	5.55%
	3.02	368.75	6.12	348.29	5.12	5.55%
	5.00	364.43	6.05	344.21	5.06	5.55%
	1.09	372.93	6.19	350.85	5.16	5.92%
	3.06	370.19	6.15	348.27	5.12	5.92%

1 - As described in section 4.2.2.2

4.4 EVALUATION OF THE ISO 5167-2 (2003) PRESSURE LOSS RATIO FOR DRY FLOW AND A NEW DATA FIT PROPOSAL

As reported by Steven, Shugart and Kutty (2018) the ISO 5167-2 (2003), represented in equation 70, present some shift from the experimental data, unfortunately they did not report a new data fit. Further, the use of ISO's correlation with a flange upstream tap, is a non-conforming way as mentioned in section 2.3.6. With these in mind, the need to develop a new data fit for the PLR_{dry} suitable for the NEMOG's installation becomes a relevant task.

To accomplish this task, the test meter configuration, exposed in Figure 34, was used, with a 6D third pressure tap. The experimental procedure implies on measure the dry

air flow through the test section meter combining pressure set up of 1, 3 and 5 barg, 150, 225 and 350 kg/h air flow rate with 0.5β and 0.68β orifice plates, totalizing 18 experimental points. For each point a 5-minute data acquisition after a 2-minute flow stabilization procedure is executed, resulting in approximately 1,500 data lectures for each experimental point. With all data gathered, the mean value and the standard deviation are calculated to estimate the expanded uncertainty for the pressure loss ratio, using section 4.2.2 procedure. The expanded uncertainty is 0.73%, (95% confidence level).

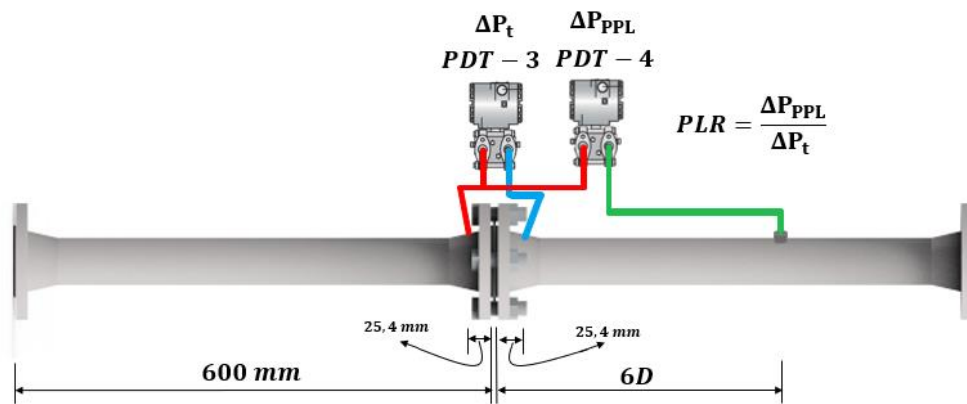


Figure 34 - PLR dry test configuration (Source: author)

Figure 35 and Figure 36 obtained data from the experimental procedure aforementioned. The black triangles represent the comparison between ISO correlation and experimental data for different betas and discharge coefficients values. The major bias occurs for 0.68β (see Figure 35) with an average 1.5% shift. However, in 0.50β (see Figure 36) this bias reduces to 0.5% averaged, which is lower than the experimental expanded uncertainty, glimpsing an statistical agreement among it. This behavior could be explained by Steven et al. (2011) and Steven, Shugart and Kutty (2018) observations, where the PLR_{dry} is governed by the traditional differential pressure (caused by the orifice restriction) for orifice plates with beta lower than 0.55, i.e. the permanent pressure loss (PPL) is almost equal to the traditional differential pressure, resulting in a more predictable phenomenon by the ISO correlation. Moreover, looking to in 0.50β data fit, at Figure 36, it can be seen that there are no statistically significant reductions on the deviation. In other hand, for 0.68β , the new

adjusted curve, written in equation 79, resulted in up to 1% of deviation reduction, indicating a better performance for the PLR_{dry} estimation.

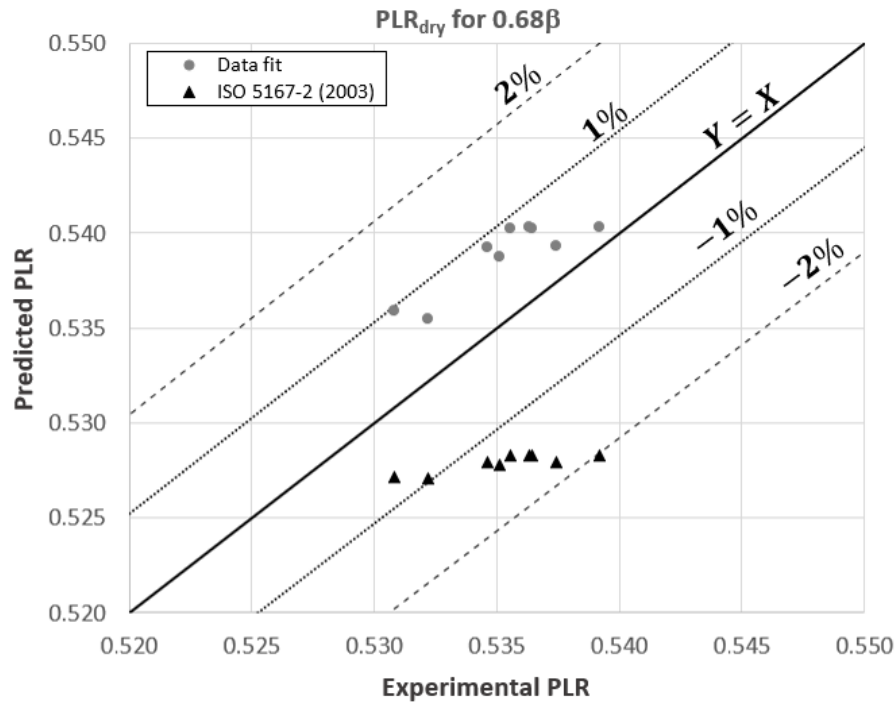


Figure 35 - ISO 5167-2 (2003)'s PLR_{dry} and the new data fit for a 0.68β orifice plate.

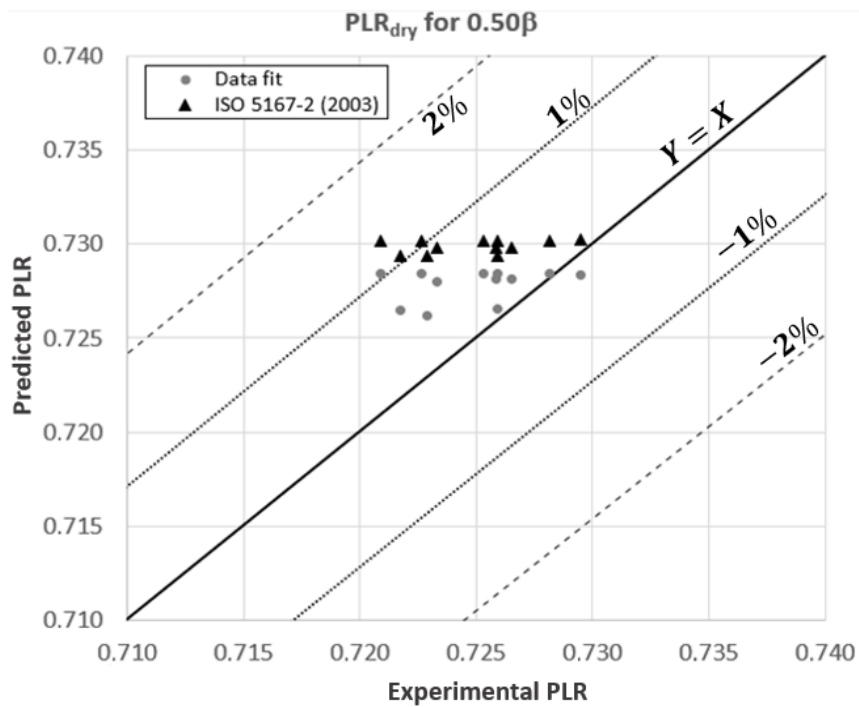


Figure 36 - ISO 5167-2 (2003)'s PLR_{dry} and the new data fit for a 0.50β orifice plate.

The adjusted curve, represented by equation 79, was developed using Minitab®'s multiple linear regression function, based on least squares and ANOVA methods, resulting in Table 13. It shows that, the relevant parameters to the metering problem be analyzing are: β , C_d and the βC_d and $C_d C_d$ interactions, all based on the statistical hypothesis test probabilities, exposed in last column, for a 5% significance level. The resultant R-squared was 98.86%.

Is important to highlight that all data used to verify the correlation and exposed in Figure 35 and Figure 36, was an additional data, which were not used to estimate the fitted equation. However, it is important to note that such data fit could not be extrapolated for other installations without further tests.

$$PLR_{dry,fit} = -185.08 - 23.45\beta + 631.7C_d + 36.70\beta C_d - 534.9C_d^2 \quad (79)$$

Table 13 - Multiple linear regression coefficients ANOVA for the $PLR_{dry,fit}$ data fit

Source	DoF	Adj SS	Adj MS	F-Value	P-Value ¹
Regression	4	558.773	139.693	10774167.43	0.000
β	1	0.004	0.004	295.70	0.000
C_d	1	0.005	0.005	388.27	0.000
$\beta \times C_d$	1	0.004	0.004	271.38	0.000
C_d^2	1	0.005	0.005	385.09	0.000
Error	62390	0.809	0.000		
Total	62394	559.582			

1 - Considering a 5% significance level to assess the null hypothesis

4.5 WET GAS FLOW TESTS

As discussed in section 2.3.1, wet gas could be considered as a flow with a maximum Lockhart-Martinelli parameter of 0.3 or equally a minimal GVF value of 95%. Ranging in those limits and on NEMOG's wet gas flow envelope mentioned in section 4.1, a test matrix was elaborated to evaluate:

- i) Orifice plate over-reading correction correlations,
- ii) ISO TR 11583 (2012) PLR to X_{LM} correlation performance for different third tap configurations, as illustrated in Figure 37 and

- iii) Correct third tap pressure shift by Petalas and Aziz (1998) pressure drop model, comparing to traditional 6D downstream pressure tap.

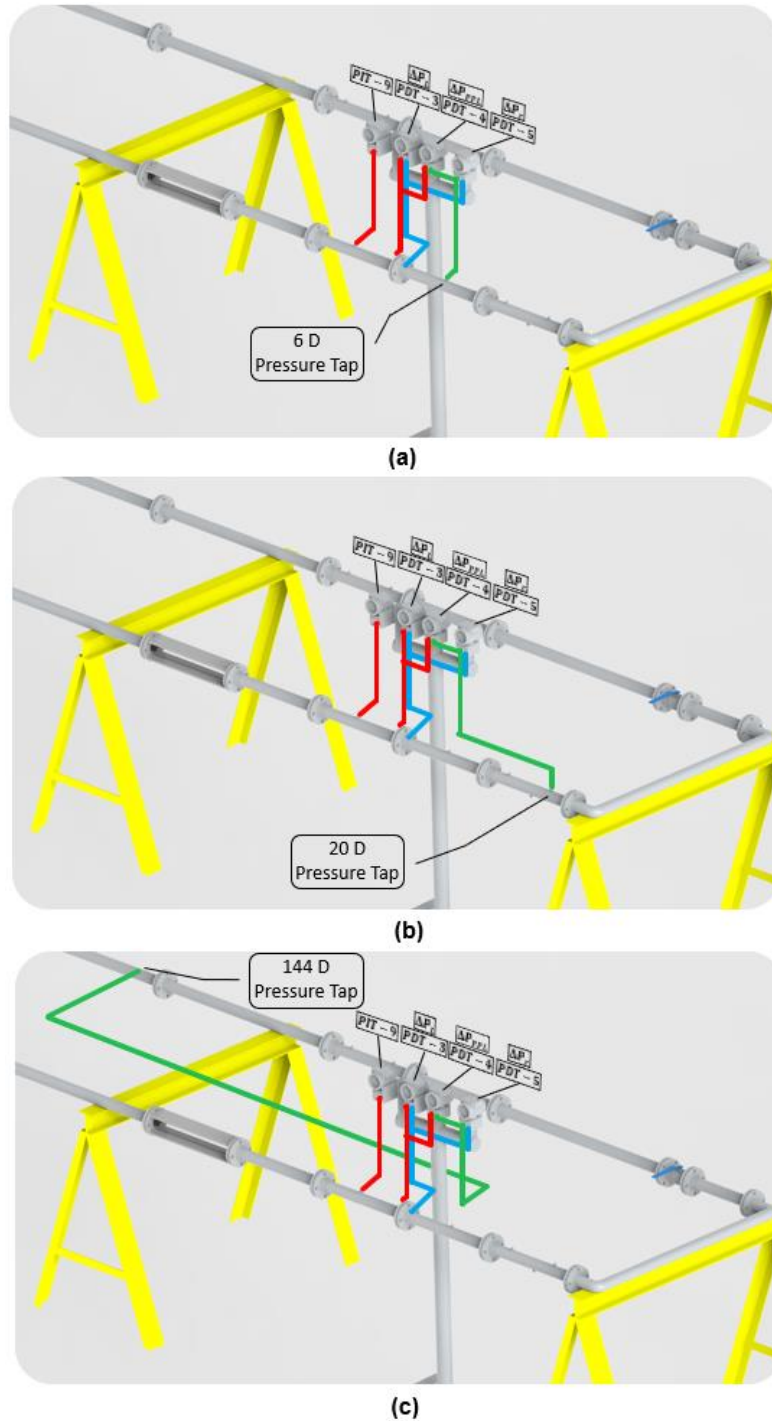


Figure 37 - Different configurations for the third downstream pressure tap: (a) 6D, (b) 20D and (c) 144D (Source: author)

Table 14 exhibit the experimental points accomplished, totalizing 54 experimental set ups.

Table 14 - Wet gas flow test matrix

3 rd pressure tap distance	β	Line pressure (barg)	Lockhart-Martinelli levels
6D	0.50	1	0.15
6D	0.50	1	0.22
6D	0.50	1	0.30
6D	0.50	3	0.15
6D	0.50	3	0.22
6D	0.50	3	0.30
6D	0.50	5	0.15
6D	0.50	5	0.22
6D	0.50	5	0.30
6D	0.68	1	0.15
6D	0.68	1	0.22
6D	0.68	1	0.30
6D	0.68	3	0.15
6D	0.68	3	0.22
6D	0.68	3	0.30
6D	0.68	5	0.15
6D	0.68	5	0.22
6D	0.68	5	0.30
20D	0.50	1	0.15
20D	0.50	1	0.22
20D	0.50	1	0.30
20D	0.50	3	0.15
20D	0.50	3	0.22
20D	0.50	3	0.30
20D	0.50	5	0.15
20D	0.50	5	0.22
20D	0.50	5	0.30
20D	0.68	1	0.15
20D	0.68	1	0.22
20D	0.68	1	0.30
20D	0.68	3	0.15
20D	0.68	3	0.22
20D	0.68	3	0.30
20D	0.68	5	0.15
20D	0.68	5	0.22
20D	0.68	5	0.30
144D	0.50	1	0.15
144D	0.50	1	0.22

(continued on the next page)

Table 14 – (continued)

3 rd pressure tap distance	β	Line pressure (barg)	Lockhart-Martinelli levels
144D	0.50	1	0.30
144D	0.50	3	0.15
144D	0.50	3	0.22
144D	0.50	3	0.30
144D	0.50	5	0.15
144D	0.50	5	0.22
144D	0.50	5	0.30
144D	0.68	1	0.15
144D	0.68	1	0.22
144D	0.68	1	0.30
144D	0.68	3	0.15
144D	0.68	3	0.22
144D	0.68	3	0.30
144D	0.68	5	0.15
144D	0.68	5	0.22
144D	0.68	5	0.30

The experimental procedure consists in:

- a. set up the 3rd pressure tap and the orifice plate configuration, for example 6D and 0.50β
- b. then run a dry air flow measurement for at least 5 minutes to estimate the actual shift between the single-phase measurement and the test section measurement for late corrections as described in section 4.3.
- c. After estimating the current maximum corrected dry air mass flow rate, the required water mass flow rates for each X_{LM} level, in each line pressure, were calculated. This water flow rate is controlled on the supervisory system by the water pump rotation in an open loop control.
- d. The line pressure is maintained and controlled by the separator vessel pressure, regulated by the gas outlet valve.
- e. For each experimental set up, i.e. 3rd tap, beta, line pressure and X_{LM} combination, a 7-minute steady state (considered as less than 1% of variability

on the test section meter) data acquisition is performed, totalizing an average 2000 valid data points.

- f. So, after performing line pressures and X_{LM} combinations, the experimental campaign is concluded, saving all data for postprocessing and
- g. Then restarting all over again, for a different third tap and orifice plate combination.

Figure 38 brings a raw data from the supervisory log, exemplifying the foregoing procedure. The first 300 seconds represents the single-phase and test section measurement comparison in dry air flow, which a bias can be seen (as described in section 4.3). Forwards, the water control valve is opened allowing mixing with air flow and forming wet gas flow at the test section. Here, the over-reading effect occurs, evidenced a higher false prediction gas mass flow rate, measured by the test section meter.

It should be noted that dry air flow rate keeps stable and unchanged, although the flow reading changes, due to the presence of liquid in the flow.

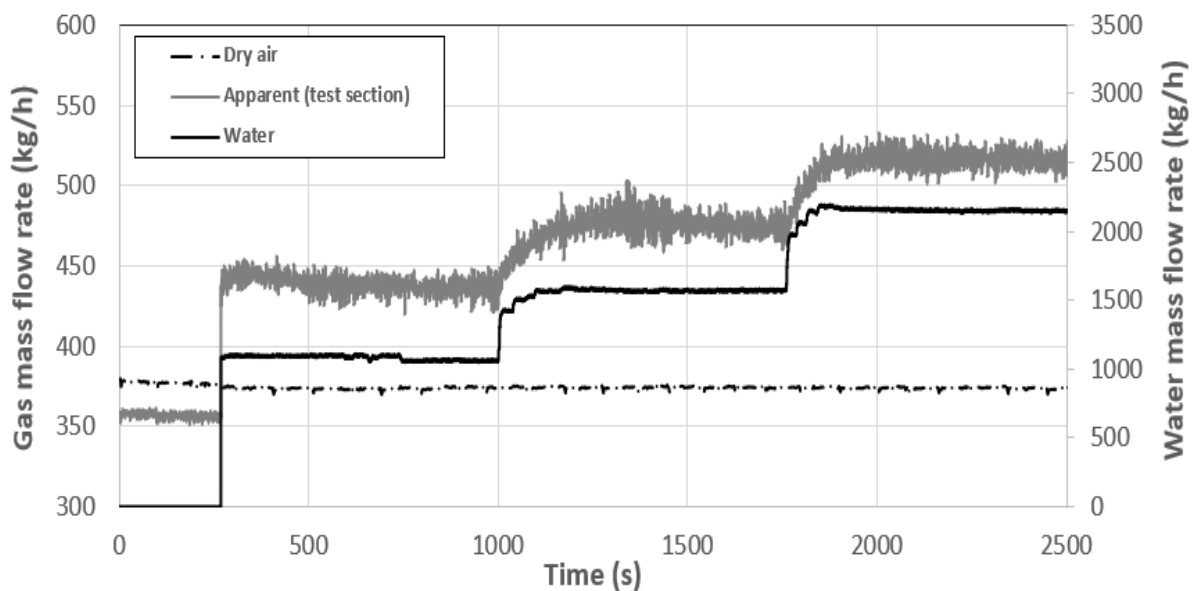


Figure 38 - Raw data from a 0.50β , 1 barg and 6D 3rd tap test (Source: author)

4.5.1 Analysis of the main orifice plate over-reading correction correlations available in literature.

The over-reading correction correlations development encompassing different primary devices such as orifice plates, Venturis and inverted cones. In equation 53, by Murdock (1962), equation 54 (Chisholm, 1977) and the most recent orifice plate correlation by Steven et al. (2011), in equation 66, were evaluated considering the NEMOG's multiphase circuit running air-water flow.

The first step is to check the validity of the single-phase flow measurement correction, comparing its effects on the over-reading estimation.

Figure 39 brings the mentioned original correlations plots, represented in lines, joint to the NEMOG's wet gas flow data in addition with Murdock, Emerson NEL and CEESI real experimental data points, gathered in Murdock (1962) and Steven, Shugart and Kutty (2018). It is important to emphasize that the Chisholm's (1977) and Steven et al.'s (2011) equations are pressure dependents, thus, to plot them on the mentioned figures, it is set up 4.5 barg average line pressure, in view of the 1 to 5 barg pressure range. This is proceeded only for viewing comparison purposes, between uncorrected and corrected data.

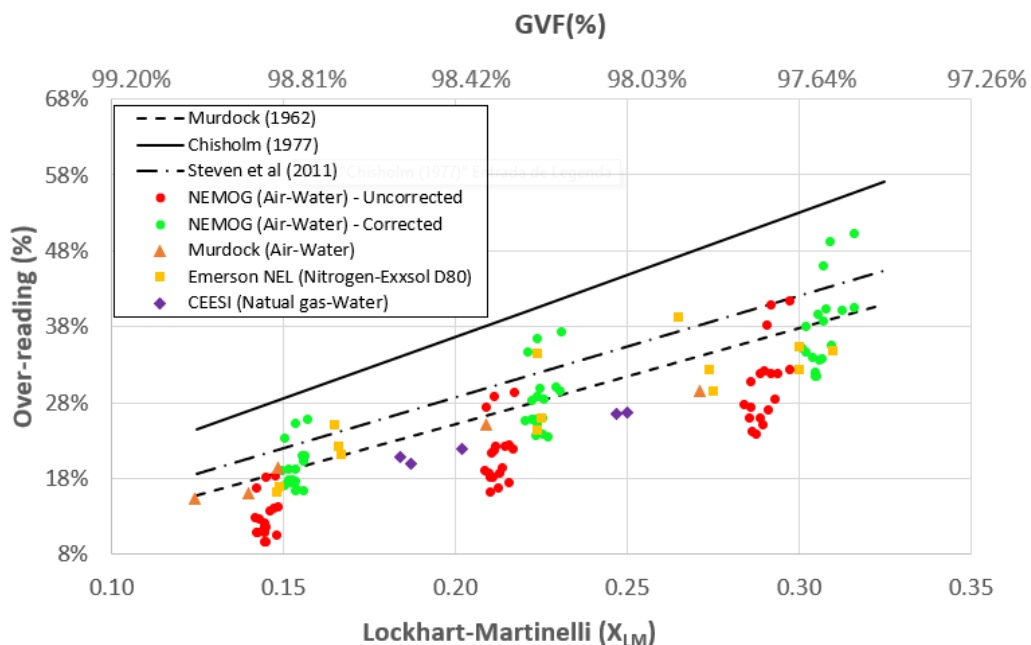


Figure 39 - NEMOG's experimental over-reading estimation based on the single-phase air flow measurement with and without the systematic shift correction (OR and X_{LM} relative expanded uncertainties are 2.24% and 1.84% respectively) (Source: author)

In Figure 39 the red dots represent the over-reading and Lockhart-Martinelli estimation, for NEMOG's data based on the single-phase air mass flow rate without corrections, resulting in a lower OR and X_{LM} values for each experimental point, a consequence of higher air mass flow rate. It shows a poor concordance between NEMOG's data, correlations and literature data, with an underestimation up to 10% for the over-reading value, showing that the use of uncorrected single-phase air mass flow rate leads to uncorrected data.

In other hand, the green dots represent the wet gas points based on the corrected single-phase air mass flow rate, exhibiting a better approximation with the literature correlations and experimental points, mainly with Murdock's and Emerson's data, reinforcing that air flow correction is valid. In addition, this figure brings some additional observations about the OR equations behavior, where X_{LM} relation can be seen as linear. Other important aspect is that many experimental points, including the literature ones, are below the curves, indicating some overestimation by them.

To better understand this behavior, Figure 40, Figure 41 and Figure 42 show the behavior of NEMOG's 1, 3 and 5 barg line pressure points respectively, in which each correlation is calculated with the corresponding pressure. Thus, it becomes evident that pressure plays an important role in the over reading effect, decreasing it as the pressure increases. Furthermore, Murdock's (1962) and Steven et al.'s (2011) presents significative concordance to experimental data for 0.50β and 0.68β respectively, running at 1 and 3 barg. Nonetheless for 5 barg this matchup fails. It could be explained by the gas Froude number limitation for Steven et al.'s work, which uses $Fr_g = 1.5$ as lower value limit in contrast with a $Fr_g \leq 1.29$ value reached in NEMOG's facility at a nominal 1 barg. This extrapolation explains the reason to raising pressure increases the discordance between data and correlation, i.e. as pressure rises, the Froude number decreases (for other parameters held constant) reaching 0.90 at 3 barg and 0.74 at 5 barg, falling far short of the correlation limit, resulting in a OR lower than the predicted.

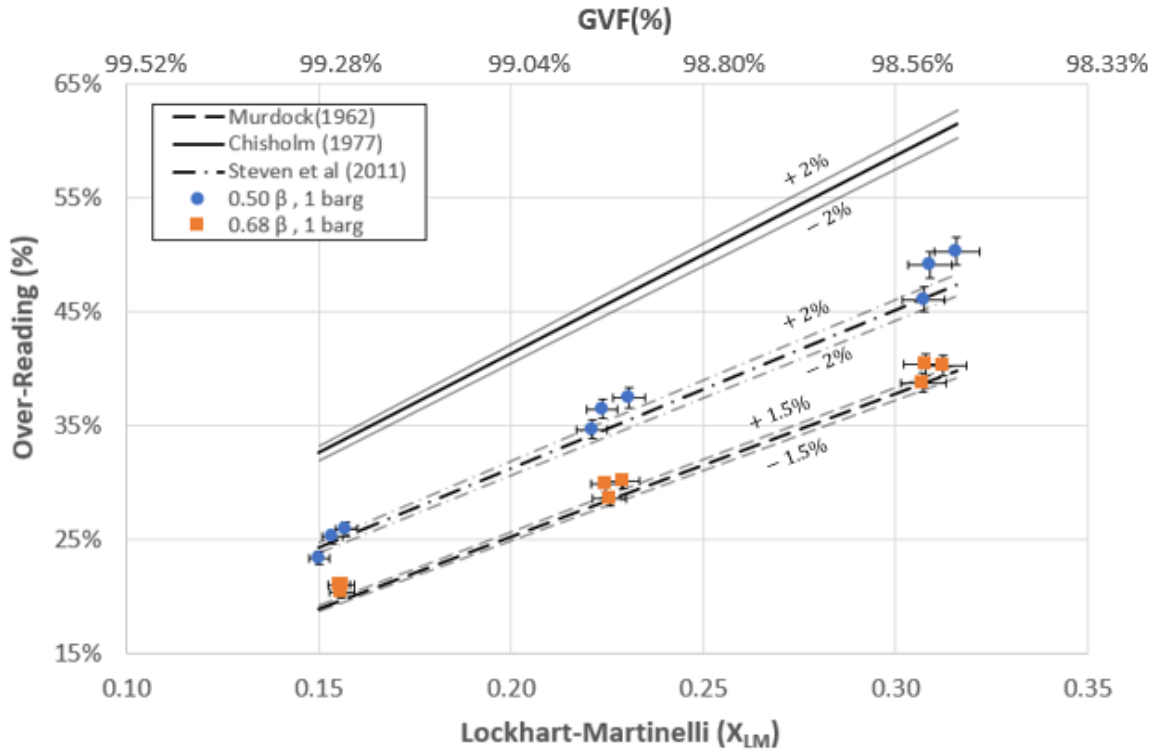


Figure 40 - Over-reading experimental data points comparison with literature correlations using air-water flow with 0.50 and 0.68 beta and 1 barg line pressure (Source: author)

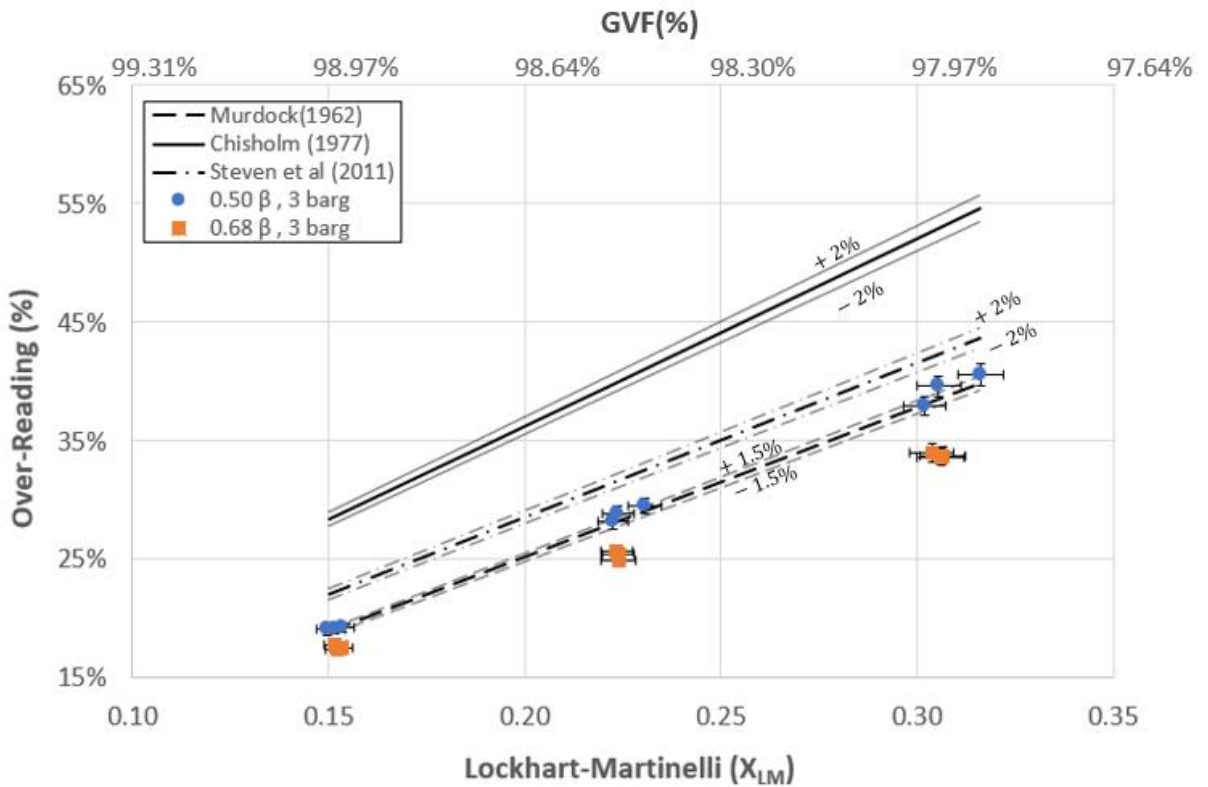


Figure 41 - Over-reading experimental data points comparison with literature correlations for air-water flow with 0.50 and 0.68 beta and 3 barg line pressure (Source: author)

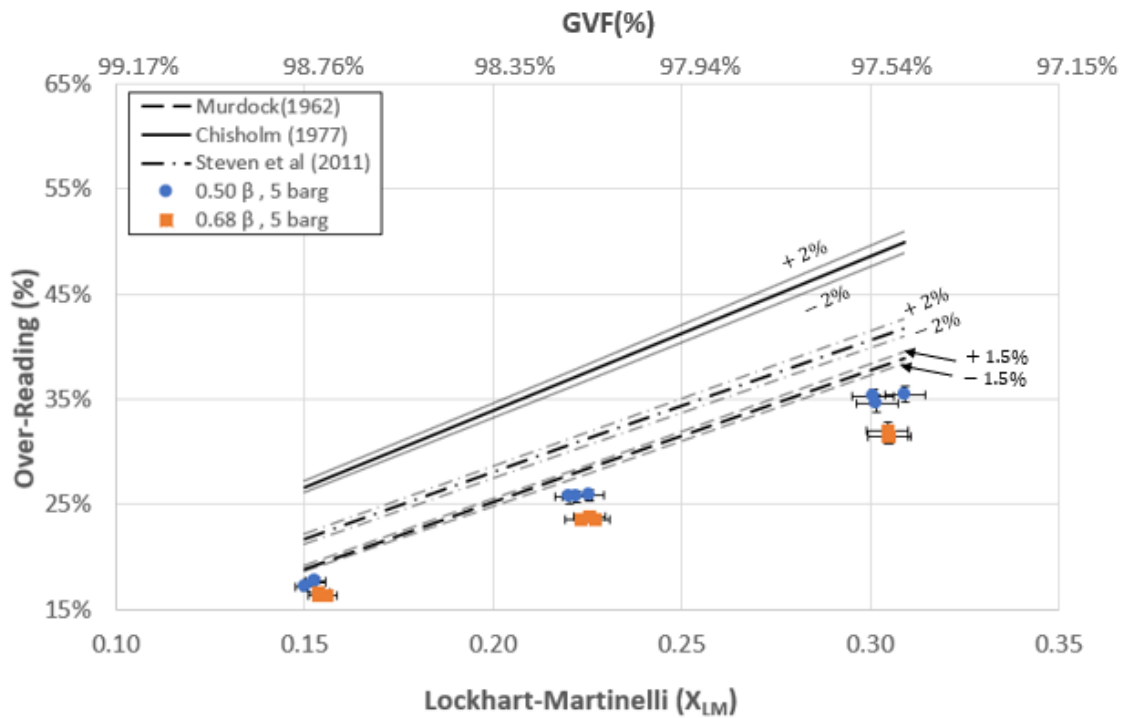


Figure 42 - Over-reading experimental data points comparison with literature correlations for air-water flow with 0.50 and 0.68 beta and 5 barg line pressure (Source: author)

For Murdock's one, the equation does not take the line pressure into account, as mentioned in section 2.3.5, using only 0.06 barg pressure to develop it. The 0.68 β , 1 barg and 0.50 β , 3 barg matches are explained since the relation $\Delta P_{TP,m}/\Delta P_{g,m}$ for both states are near to the values found by Murdock in his experimental work for air-water flow.

Another relevant observation in Figure 40, Figure 41 and Figure 42 is the beta effect, where the over-reading reduces with the beta increase. Indeed, as the over-reading phenomenon relies on the liquid accumulation, area reduction and other flow dynamics changes, explained in section 2.3.4, the beta increase results in a orifice area increase, reducing the four mentioned effects. However, this beta effect is more noticeable at low pressure and high gas wetness, e.g., at 1 barg and $X_{LM} = 0.3$, the 0.50 β has a OR almost 22% higher than in 0.68 β as average, whereas at 5 barg and $X_{LM} = 0.15$ this difference drops to 6% as average. This behavior explains why this effect was negligible, as mentioned by many authors in literature, as they used pressure levels such 10 barg or higher, and why Steven et al.'s (2011) correlation fails to predict the 0.68 β over-reading.

4.5.2 ISO TR 11583 (2012) PLR to X_{LM} correlation performance in air-water flow and new data fits correlations considering two extra 3rd tap configurations

ISO TR 11583 (2012) is one of the first attempt to consolidate a wet gas measurement methodology for Venturi and orifice meters, considering the pressure loss as one of the techniques to estimate the liquid amount on the flow. For orifice plates, the correlation suggested to estimate the over-reading is Steven and Hall's (2009) one, which is very similar to Steven et al.'s (2011), tested in previous section. In addition, this technical report brought different methods, such as trace techniques, separator vessel readings and a pressure loss correlation, to estimate the X_{LM} , required to perform the gas flow rate computation. This last methodology is based on Figure 28 arrangements, considering 6D additional tap and applying equations 71 and 72, as exposed in section 2.3.6.

The first step in this topic is to verify the viability of pressure loss methodology for NEMOG's installation, due to parameters limitations and then, use wet gas data gathered to evaluate the technique performance, as discussed in the beginning of section 4.5.

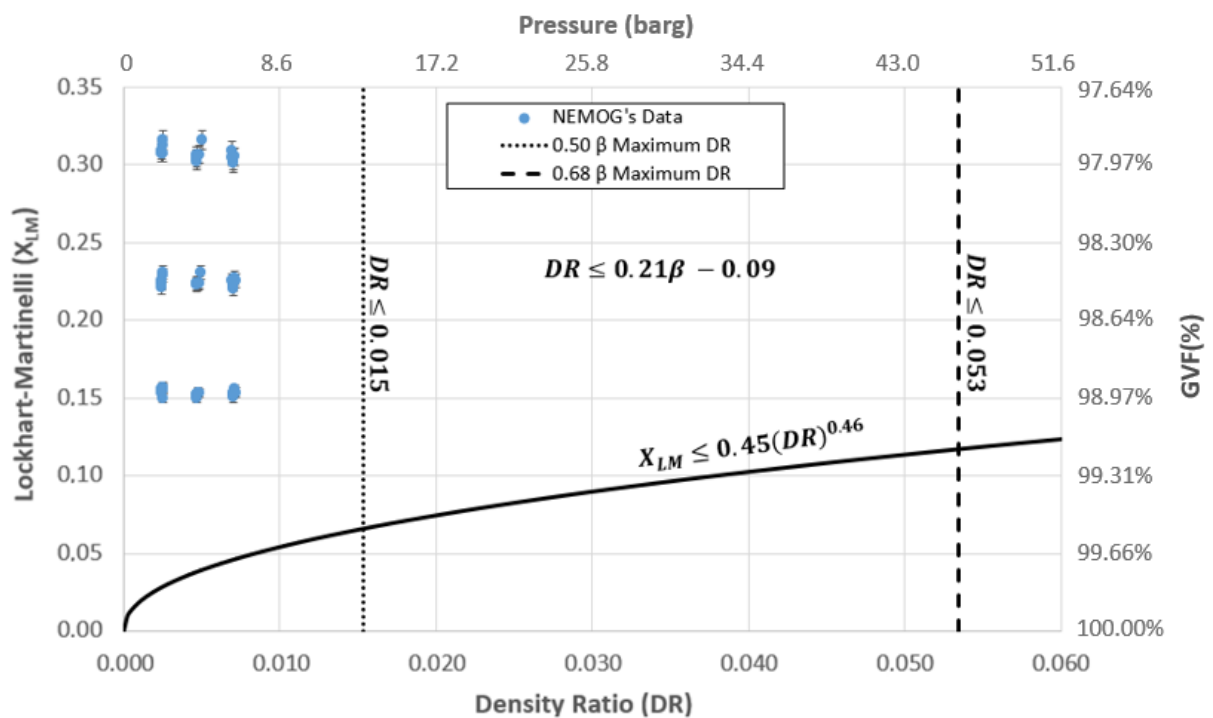


Figure 43 - ISO TR 11583 (2012) X_{LM} and DR limits of applicability with NEMOG's data envelope (Source: author)

Figure 43 brings both X_{LM} and DR limits of applicability for the PLR to X_{LM} correlation, showing a limited range of liquid content for lower density ratios i.e., lower line pressures), result of a small data set to perform the data fit, as reported by Steven, Shugart and Kutty (2018). Looking at NEMOG's data, these are within the DR boundaries, being lower than the 0.015 for 0.50β and lower than the 0.053 for 0.68β . However, they are way beyond the X_{LM} of 0.04 for 5 barg, or even the X_{LM} of 0.02 for 1 barg.

Thus, the use of NEMOG's data led to a Lockhart-Martinelli range extrapolation, resulting in a X_{LM} estimation with up to 80% deviation for 0.68β and 1 barg, as displayed in Figure 44, for estimated expanded uncertainty of 0.93%, following the ISO correlation. Moreover, the least deviation at 0.50β could be explained by the Y parameter in equation 71, which is a function of ISO 5157-2 PLR_{dry} and the experimental PLR_{wet} . So, the better fit of the ISO 5157-2 PLR_{dry} on 0.50β , seen in Figure 36, result in lower error carried to X_{LM} equation. Additionally, the data points high scatter at 0.50β , is a consequence of the sensitivity coefficient between the X_{LM} and PLR_{wet} , represented by equation 80 and illustrated in Table 15 by two examples of PLR_{wet} offset effect in X_{LM} estimation.

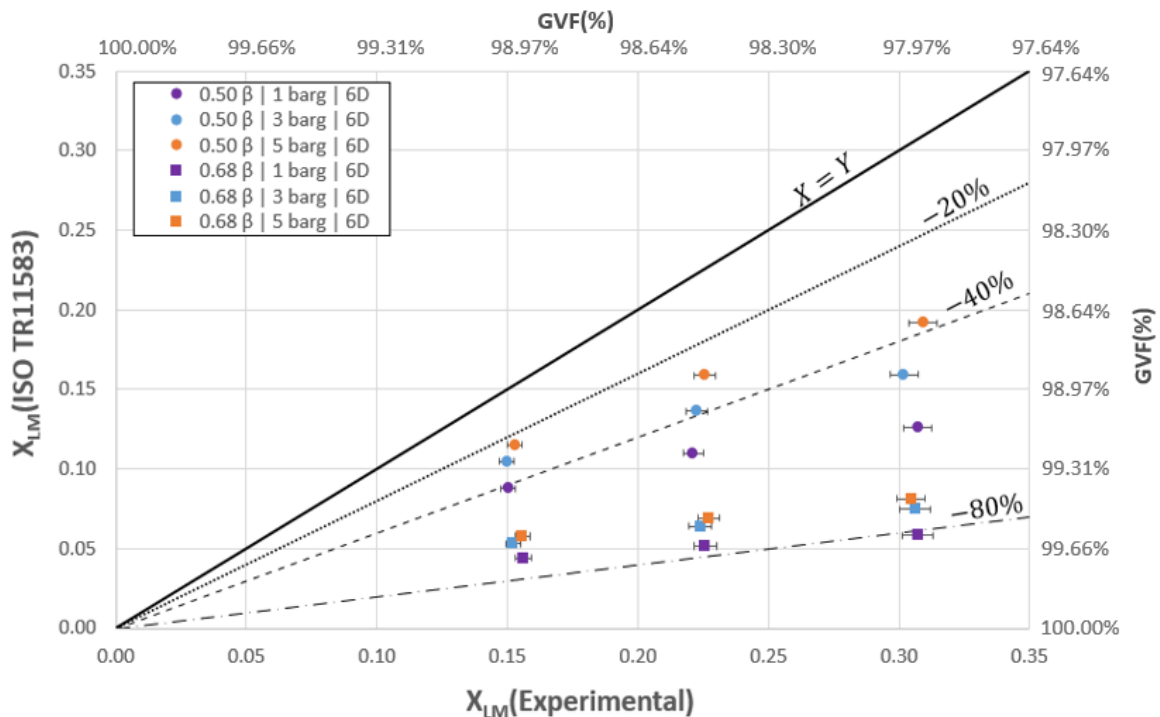


Figure 44 - ISO TR 11583 (2012) PLR to X_{LM} extrapolation test with air-water flow (Source: author)

$$\frac{\partial(X_{LM})}{\partial(PLR_{wet})} = -\frac{6.41}{\beta^{4.9}}(DR)^{0.92} \quad (80)$$

Table 15 - PLR_{wet} sensitivity in X_{LM} estimation by ISO TR 11583 (2012) correlation

β	X_{LM} (real)	DR	Sensitivity (Eq. 80)	PLR_{dry}	PLR_{wet} offset (%)	PLR_{wet}	X_{LM} (calculated)	Shift ¹
0.50	0.15	0.0070	-1.96	0.730	1%	0.797	0.13	13.4%
					0%	0.789	0.12	Base value
					-1%	0.781	0.10	-13.4%
0.68	0.16	0.0070	-0.43	0.529	1%	0.666	0.06	5.0%
					0%	0.660	0.06	Base value
					-1%	0.653	0.05	-5.0%

1 - From the X_{LM} (calculated) at 0% offset

For 0.50β , 5 barg (0.0070 DR), considering the PLR_{wet} data gathered experimentally as base value, (see Table 15 at 0% offset), the resultant sensitivity coefficient is -1.92, which represents 4.6 times higher than sensitivity coefficient for 0.68β orifice plate. Consequently, a simply 1% increase in PLR_{wet} results in a 13.4% X_{LM} estimation shift, so taking the 0.8 expanded uncertainty for the experimental PLR_{wet} , it is expected that the 0.50β data points would be more scattered.

Albeit the huge deviation found on the ISO TR 11583 (2012) extrapolation, data presents a reasonably linear tendency, showing that the equation could be improved with more experimental data to cover this higher wetness and low-pressure level.

For that, a new data fit was executed, using 6D installation data based on $PLR_{dry,fit}$, 0.50β and 0.68β , $0.0024 \leq DR \leq 0.0071$ (1 to 5 barg) and $0.74 \leq Fr_g \leq 1.29$ parameters ranges. The Minitab®'s multiple linear regression function, based on least squares and ANOVA methods, was used to perform this task resulting in equation 81 using a significance level of 5%, where Y is given by equation 71. The new data fit estimation is plotted in Figure 45, using additional data (not used on correlation's development), showing a good agreement between experimental and calculated values, with 89% of the points beneath 5% of accuracy and 100% beneath 10% of accuracy all with a 95% confidence level. Table 16 summaries the ANOVA for the regression coefficients.

$$X_{LM} = -0.1080 - 0.5498\beta + 77.40DR + 6.602Y - 4853DR^2 - 7.681(\beta \times Y) + 168.5(DR \times Y) \quad (6D) \quad (81)$$

Table 16 - Multiple linear regression coefficients ANOVA for 6D PLR to X_{LM} new data fit

Source	DoF	Adj SS	Adj MS	F-Value	P-Value ¹
Regression	6	0.277863	0.04631	640.95	0.000
β	1	0.004992	0.004992	69.1	0.000
DR	1	0.008898	0.008898	123.15	0.000
Y	1	0.026576	0.026576	367.82	0.000
DR²	1	0.005835	0.005835	80.76	0.000
$\beta \times Y$	1	0.020521	0.020521	284.02	0.000
DR \times Y	1	0.008800	0.0088	121.79	0.000
Error	65	0.004696	0.000072		
Total	71	0.282559			

1 - Considering a 5% significance level to assess the null hypothesis

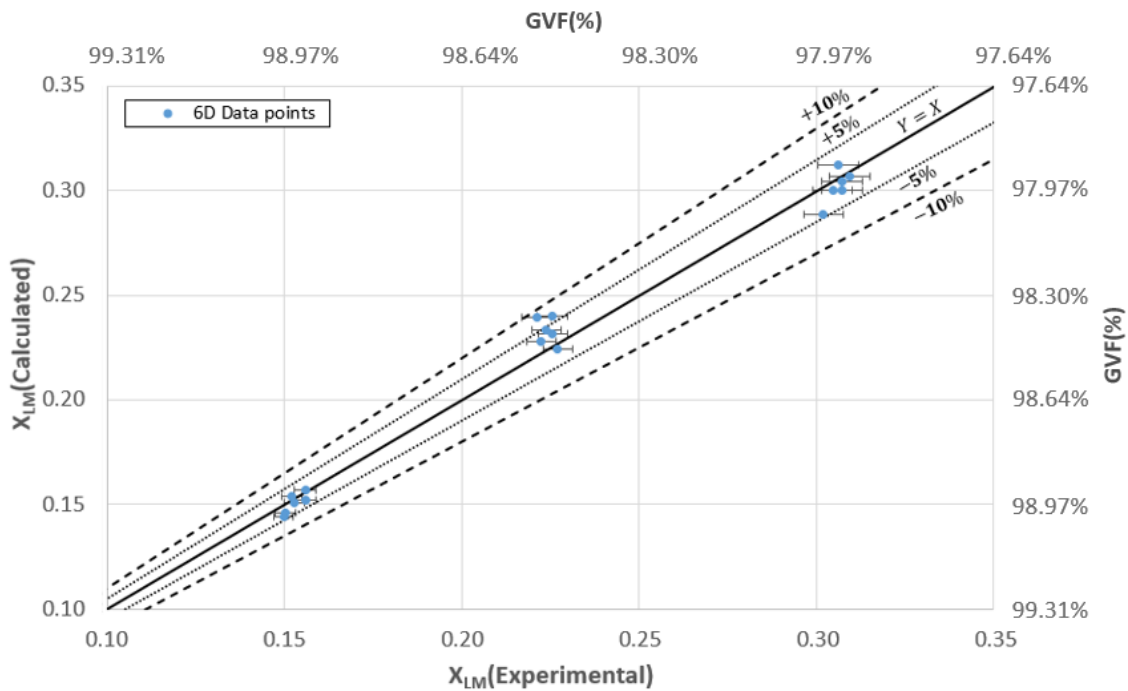


Figure 45 - 6D PLR to X_{LM} new data fit results for 0.50 β and 0.68 β , 1, 3 and 5 barg and 0.15 to 0.31 Lockhart-Martinelli (Source: author)

Although the performance of the new data fit is relevant for the 6D third pressure tap, considering that it is a two-phase flow phenomenon, another limiting factor in this liquid loading estimation methodology, the fixed 6D third tap location, need to be better investigated, as long as this rigid requirement results in a CapEx barrier for new

implementations, in already existent single-phase gas orifice meters, which most doesn't count with an additional exactly 6D distance pressure tap. In such wise, two additional distances were tested on the NEMOG's test loop:

- i) one at 20D and
- ii) other at 144D,

where the first one was in straight forward pipeline and the latter consisted in straight forward pipeline with two 90° elbows in the same plane, as exposed in Figure 37. This new data gathered led to the development of two new equations based on $PLR_{dry,fit}$, 0.50β and 0.68β , $0.0024 \leq DR \leq 0.0071$ (1 to 5 barg) and $0.74 \leq Fr_g \leq 1.29$ parameters ranges, processed with the same previous mentioned Minitab®'s methodology.

The resultant mathematical relations are exposed in equations 82 and 83, with R-squared were 98.01% and 94.93% respectively, followed by the ANOVAS in

Table 17 and Table 18. One interesting observation regarding the ANOVA in Table 18, is the loss of statistical significance on the β on its own, comparing to 6D and 20D ANOVAS, been only significant on the combined effect with Y parameter, represented by the interaction row $\beta \times Y$. It could be a result of the distance from the orifice plate. Additionally, the $DR \times Y$ combined effect were eliminated too, due to the probability value higher than 5% (significance level chosen).

$$X_{LM} = 0.1001 - 1.0413\beta + 80.06DR + 6.503Y - 5933DR^2 - 7.558(\beta \times Y) + 138.4(DR \times Y) \quad (20D) \quad (82)$$

Table 17 - Multiple linear regression coefficients ANOVA for 20D PLR to X_{LM} new data fit

Source	DoF	Adj SS	Adj MS	F-Value	P-Value
Regression	6	0.276186	0.046031	533.83	0.000
β	1	0.009568	0.009568	110.96	0.000
DR	1	0.013004	0.013004	150.81	0.000
Y	1	0.026383	0.026383	305.97	0.000
DR^2	1	0.011351	0.011351	131.64	0.000
$\beta \times Y$	1	0.018372	0.018372	213.06	0.000
$DR \times Y$	1	0.012019	0.012019	139.39	0.000
Error	65	0.005605	0.000086		
Total	71	0.281791			

1 - Considering a 5% significance level to assess the null hypothesis

$$X_{LM} = -0.9312 + 167.02DR + 5.365 Y - 10442 DR^2 - 7.142\beta \times Y \tag{144D} \tag{83}$$

Table 18 - Multiple linear regression coefficients ANOVA for 144D PLR to X_{LM} new data fit

Source	DoF	Adj SS	Adj MS	F-Value	P-Value
Regression	4	0.27476	0.068689	313.51	0.000
<i>DR</i>	1	0.09196	0.091959	419.71	0.000
<i>Y</i>	1	0.27067	0.270674	1235.39	0.000
<i>DR</i> ²	1	0.04293	0.04293	195.94	0.000
$\beta \times Y$	1	0.26905	0.269049	1227.97	0.000
Error	65	0.01468	0.000219		
Total	71	0.28944			

1 - Considering a 5% significance level to assess the null hypothesis

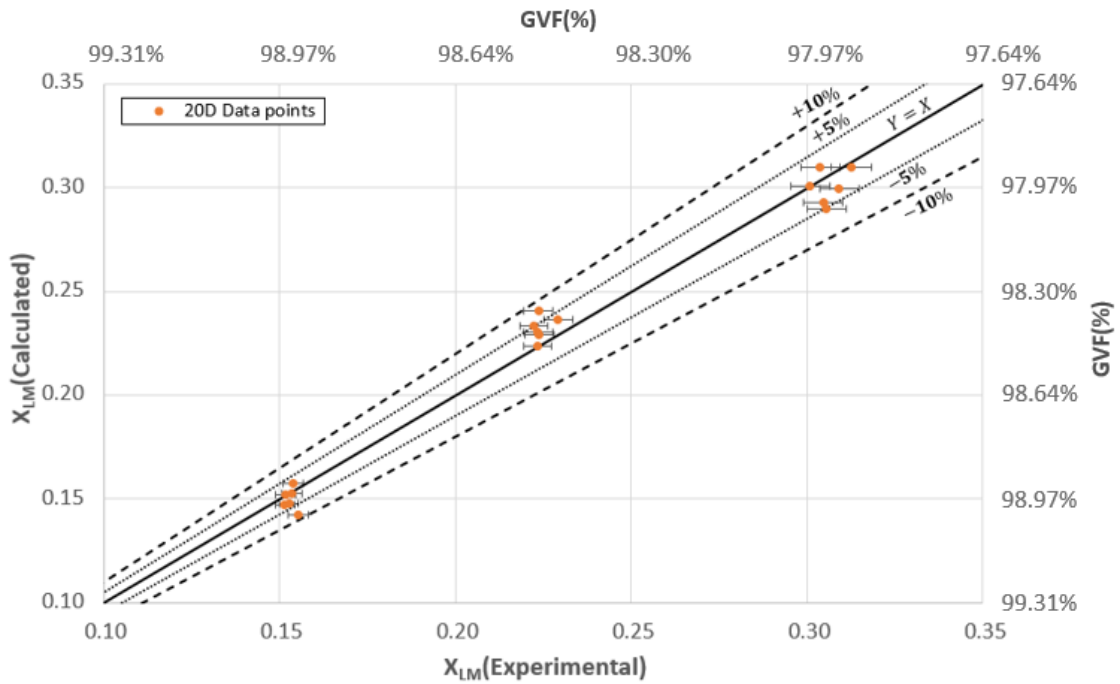


Figure 46 - 20D PLR to X_{LM} new data fit results for 0.50β and 0.68β , 1, 3 and 5 barg and 0.15 to 0.31 Lockhart-Martinelli (Source: author)

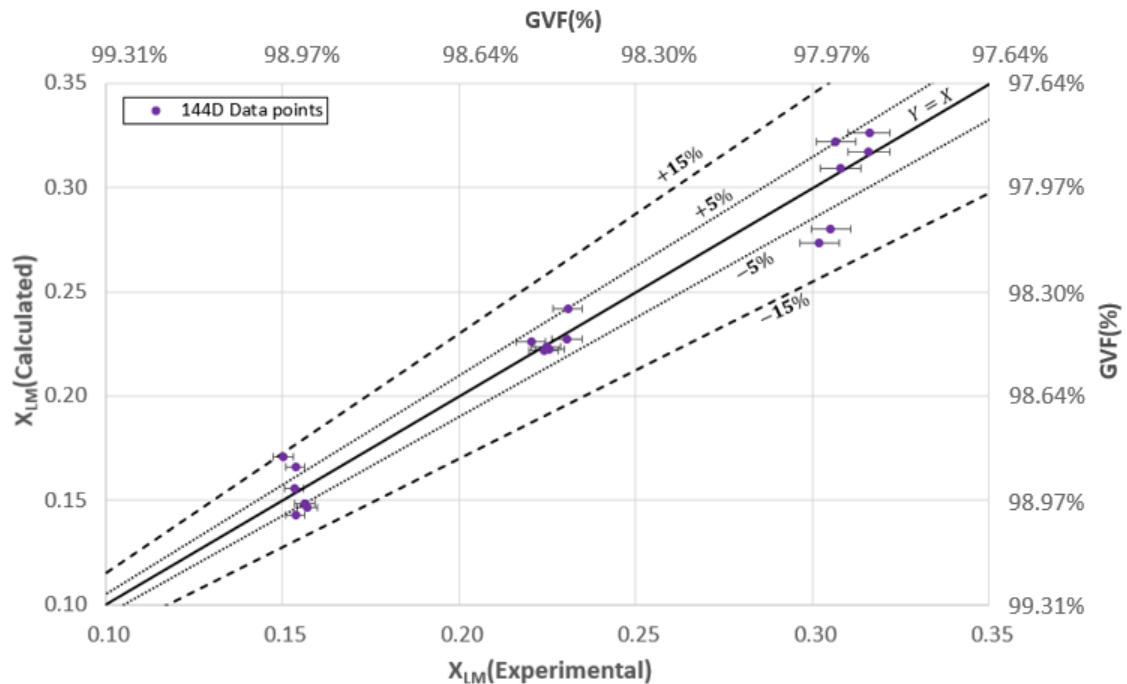


Figure 47 - 144D PLR to X_{LM} new data fit results for 0.50β and 0.68β , 1, 3 and 5 barg and 0.15 to 0.31 Lockhart-Martinelli (Source: author)

Continuing the analysis, Figure 46 brings the 20D equation plot, where 78% of the data used were within $\pm 5\%$ of accuracy and 100% within $\pm 10\%$ of accuracy. Then, Figure 47 plots the 144D equation, where 55% of the data used were within $\pm 5\%$ of accuracy and 100% within $\pm 15\%$ of accuracy, albeit scattering increases in this distance, mainly in high Lockhart-Martinelli values.

These equations are not the ultimate solution for the X_{LM} estimation, mainly for being installation dependents, requiring further investigations for external uses, but they show that is possible to correlate different pressure taps with the wetness and it opens the possibility to develop correlations for different installations and even the use of machine learning to develop new algorithms to estimate the liquid content.

4.5.3 Lockhart-Martinelli estimation using ISO TR 11583 (2012) equation with 3rd tap correction to 6D position using Petalas and Aziz (1998) two phase flow pressure drop model

As exposed in previous section, the data fit equation seems to be an alternative to the X_{LM} estimation in wet gas measurement methodologies, however this technique is very

installation dependent, requiring a new data acquisition and treatment in each desired installation to implement the wet gas measurement, becoming unfeasible in some cases.

In that sake, this work analyzes an alternative methodology to overcome the third tap position issue in ISO TR 11583 (2012) pressure loss technique, by using Petalas and Aziz (1998) two-phase flow pressure drop model to bring the farther positioned additional pressure tap back to the required 6D distance in a virtual manner, as exemplified in Figure 48, where pressure head loss, estimated by the pressure drop model, is discounted from the permanent pressure loss (PPL) measurement at 20D 3rd tap.

Following this line, the first step was to validate the two-phase flow pressure drop model in air-water flow, at NEMOG's facility. To do it so, an 2650 mm straight pipeline on the return branch was chosen to be the pressure drop validation section measurements with PDT-06 differential pressure transmitter (Appendix C), as illustrated in Figure 49, where 36 experimental points were tested using the maximum air mass flow rate (360 kg/h) with nine different water mass flow rates (to comply with the three X_{LM} levels used on previous procedures), three line pressure levels (1, 3 and 5 barg) and 0.50β , 0.68β and no orifice plate configurations.

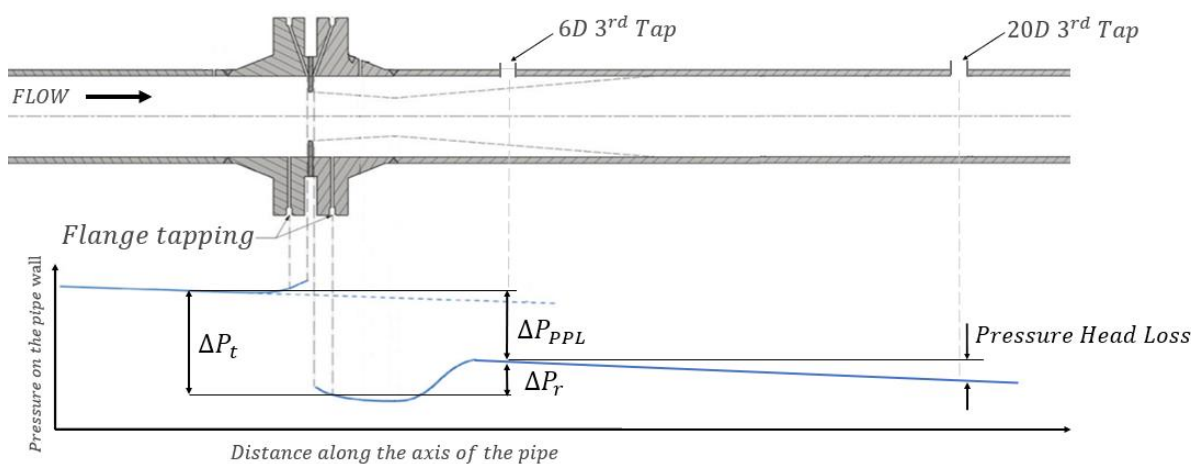


Figure 48 - Exemplification of the third pressure tap correction from 20D to 6D using Petalas and Aziz (1998) two phase flow pressure drop model (Source: author)

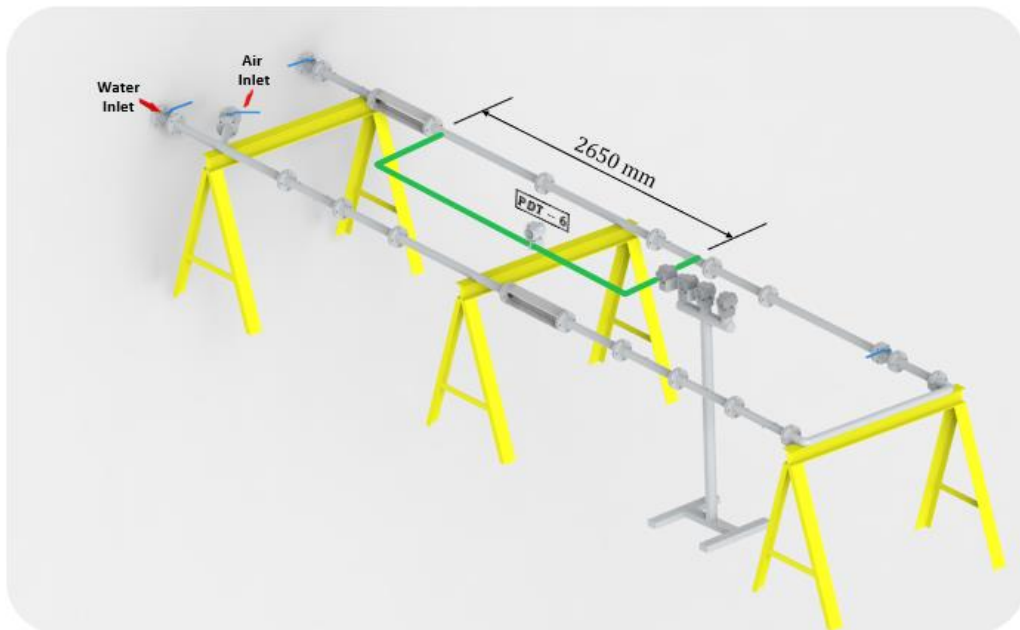


Figure 49 - Experimental configuration in two-phase pressure drop measurement for Petalas and Aziz's (1998) model validation and adjustments (Source: author)

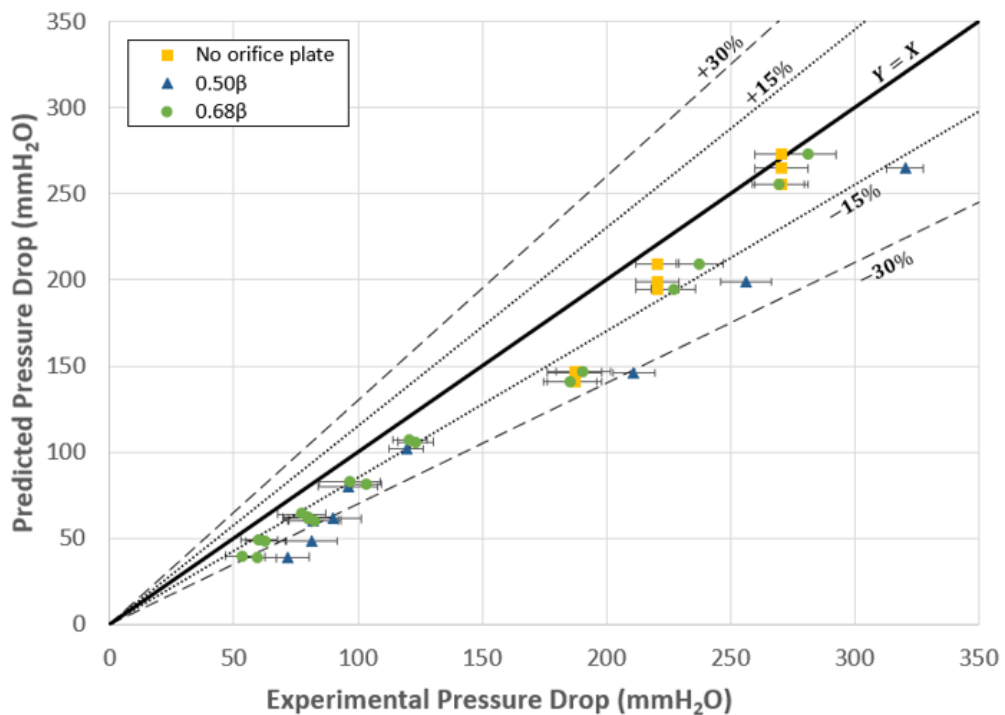


Figure 50 - Petalas and Aziz (1998) two-phase pressure drop model experimental validation without pipe roughness adjustment (Source: author)

Figure 50 shows the model behavior using a standard internal roughness for steel pipes. The model predicted 11% of the 0.50β data, 39% of the 0.68β data and 66% of

the no orifice data within 15% accuracy. Comparing the 0.50β results with the no orifice plate results, 0.50β had a considerable influence on the flow dynamic, even with measurements far from the orifice flange and this influence was not considered on the model. Another inference from this same figure is that the model had a better response in high experimental pressure drop, i.e. high water flow rates, evidenced on the experimental points above 200 mmH₂O.

To improve the model agreement with the NEMOG's test loop configuration, an iterative modification on the pipe internal roughness was performed for each of the three configurations. This approach was chosen to consider the orifices and other unconsidered pressure drop local effects such as flange misalignment and pipe internal corrosion. So, three new virtual internal roughness were found, 1.5 μm without orifice plate, 2 μm for 0.68β and 5 μm for 0.50β . Figure 51 brings the results, evidently increasing the model performance, resulting in 100% of the data within 15% accuracy and 61% of the data beneath 5% accuracy.

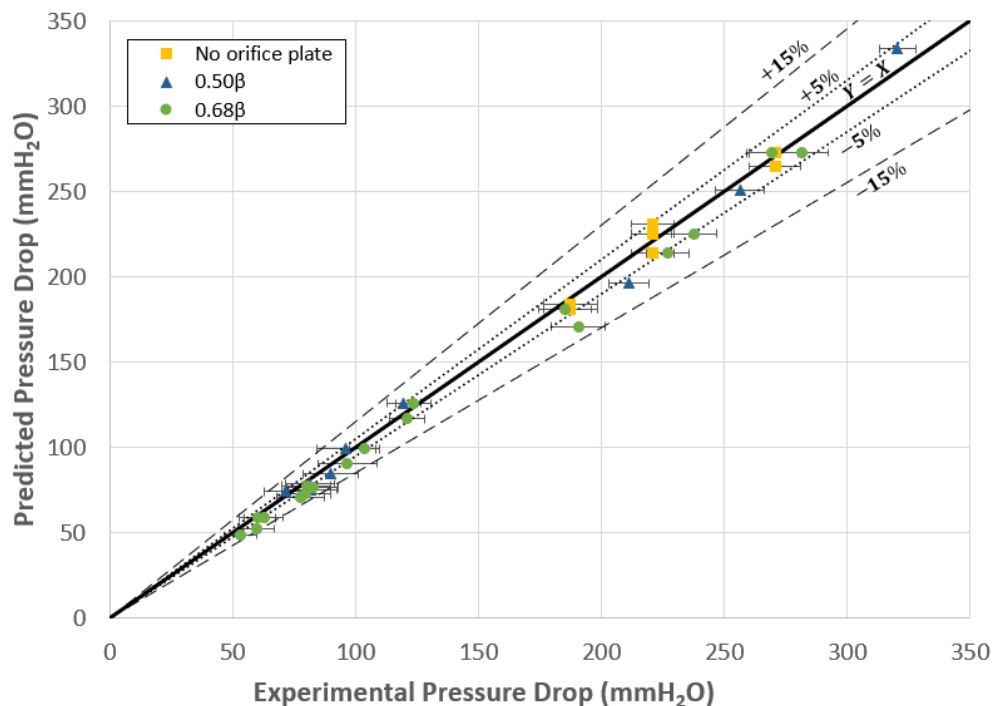


Figure 51 - Petalas and Aziz (1998) two-phase pressure drop model experimental validation with pipe roughness adjustment (Source: author)

After this model adjustment for NEMOG's test loop, the pressure head losses were estimated by the adjusted model considering a straight pipe length, for all experimental data points gathered at 20D and 144D third pressure tap, where the set pipe length on the model was equal to the difference between the 6D and the actual 3rd tap distance. Then those head losses were subtracted from the measured PPL, obtaining an adjusted PPL, which was used on the ISO TR 11583 (2012) standard procedure to estimate the Lockhart-Martinelli.

Table 19 exposes the results of the 20D data, where the results of ISO TR 11583 (2012) at 6D were used as reference, although these did not agree with the actual X_{LM} values (due to correlation limitations disserted on section 4.5.2). This methodology had a satisfactory performance considering all the complexity and uncertainty involved behind, estimating the Lockhart-Martinelli at a maximum shift of 9.96% and 4.29% shift as average. Figure 52 consolidate those results comparing the uncorrected estimation with the corresponding corrected estimation.

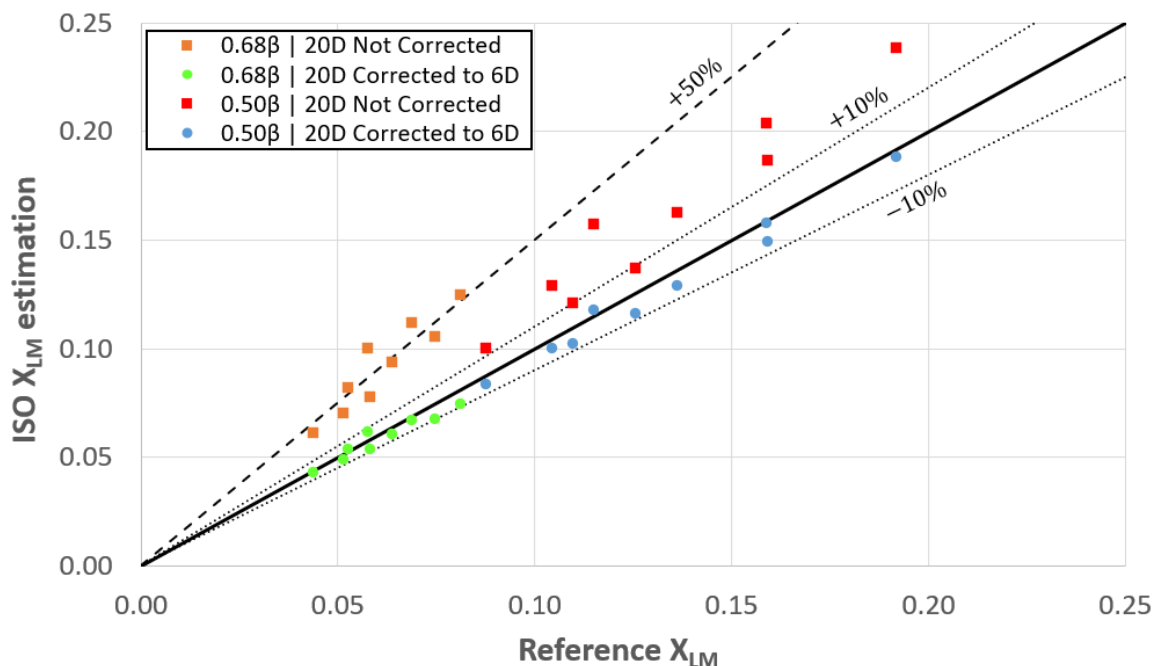


Figure 52 - Comparison between uncorrected and corrected Lockhart-Martinelli estimation using adjusted PPL by Petalas and Aziz (1998) model in ISO TR 11583 (2012) (Source: author)

Table 19 - ISO TR 11583 (2012) results using the adjusted Petalas and Aziz (1998) model to correct the 3rd pressure tap from 20D to 6D

β	Pressure (barg)	Real X_{LM}	ISO X_{LM} estimation at 6D (ref.)	ISO X_{LM} estimation at 20D	ISO X_{LM} estimation 20D to 6D	Shift ¹
0.68	1.08	0.16	0.0438	0.0606	0.0426	-2.84%
	1.09	0.23	0.0516	0.0701	0.0485	-5.95%
	1.07	0.31	0.0583	0.0774	0.0531	-8.84%
	3.04	0.15	0.0529	0.0817	0.0536	1.22%
	2.99	0.22	0.0639	0.0934	0.0601	-5.89%
	3.00	0.30	0.0749	0.1051	0.0675	-9.96%
	5.11	0.15	0.0577	0.0996	0.0612	6.07%
	5.09	0.22	0.0691	0.1115	0.0668	-3.39%
	4.98	0.30	0.0815	0.1243	0.0743	-8.86%
0.50	1.10	0.15	0.0879	0.0999	0.0833	-5.26%
	1.09	0.22	0.1100	0.1208	0.1020	-7.30%
	1.13	0.31	0.1257	0.1368	0.1158	-7.87%
	3.01	0.15	0.1046	0.1288	0.0996	-4.72%
	3.00	0.22	0.1365	0.1623	0.1286	-5.77%
	3.01	0.31	0.1594	0.1860	0.1491	-6.44%
	4.97	0.15	0.1153	0.1569	0.1172	1.60%
	4.97	0.22	0.1589	0.2031	0.1573	-1.04%
	4.98	0.30	0.1919	0.2381	0.1879	-2.06%

1 - Using ISO X_{LM} estimation at 6D as reference value and comparing to the 20D to 6D corrected value

Unfortunately, the 20D performance was not reached in 144D, with relevant differences on the X_{LM} estimation as exposed in Table 20.

Those results could be explained by the fact that the model was developed for straight forward pipe head loss estimation and the 144D pipelined have two 90° elbows, which add complexities on the two-phase pressure drop phenomenon. One attempt to overcome this limitation was to use the single-phase approach for the local pressure drop, but with no further successes, reinforcing the two-phase pressure drop complexity.

Table 20 - ISO TR 11583 (2012) results using the adjusted Petalas and Aziz (1998) model to correct the 3rd pressure tap from 144D to 6D

β	Pressure (barg)	Real X_{LM}	ISO X_{LM} estimation at 6D	ISO X_{LM} estimation at 20D	ISO X_{LM} estimation at 20D corrected to 6D	Shift ¹
0.68	1.12	0.16	0.0438	0.2547	0.0429	-2.24%
	1.04	0.22	0.0516	0.2747	0.0297	-42.40%
	1.07	0.31	0.0583	0.3054	0.0263	-54.88%
	3.10	0.15	0.0529	0.3353	0.0017	-96.80%
	3.11	0.22	0.0639	0.3776	-0.0159	-124.85%
	3.12	0.31	0.0749	0.4417	-0.0086	-111.49%
	5.07	0.15	0.0577	0.4198	-0.0249	-143.08%
	5.13	0.23	0.0691	0.4565	-0.0664	-196.01%
	5.05	0.31	0.0815	0.5046	-0.0800	-198.17%
0.50	1.09	0.16	0.0879	0.3079	0.0984	12.00%
	1.11	0.23	0.1100	0.3505	0.0959	-12.78%
	1.10	0.32	0.1257	0.3856	0.1145	-8.94%
	3.06	0.15	0.1046	0.3971	0.0275	-73.68%
	3.18	0.23	0.1365	0.4672	0.0257	-81.14%
	3.26	0.32	0.1594	0.5434	0.0437	-72.60%
	4.98	0.15	0.1153	0.4885	-0.0040	-103.44%
	4.99	0.22	0.1589	0.5489	-0.0139	-108.76%
5.02	0.30	0.1919	0.6023	-0.0458	-123.87%	

1 - Using ISO X_{LM} estimation at 6D as reference value and comparing to the 20D to 6D corrected value

5 CONCLUSION

5.1 FINAL REMARKS

Occurrence of wet gas flows are very usual in many industrial processes, mainly in oil industries. On those, flow measurement is based in differential pressure devices at least on 40% of the cases, being the orifice plate the most used. However, in case of two-phase applications, the liquid loading causes a positive bias on the pressure differential readings, due to phases interactions called over-reading and leading to an erroneous gas flow rate prediction up to 50%. Through decades apart, empirical correlations were proposed to estimate and correct this overestimation for different differential pressure devices, such as orifice plates, venture tubes and inverted cones. However, all proposals need some information about the liquid, which in most of the time is not available instantly, forcing the use of other means to “guesstimate” the liquid content with past unprecise data, inducing extra uncertainty on the gas flow rate prediction process.

To overcome this barrier, industry has been developing an all in one two-phase wet gas flow meters (WGFMs), with liquid loading estimation and over-reading correction on the same meter. In 2012, ISO TR 11583 (2012) released a methodology to wet gas measurement, based on orifice plates or Venturi, but providing for the installation of pressure loss ratio (PLR) to liquid content relationship, limited by 6D 3rd pressure tap, high pressure levels and low gas wetness.

To investigate this methodology, this work relied on a multiphase flow circuit presented on chapter **Erro! Fonte de referência não encontrada.**, located at the Research Group for Studies on Oil&Gas Flow and Measurement (NEMOG), located at Federal University of Espírito Santo, Vitória, Brazil.

The first step was to validate the test section orifice meter in single-phase air flow, comparing to the single-phase air mass flow meter at the high flow rate branch. ISO 5167-2 (2003) requirements were fulfilled, but after several test procedures comparing the two meters estimations, a systematic shift of -6% as average was found with no evident justification for it. So, another measurement comparison was performed, now in a water flow, using the Coriolis meter as reference, finding an average shift of -2%.

After that, the test section measurements were considered valid and the single-phase air flow measurements were adjusted based on the systematic shift estimated for each experimental procedure.

Second, the ISO 5167-2 (2003) pressure loss ratio for dry flow was evaluated in an air-water flow combining 1, 3 and 5 barg line pressure level, 150, 225 and 350 kg/h air flow rate with 0.5β and 0.68β orifice plates, totalizing 18 experimental points. The results showed a better performance by the ISO correlation, using a 0.50β , with an average shift of 0.5% from the experimental measurements, while for 0.68β this shift raised to 1.5%. This behavior could be explained by the fact that for 0.50β the permanent pressure loss is almost equal to the traditional differential pressure, so the pressure drop phenomenon becomes near to a localized pressure drop, which becomes more predictable. In addition, a new data fitted equation was proposed, resulting in up to 1% of deviation reduction for 0.68β , but for 0.50β , there were no significant reductions, statistically speaking.

After that, the wet gas experiments were executed for mixtures of air and water at 1, 3 and 5 barg pressure line (0.0025, 0.0048 and 0.0071 density ratio), 360 kg/h air mass flow rate, 0.15, 0.22 and 0.30 Lockhart-Martinelli parameter and 0.74, 0.90 and 1.29 gas Froude number. Considering those data points, the first evaluation was the orifice plate over-reading correlations proposals, published by Murdock (1962), Chisholm (1977) and Steven et al. (2011). It was found that the NEMOG's experimental points match with wet gas data points gathered at CEESI and NEL. Furthermore, for Froude number at 1.29 the Steven et al.'s predicts very well the over-reading value, with an 2.5% accuracy for 0.50β . However, as pressure increase, i.e. Froude number decreasing, the Steven et al.'s performance decline, due to the correlation 1.5 Froude number lower limit. Another limitation to this correlation is related to the beta value effect, evidenced in low line pressure, where the beta increase results in a over-reading reduction. As the Steven et al. (2011) used line pressures above 10 barg, this effect was not evidenced and was not considered. For Murdock's one, experimental data for 0.68β , 1 barg and 0.50β , 3 barg had a good prediction, within 2% of accuracy, but those matches are explained since the relation $\Delta P_{TP,m}/\Delta P_{g,m}$ for both states are near to the values found by Murdock in his experimental work for air-water flow.

In sequence, the ISO TR 11583 (2012) methodology was experimentally evaluated in X_{LM} values above the maximum limit required, i.e. an extrapolation performance using the air-water data points acquired at NEMOG facility. The results were poor, with up to 80% shift, showing that extrapolations are not tolerable and the necessity of further improvements. On that line, it was proposed a new data fitting equation for the X_{LM} estimation by means of pressure loss ratio (PLR) using a 6D third tap, resulting in 89% of the points beneath 5% of accuracy and 100% beneath 10% of accuracy all with a 95% confidence level. Furthermore, to overcome the limitation of 6D third tap fixed location, it was test two new distances, 20D and 144D, resulting in $\pm 10\%$ and $\pm 15\%$ of accuracy respectively.

Finally, the last contribution of this work was the analysis of an alternative methodology to overcome the third tap position issue in ISO TR 11583 (2012) pressure loss technique, by using Petalas and Aziz (1998) two-phase flow pressure drop model to bring the farther positioned additional pressure tap back to the required 6D distance in a virtual manner. After Petalas and Aziz model adjustments for NEMOG test loop and flow conditions, it was used to estimate de head loss between the 6D and the new third tap distance. This methodology had a satisfactory performance considering all the complexity and uncertainty involved behind, estimating the Lockhart-Martinelli at a maximum shift of 9.96% and 4.29% shift as average. However, for the 144D third tap, the methodology failed in predict the Lockhart-Martinelli since Petalas and Aziz model was not suitable to curved pipes, demanding further improvements to have a satisfactory result.

5.2 CORRELATIONS SUMMARY

Pressure loss ratio for dry air flow: this equation considers 150, 225 and 350 kg/h dry air mass flow rates, for 1, 3 and 5 barg line pressure, using 0.50β and 0.68β orifice plate sizes and a range of temperature from 24°C to 30°C

$$PLR_{dry,fit} = -185.08 - 23.45\beta + 631.7C_d + 36.70\beta C_d - 534.9C_d^2$$

Lockhart- Martinelli estimation by means of Pressure Loss Ratio (PLR): this equations considers 1,3 and 5 barg pressure line (0.0025, 0.0048 and 0.0071 density ratio), 360 kg/h air mass flow rate, 0.15 ,0.22 and 0.30 Lockhart-Martinelli parameter, 0.74, 0.90 and 1.29 gas Froude number and a range of temperature from 24°C to 30°C

- **For 6D downstream third pressure tapping:**

$$X_{LM} = -0.1080 - 0.5498\beta + 77.40DR + 6.602Y - 4853DR^2 - 7.681(\beta \times Y) + 168.5(DR \times Y)$$

Accuracy: 10%

- **For 20D downstream third pressure tapping:**

$$X_{LM} = 0.1001 - 1.0413\beta + 80.06DR + 6.503Y - 5933DR^2 - 7.558(\beta \times Y) + 138.4(DR \times Y)$$

Accuracy: 10%

- **For 144D downstream third pressure tapping:**

$$X_{LM} = -0.9312 + 167.02DR + 5.365Y - 10442DR^2 - 7.142\beta \times Y$$

Accuracy: 15%

5.3 PROPOSAL FOR FUTURE WORK

Literature review and results presented in this dissertation provide some proposal to further investigation.

- Investigate the ISO 5167-2 pressure loss ratio equation behavior in other orifice plate beta values, using larger line pressures and air flow rates.
- Verify the over-reading estimation correlations for orifice plates in Froud number higher than 1.5 and lower Lockhart-Martinelli values.
- Check the validity of ISO TR 11583 at low Lockhart-Martinelli values and low line pressure, i.e low density ratio.

- Improve the experimental range for the Lockhart-Martinelli estimation using ISO TR 11583 (2012) equation with 3rd tap correction to 6D position using Petalas and Aziz (1998) two phase flow pressure drop model, with third tap distances further than 20D in straight pipeline.
- Couple the ISO TR 11583 (2012) algorithm with the Petalas and Aziz (1998) model considering the phase slip ratio.

REFERENCES

- API - AMERICAN PETROLEUM INSTITUTE. **State of the Art Multiphase Flow Metering Report**, 2004.
- BARNEA, D. A unified model for predicting flow-pattern transitions for the whole range of pipe inclinations. **International Journal of Multiphase Flow**, v. 13, n. 1, 1987.
- CHISHOLM, D. Research Note: Two-Phase Flow through Sharp-Edged Orifices. **Journal of Mechanical Engineering Science**, v. 19, n. 3, p. 128–130, jun. 1977.
- CHISHOLM, D.; ROONEY, D. H. Research Note: Pressure Drop During Steam/Water Flow Through Orifices. **JNL. MECH. ENGG. SCIENCE**, v. 16, n. 5, p. 353–355, 1974.
- COLLINS, A.; CLARK, S. Evolution of Wet Gas Venturi Metering and Wet Gas Correction Algorithms Contributed Paper. **Measurement + Control**, v. 46, 2013.
- CORNELIUSSEN, S. et al. **Handbook of multiphase flow metering**. Oslo: Norwegian Society for Oil and Gas Measurement, 2005. v. 55
- DE LEEUW, R. Liquid Correction of Venturi Meter Readings in Wet Gas Flow. **North Sea Flow Measurement Workshop**, 1997.
- DELMÉE, G. J. **Manual de medição de vazão**. 3. ed. São Paulo: Blucher, 2003.
- FOX, R. W.; MCDONALD, A. T.; MITCHELL, J. W. **Fox and McDonald's introduction to fluid mechanics**. 8. ed. Hoboken: John Wiley & Sons, 2020.
- HALL, A.; GRIFFIN, D.; STEVEN, R. **A Discussion on Wet Gas Flow Parameter Definitions**. 2007.
- ISO 5167-1. Measurement of fluid flow by means of pressure differential devices inserted in circular cross-section conduits running full-Part 1: General principles and requirements. **International Standard Organization**, 2003.
- ISO 5167-2. Measurement of fluid flow by means of pressure differential devices inserted in circular-cross section conduits running full-Part 2: Orifice plates. **International Standard Organization**, 2003.

ISO TR 11583. Measurement of wet gas flow by means of pressure differential devices inserted in circular cross-section conduits. **International Standard Organization**, 2012.

ISO TR 12748. Natural Gas-Wet gas flow measurement in natural gas operations. **International Standard Organization**, 2015.

JCGM. **Evaluation of measurement data-Guide to the expression of uncertainty in measurement**. 1st ed. 2008.

LOCKHART, R. W.; MARTINELLI, R. C. Proposed correlation of data for isothermal two-phase, two-component flow in pipes. **Chem. Eng. Prog.**, v. 45, n. 1, p. 39–48, 1949.

MUKHERJEE, H.; BRILL, J. P. Pressure drop correlations for inclined two-phase flow. **Journal of Energy Resources Technology, Transactions of the ASME**, v. 107, n. 4, 1985.

MURDOCK, J. W. Two-Phase Flow Measurement with Orifices. **The American Society of Mechanical Engineers**, 1962.

OLIEMANS, R. V. A.; POTS, B. F. M.; TROMPÉ, N. Modelling of annular dispersed two-phase flow in vertical pipes. **International Journal of Multiphase Flow**, v. 12, n. 5, 1986.

PETALAS, N.; AZIZ, K. **A Mechanistic Model for Multiphase Flow in Pipes**. Annual Technical Meeting. **Anais**.1998.

READER-HARRIS, M.; FORSYTH, C.; BOUSSOUARA, T. The calculation of the uncertainty of the orifice-plate discharge coefficient. **Flow Measurement and Instrumentation**, v. 82, 2021.

READER-HARRIS, M.; NEL, T.; GRAHAM, E. An Improved Model For Venturi-Tube Over-Reading In Wet Gas. **27th International North Sea Flow Measurement Workshop**, v. 20, 2009.

STEVEN, R. Horizontally Installed Differential Pressure Meter Wet Gas Flow Performance Review. **North Sea flow measurement workshop**, 2006.

STEVEN, R. **V-Cone Wet Gas Metering**, 2007.

STEVEN, R. A dimensional analysis of two-phase flow through a horizontally installed Venturi flow meter. **Flow Measurement and Instrumentation**, v. 19, n. 6, p. 342–349, dez. 2008.

STEVEN, R. et al. **Horizontally Installed Orifice Plate Meter Response to Wet Gas Flows**, 2011.

STEVEN, R.; HALL, A. Orifice plate meter wet gas flow performance. **Flow Measurement and Instrumentation**, v. 20, n. 4–5, p. 141–151, ago. 2009.

STEVEN, R.; KEGEL, T.; BRITTON, C. An update on V-Cone meter wet gas flow metering research. **Flomeko - 13th International Flow Measurement Conference**, 2005.

STEVEN, R. N. Wet gas metering with a horizontally mounted Venturi meter. **Flow Measurement and Instrumentation**, v. 12, p. 361–372, 2002.

STEVEN, R.; SHUGART, C.; KUTTY, R. Orifice Meter Multiphase Wet Gas Flow Performance-The Pressure Loss Ratio Solution to the “Ill-Posed” Problem. **North Sea Flow Measurement Workshop**, p. 22–24, 2018.

STEVEN, R.; TING, F.; STOBIE, G. A re-evaluation of axioms regarding orifice meter wet gas flow performance. **SE Asia Hydrocarbon Flow Measurement Workshop**, 2007.

STEWART, D. et al. Wet Gas Metering with V-Cone Meters. **North Sea Flow Measurement Workshop**, 2002.

TAITEL, Y.; DUKLER, A. E. A theoretical approach to the Lockhart-Martinelli correlation for stratified flow. **International Journal of Multiphase Flow**, v. 2, p. 591–595, 1975.

TAITEL, Y.; DUKLER, A. E. A model for predicting flow regime transitions in horizontal and near horizontal gas-liquid flow. **AIChE Journal**, v. 22, n. 1, 1976.

TING, V. C. Effects of Nonstandard Operating Conditions on the Accuracy of Orifice Meters. **SPE Production and Facilities**, 1993.

WALLIS, G. B. **One-dimensional Two-phase Flow**. Darmonth: McGraw-Hill, 1969.

XIAO, J. J.; SHOHAM, O.; BRILL, J. P. **Comprehensive mechanistic model for two-phase flow in pipelines**. Proceedings - SPE Annual Technical Conference and Exhibition. **Anais...**1990.

APPENDIX A



Laboratório de calibração
acreditado pela Cgcre
de acordo com a ABNT NBR ISO/IEC 17025
sob número 0247



CERTIFICADO DE CALIBRAÇÃO VOLUMÉTRICA N° LMV 39898-20

Folha: 1 de 3

CLIENTE: FUNDAÇÃO ESPÍRITO SANTENSE DE TECNOLOGIA
ENDEREÇO CLIENTE: Avenida Fernando Ferrari, 845, Campus Universitário, Bairro Goiabeiras - Vitória/ES - CEP: 29075-010
PROCESSO CLIENTE: 117842020 **PROCESSO METROVAL:** OP 200548

1-IDENTIFICAÇÃO DO INSTRUMENTO

Instrumento: Medidor de Vazão (Calibrado na sua função de totalizador de volume)
Tipo: Mássico **N° de série:** 0190420
Identificação (TAG): FIT-002 **Fabricante:** METROVAL
Modelo: SMT-100 **Data da calibração:** 15/05/2020
Faixa de operação: (8 a 80) m³/h
Diâmetro nominal: 100 mm **Fator do medidor²:** 63,00341797
Classe de pressão: #150
Conversor:
Modelo: MTM-01-M **Número de série:** 02080320

2-PADRÕES UTILIZADOS

DESCRIÇÃO	CERTIFICADO	LABORATÓRIO	CALIBRAÇÃO	VALIDADE
TANQUE PADRÃO 5000 L - TQ 10001	DIMCI 1032/2013	INMETRO	13/07/2012	10/07/2024
TERMÔMETRO DIGITAL - B09-TT-01	LT 249 630	ESCALA	17/02/2020	06/02/2022
MANÔMETRO DIGITAL - B09-PT-01	LP 249 631	ESCALA	17/02/2020	16/02/2022
TERMOHIGRÔMETRO - 41.17	LT 175710	ESCALA	01/06/2017	31/05/2020
TERMÔMETRO DIGITAL - B09-TT-02	LT 249 632	ESCALA	17/02/2020	16/02/2022
TERMÔMETRO DIGITAL - B09-TT-03	LT 249 633	ESCALA	17/02/2020	16/02/2022
TERMÔMETRO DIGITAL - B09-TT-04	LT 249 634	ESCALA	17/02/2020	16/02/2022

3-PROCEDIMENTO DE CALIBRAÇÃO

A calibração foi feita pelo método de comparação do volume circulado pelo medidor sob calibração e o volume coletado no tanque volumétrico padrão, conforme procedimentos internos LPTI-02 e LPTI-09 nas suas últimas revisões.

4-CONDIÇÕES DE CALIBRAÇÃO

FLUIDO	VISCOSIDADE	UMIDADE RELATIVA	TEMPERATURA AMBIENTE
ÁGUA	1, mm ² /s	46 %	26,8 °C

Local da calibração: Instalação permanente

Nova Odessa, 19 de maio de 2020.


Wagner Gaia Donato
Signatário

Endereço:
Rua Christiano Kilmeyers, 819
CEP 13380-296 - Nova Odessa - SP
Fone: +55 19 2127-9400

www.metroval.com.br

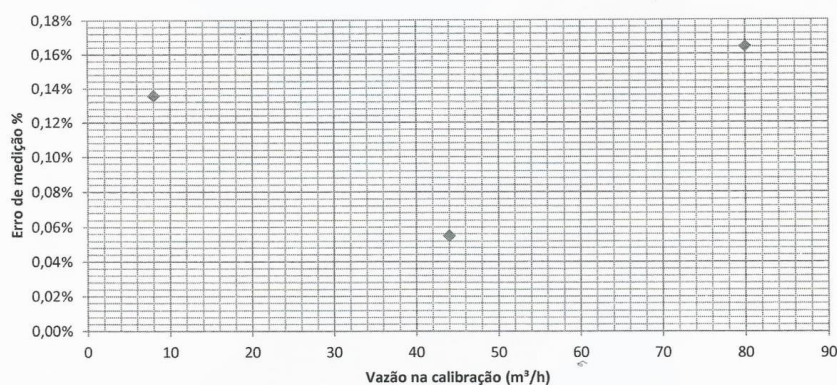
CERTIFICADO DE CALIBRAÇÃO VOLUMÉTRICA N° LMV 39898-20

Folha: 2 de 3

5-RESULTADOS ("AS FOUND" = "AS LEFT")

Vazão na calibração ^a	Temperatura Medidor sob calibração	Pressão Medidor sob calibração	Volume referência ^b	Volume Medidor ^c	MF	Erro de medição	Repetibilidade				
							Calculada mediante: Desvio-padrão	U	k	yeff	n ^a
m ³ /h	°C	kPa	L	L	adimensional	%	%	%			
8,0	25,6	68,6	4998,05	5004,84	0,99864	0,14%	0,007%	0,17%	2,00	178454	3
44,0	25,6	65,7	4992,59	4995,33	0,99945	0,05%	0,007%	0,17%	2,00	226883	3
80,0	25,6	63,7	4997,67	5005,90	0,99836	0,16%	0,007%	0,17%	2,00	216320	3

6-GRÁFICO



Nova Odessa, 19 de maio de 2020.


 Wagner Gaia Donato
 Signatário

 Endereço:
 Rua Christiano Kilmeyers, 819
 CEP 13380-296 - Nova Odessa - SP
 Fone: +55 19 2127-9400

www.metroval.com.br

CERTIFICADO DE CALIBRAÇÃO VOLUMÉTRICA N° LMV 39898-20

Folha: 3 de 3

7-NOTAS

• O presente certificado de calibração atende aos requisitos da ABNT NBR ISO/IEC 17025 e é válido apenas para o instrumento de medição/padrão acima declarados, não sendo extensivo a quaisquer outros instrumentos de medição, ainda que similares.

• Vazão na calibração é meramente informativa (a).

• Volume indicado no padrão que está corrigido pelo seu certificado de calibração e pela temperatura e pressão nas condições do medidor (b).

• Volume totalizado nas condições de pressão e temperatura registradas no medidor (c).

• Equações:

$$MF = \frac{\text{Volume referência}}{\text{Volume Medidor}} \quad \text{Volume Medidor} = \frac{\text{N}^\circ \text{ de pulsos}}{\text{Kfactor (pulsos/L)}} \quad \text{Erro (\%)} = \frac{\text{Volume Medidor} - \text{Volume referência}}{\text{Volume referência}} \times 100$$

• A incerteza expandida da medição U relatada é declarada como a incerteza padrão da medição multiplicada pelo fator de abrangência k, o qual para uma distribuição t, com os graus de liberdade efetivos relatados (ν_{eff}) correspondente a uma probabilidade de abrangência de aproximadamente 95%. A incerteza padrão da medição foi determinada de acordo com a publicação EA-4/02.

• Incerteza expandida da medição do volume com a bancada utilizada é 0,16 %, já incluso no cálculo de incerteza expandida de cada ponto.

• Os resultados acima relatados são validos nas condições de calibração. Cabe ao usuário estimar as mudanças nos resultados aqui apresentados por utilizar o medidor em condições diferentes às quais foi calibrado e as contribuições adicionais de incerteza.

• *Os resultados declarados são a média de pelo menos três medições. O número de corridas n utilizado para os cálculos correspondente para cada vazão é declarado na tabela de resultados.

• É proibida a reprodução parcial deste certificado. A reprodução de partes do certificado de calibração requer aprovação escrita do laboratório.

• Este certificado atende aos requisitos de acreditação pela Cgcre, o qual avaliou a competência do laboratório e comprovou sua rastreabilidade a padrões nacionais de medida ou ao Sistema Internacional de Unidades - SI.


• 1 m³ = 1000L , 1h=60 min

• ¹Este fator se refere à saída de pulsos por unidade de volume proporcionada pelo medidor em calibração. Caso seja utilizado em conjunto com um computador de vazão, este valor deve ser atualizado nele.

• ²Este fator se refere à constante utilizada pelo medidor para proporcionar a indicação de vazão e volume. Esta informação se encontra inserida na unidade eletrônica do medidor.

• A viscosidade de 1 mm²/s é a média da viscosidade da ÁGUA na temperatura média de calibração de 25,6°C.

Nova Odessa, 19 de maio de 2020 .

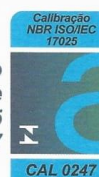

 Wagner Galá Donato
 Signatário

 Endereço:
 Rua Christiano Kilmeyers, 819
 CEP 13380-296 - Nova Odessa - SP
 Fone: +55 19 2127-9400

www.metroval.com.br



Laboratório de calibração
acreditado pela Cgcre
de acordo com a ABNT NBR ISO/IEC 17025
sob número 0247



CERTIFICADO DE CALIBRAÇÃO VOLUMÉTRICA N° LMV 39897-20

Folha: 1 de 3

CLIENTE: FUNDAÇÃO ESPIRITO SANTENSE DE TECNOLOGIA
ENDEREÇO CLIENTE: Avenida Fernando Ferrari, 845, Campus Universitário, Bairro Goiabeiras - Vitória/ES - CEP: 29075-010
PROCESSO CLIENTE: 117842020 **PROCESSO METROVAL:** OP 200548

1-IDENTIFICAÇÃO DO INSTRUMENTO

Instrumento: Medidor de Vazão (Calibrado na sua função de totalizador de volume)
Tipo: Mássico **N° de série:** 0140420
Identificação (TAG): FIT-005 **Fabricante:** METROVAL
Modelo: SMT-50 **Data da calibração:** 14/05/2020
Faixa de operação: (2 a 20) m³/h
Diâmetro nominal: 100 mm **Fator do medidor²:** 17,43059158
Classe de pressão: #150
Conversor:
Modelo: MTM-01-M **Número de série:** 02100320

2-PADRÕES UTILIZADOS

DESCRIÇÃO	CERTIFICADO	LABORATÓRIO	CALIBRAÇÃO	VALIDADE
TANQUE PADRÃO 1000 L - TQ 1004	DIMCI 2158/2012	INMETRO	13/07/2012	10/07/2024
TERMÔMETRO DIGITAL - B11-TT-01	LT 249 640	ESCALA	17/02/2020	16/02/2022
MANÔMETRO DIGITAL - B09-PT-01	LP 249 631	ESCALA	17/02/2020	16/02/2022
TERMOHIGRÔMETRO - 41.17	LT 175710	ESCALA	01/06/2017	31/05/2020
TERMÔMETRO DIGITAL - B11-TT-04	LT 249 639	ESCALA	17/02/2020	16/02/2022
TERMÔMETRO DIGITAL - B11-TT-05	LT 249 637	ESCALA	17/02/2020	16/02/2022
TERMÔMETRO DIGITAL - B11-TT-06	LT 249 638	ESCALA	17/02/2020	16/02/2022

3-PROCEDIMENTO DE CALIBRAÇÃO


A calibração foi feita pelo método de comparação do volume circulado pelo medidor sob calibração e o volume coletado no tanque volumétrico padrão, conforme procedimentos internos LPTI-02 e LPTI-09 nas suas últimas revisões.

4-CONDIÇÕES DE CALIBRAÇÃO

FLUIDO	VISCOSIDADE	UMIDADE RELATIVA	TEMPERATURA AMBIENTE
ÁGUA	1, mm ² /s	48 %	26,4 °C

Local da calibração: Instalação permanente

Nova Odessa, 19 de maio de 2020.


Wagner Gaia Donato
Signatário

Endereço:
Rua Christiano Kilmeyers, 819
CEP 13380-296 - Nova Odessa - SP
Fone: +55 19 2127-9400

www.metroval.com.br

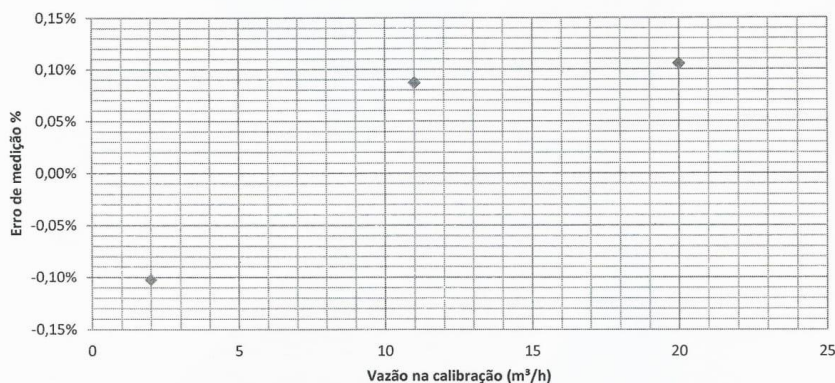
CERTIFICADO DE CALIBRAÇÃO VOLUMÉTRICA N° LMV 39897-20

Folha: 2 de 3

5-RESULTADOS ("AS FOUND" = "AS LEFT")

Vazão na calibração ^a	Temperatura Medidor sob calibração	Pressão Medidor sob calibração	Volume referência ^b	Volume Medidor ^c	MF	Erro de medição	Repetibilidade				n ^a
							Calculada mediante: Desvio- padrão	U	k	yeff	
m ³ /h	°C	kPa	L	L	adimensional	%	%	%			
2,0	25,2	115,7	1014,86	1013,82	1,00102	-0,10%	0,011%	0,17%	2,00	43334	3
11,0	25,3	72,5	1015,04	1015,93	0,99913	0,09%	0,012%	0,17%	2,00	32398	3
20,0	25,4	65,7	1014,65	1015,72	0,99895	0,11%	0,012%	0,17%	2,00	35971	3

6-GRÁFICO



Nova Odessa, 19 de maio de 2020.


 Wagner Gaia Donato
 Signatário

 Endereço:
 Rua Christiano Kilmeyers, 819
 CEP 13380-296 - Nova Odessa - SP
 Fone: +55 19 2127-9400

www.metroval.com.br



Laboratório de calibração
acreditado pela Cgcre
de acordo com a ABNT NBR ISO/IEC 17025
sob número 0247



CERTIFICADO DE CALIBRAÇÃO VOLUMÉTRICA N° LMV 39897-20

Folha: 3 de 3

7-NOTAS

• O presente certificado de calibração atende aos requisitos da ABNT NBR ISO/IEC 17025 e é válido apenas para o instrumento de medição/padrão acima declarados, não sendo extensivo a quaisquer outros instrumentos de medição, ainda que similares.

• Vazão na calibração é meramente informativa (a).

• Volume indicado no padrão que está corrigido pelo seu certificado de calibração e pela temperatura e pressão nas condições do medidor (b).

• Volume totalizado nas condições de pressão e temperatura registradas no medidor (c).

• Equações:

$$MF = \frac{\text{Volume referência}}{\text{Volume Medidor}} \quad \text{Volume Medidor} = \frac{\text{N}^\circ \text{ de pulsos}}{\text{Kfactor (pulsos/L)}} \quad \text{Erro (\%)} = \frac{\text{Volume Medidor} - \text{Volume referência}}{\text{Volume referência}} \times 100$$

• A incerteza expandida da medição U relatada é declarada como a incerteza padrão da medição multiplicada pelo fator de abrangência k, o qual para uma distribuição t, com os graus de liberdade efetivos relatados (yeff) correspondente a uma probabilidade de abrangência de aproximadamente 95%. A incerteza padrão da medição foi determinada de acordo com a publicação EA-4/02.

• Incerteza expandida da medição do volume com a bancada utilizada é 0,16 %, já incluso no cálculo de incerteza expandida de cada ponto.

• Os resultados acima relatados são validos nas condições de calibração. Cabe ao usuário estimar as mudanças nos resultados aqui apresentados por utilizar o medidor em condições diferentes às quais foi calibrado e as contribuições adicionais de incerteza.

•²Os resultados declarados são a média de pelo menos três medições. O número de corridas n utilizado para os cálculos correspondente para cada vazão é declarado na tabela de resultados.

•É proibida a reprodução parcial deste certificado. A reprodução de partes do certificado de calibração requer aprovação escrita do laboratório.

• Este certificado atende aos requisitos de acreditação pela Cgcre, o qual avaliou a competência do laboratório e comprovou sua rastreabilidade a padrões nacionais de medida ou ao Sistema Internacional de Unidades - SI.

• 1 m³ = 1000L , 1h=60 min

•¹Este fator se refere à saída de pulsos por unidade de volume proporcionada pelo medidor em calibração. Caso seja utilizado em conjunto com um computador de vazão, este valor deve ser atualizado nele.

•²Este fator se refere à constante utilizada pelo medidor para proporcionar a indicação de vazão e volume. Esta informação se encontra inserida na unidade eletrônica do medidor.

• A viscosidade de 1 mm²/s é a média da viscosidade da ÁGUA na temperatura média de calibração de 25,3°C.

Nova Odessa, 19 de maio de 2020 .


Wagner Gaia Donato
Signatário

Endereço:
Rua Christiano Kilmeyers, 819
CEP 13380-296 - Nova Odessa - SP
Fone: +55 19 2127-9400

www.metroval.com.br

APPENDIX B


FABRICANTE		NÚM. SÉRIE		MODELO		PROX. CAL.		NÚM. CERTIFICADO	
Presys		060.10.15		MCS-XV		01/09/2022		R4756.09.21	
Presys		060.10.15		MCS-XV		01/09/2022		R4758.09.21	


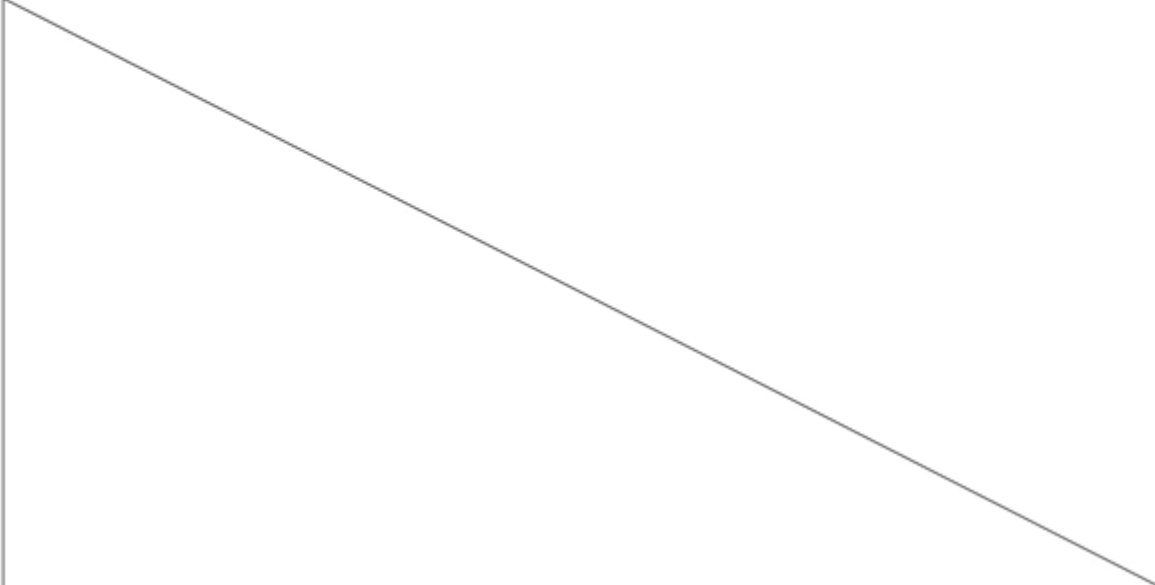
Calibração preliminar realizada por: Ulisses Reis CONDIÇÕES DE CALIBRAÇÃO: UMIDADE: 50,00 % TEMPERATURA: 25,00 °C DATA 27/10/2021


Calibração (mmH2O)	Referência (nmH2O)	Cal. Corr. (mmH2O)	Ref. Corr. (nmH2O)	Leitura 1 (nmH2O)	Leitura 2 (nmH2O)	Média (nmH2O)	Erro (nmH2O)	U (nmH2O)	k
0	0,00	-2	-1,50	-0,44	-0,44	-0,44	1,06	10,27	2,509
2333	2333,33	2333	2333,58	2343,69	2341,15	2342,42	8,84	14,29	2,332
4667	4666,67	4665	4665,17	4679,98	4683,74	4681,86	16,69	14,93	2,292
7000	7000,00	7001	7001,25	7025,20	7029,49	7027,34	26,10	15,53	2,295
0	0,00	-2	-1,50	-0,44	-0,44	-0,44	1,06	10,27	2,509
2333	2333,33	2333	2333,58	2343,69	2341,15	2342,42	8,84	14,29	2,332
4667	4666,67	4665	4665,17	4679,98	4683,74	4681,86	16,69	14,93	2,292
7000	7000,00	7001	7001,25	7025,20	7029,49	7027,34	26,10	15,53	2,295


OBSERVAÇÕES:
 O campo Ref. Corr. corresponde ao Valor Convencional. O campo Média corresponde à Indicação. A incerteza de medida U está associada à Indicação.
 A incerteza expandida foi calculada para uma probabilidade de abrangência de 95,45%.
 A incerteza padrão de medição foi determinada de acordo com a publicação EA-402.
 Os resultados apresentados referem-se exclusivamente ao instrumento calibrado.
 Este documento não pode ser reproduzido sem a aprovação do laboratório, exceto se reproduzido na íntegra.

DATA DE CALIBRAÇÃO: 27/10/2021	RESPONSÁVEL	DATA DE EMISSÃO: 27/10/2021
---------------------------------------	--------------------	------------------------------------

 NÚCLEO DE ESTUDOS EM ESCOAMENTO E MEDIÇÃO DE ÓLEO E GÁS CERTIFICADO DE CALIBRAÇÃO NÚMERO 0035.2863.21									
TAG: PDT-4		MODELO: LD301 D2							
NÚMERO DE SÉRIE: 365204-2020		FABRICANTE: Smar							
FAIXA DE SAÍDA ESCALONADA De 4.0000 a 20.0000 mA (Sinal) De 0.00 a 5050.00 mmH2O (Escala)		ERRO MÁXIMO = 0.5% SPAN(SPAN = 5050 mmH2O)							
FAIXA DE ENTRADA: 0 a 5050 mmH2O (Pressure)		SETOR: Circuito multifásico							
PADRÃO:									
<i>FABRICANTE</i>	<i>NÚM. SÉRIE</i>	<i>MODELO</i>	<i>PROX. CAL.</i>	<i>NÚM. CERTIFICADO</i>					
Presys	060.10.15	MCS-XV	01/09/2022	R4756.09.21					
Presys	060.10.15	MCS-XV	01/09/2022	R4758.09.21					
Calibração preliminar realizada por: Ulisses Reis				CONDICÕES DE CALIBRAÇÃO: UMIDADE: 50,00 % TEMPERATURA: 25,00 °C DATA 27/10/2021					
Calibração (mmH2O)	Referência (mmH2O)	Cal. Corr. (mmH2O)	Ref. Corr. (mmH2O)	Leitura 1 (mmH2O)	Leitura 2 (mmH2O)	Média (mmH2O)	Erro (mmH2O)	U (mmH2O)	k
0,00	0,00	0,24	0,24	-0,66	-0,66	-0,66	-0,90	14,10	2,383
1683,33	1683,33	1683,11	1683,19	1693,17	1692,10	1692,64	9,45	14,21	2,350
3366,67	3366,67	3366,52	3366,69	3385,99	3383,69	3384,84	18,15	14,19	2,356
5050,00	5050,00	5050,23	5050,48	5081,34	5079,86	5080,60	30,12	14,16	2,358
0,00	0,00	0,24	0,24	-0,66	-0,66	-0,66	-0,90	14,10	2,383
1683,33	1683,33	1683,11	1683,19	1693,17	1692,10	1692,64	9,45	14,21	2,350
3366,67	3366,67	3366,52	3366,69	3385,99	3383,69	3384,84	18,15	14,19	2,356
5050,00	5050,00	5050,23	5050,48	5081,34	5079,86	5080,60	30,12	14,16	2,358
OBSERVAÇÕES: O campo Ref. Corr. corresponde ao Valor Convencional. O campo Média corresponde à Indicação. A incerteza de medida U está associada à Indicação. A incerteza expandida foi calculada para uma probabilidade de abrangência de 95,45%. A incerteza padrão de medição foi determinada de acordo com a publicação EA-402. Os resultados apresentados referem-se exclusivamente ao instrumento calibrado. Este documento não pode ser reproduzido sem a aprovação do laboratório, exceto se reproduzido na íntegra.									
DATA DE CALIBRAÇÃO: 27/10/2021			RESPONSÁVEL			DATA DE EMISSÃO: 27/10/2021			

 NÚCLEO DE ESTUDOS EM ESCOAMENTO E MEDIÇÃO DE ÓLEO E GÁS CERTIFICADO DE CALIBRAÇÃO NÚMERO 0034.2863.21									
TAG: PDT-5	MODELO: LD301 D2								
NÚMERO DE SÉRIE: 365203-2020	FABRICANTE: Smar								
FAIXA DE SAÍDA ESCALONADA De 4.0000 a 20.0000 mA (Sinal) De 0.00 a 2500.00 mmH2O (Escala)	ERRO MÁXIMO = 0.5% SPAN(SPAN = 2500 mmH2O)								
FAIXA DE ENTRADA: 0 a 2500 mmH2O (Pressure)	SETOR: Circuito multifático								
PADRÃO:									
<i>FABRICANTE</i>	<i>NÚM. SÉRIE</i>	<i>MODELO</i>	<i>PROX. CAL.</i>	<i>NÚM. CERTIFICADO</i>					
Presys	060.10.15	MCS-XV	01/09/2022	R4756.09.21					
Presys	060.10.15	MCS-XV	01/09/2022	R4758.09.21					
Calibração preliminar realizada por: Ulisses Reis CONDIÇÕES DE CALIBRAÇÃO: UMIDADE: 50,00 % TEMPERATURA: 25,00 °C DATA 27/10/2021									
Calibração (mmH2O)	Referência (mmH2O)	Cal. Corr. (mmH2O)	Ref. Corr. (mmH2O)	Leitura 1 (mmH2O)	Leitura 2 (mmH2O)	Média (mmH2O)	Erro (mmH2O)	U (mmH2O)	k
0,00	0,00	2,87	2,87	-0,22	-0,22	-0,22	-3,09	14,11	2,373
833,33	833,33	834,11	834,15	834,98	835,47	835,22	1,07	14,51	2,332
1666,67	1666,67	1666,82	1666,91	1672,81	1672,58	1672,70	5,79	14,09	2,384
2500,00	2500,00	2501,71	2501,83	2512,52	2509,03	2510,78	8,94	14,42	2,329
0,00	0,00	2,87	2,87	-0,22	-0,22	-0,22	-3,09	14,11	2,373
833,33	833,33	834,11	834,15	834,98	835,47	835,22	1,07	14,51	2,332
1666,67	1666,67	1666,82	1666,91	1672,81	1672,58	1672,70	5,79	14,09	2,384
2500,00	2500,00	2501,71	2501,83	2512,52	2509,03	2510,78	8,94	14,42	2,329
OBSERVAÇÕES: O campo Ref. Corr. corresponde ao Valor Convencional. O campo Média corresponde à Indicação. A incerteza de medida U está associada à Indicação. A incerteza expandida foi calculada para uma probabilidade de abrangência de 95,45%. A incerteza padrão de medição foi determinada de acordo com a publicação EA-4/02. Os resultados apresentados referem-se exclusivamente ao instrumento calibrado. Este documento não pode ser reproduzido sem a aprovação do laboratório, exceto se reproduzido na íntegra.									
DATA DE CALIBRAÇÃO: 27/10/2021			RESPONSÁVEL				DATA DE EMISSÃO: 27/10/2021		
									

		NÚCLEO DE ESTUDOS EM ESCOAMENTO E MEDIÇÃO DE ÓLEO E GÁS CERTIFICADO DE CALIBRAÇÃO NÚMERO 0043.2863.22						
TAG: PDT6				MODELO: LD301				
NÚMERO DE SÉRIE: 347314-2016				FABRICANTE: SMAR				
FAIXA DE SAÍDA ESCALONADA De 4.0000 a 20.0000 mA (Sinal) De 0.0 a 9000.0 mmH2O (Escala)				ERRO MÁXIMO = 0.1% SPAN(SPAN = 9000.0 mmH2O)				
FAIXA DE ENTRADA: 0 a 1000 mmH2O (Pressure)				SETOR:				
PADRÃO:								
<i>FABRICANTE</i>		<i>NÚM. SÉRIE</i>		<i>MODELO</i>		<i>PROX. CAL.</i>	<i>NÚM. CERTIFICADO</i>	
Presys		060.10.15		MCS-XV		01/09/2022	R4756.09.21	
Presys		060.10.15		MCS-XV		01/09/2022	R4758.09.21	
Calibração preliminar realizada por: Ulisses Reis CONDIÇÕES DE CALIBRAÇÃO: UMIDADE: 50,00 % TEMPERATURA: 25,00 °C DATA 07/03/2022								
Calibração (mmH2O)	Referência (mmH2O)	Cal. Corr. (mmH2O)	Ref. Corr. (mmH2O)	Leitura I (mmH2O)	Média (mmH2O)	Erro (mmH2O)	U (mmH2O)	k
0,00	0,0	-0,67	-0,7	-0,2	-0,2	0,5	7,1	2,166
15,00	15,0	17,27	17,3	-0,2	-0,2	-17,5	14,1	2,384
30,00	30,0	29,43	29,4	25,2	25,2	-4,2	14,1	2,384
100,00	100,0	101,07	101,1	93,1	93,1	-8,0	14,1	2,384
500,00	500,0	500,59	500,6	494,9	494,9	-5,7	14,1	2,384
1000,00	1000,0	1005,67	1005,7	998,0	998,0	-7,7	14,1	2,384
OBSERVAÇÕES: O campo Ref. Corr. corresponde ao Valor Convencional. O campo Média corresponde à Indicação. A incerteza de medida U está associada à Indicação. A incerteza expandida foi calculada para uma probabilidade de abrangência de 95,45%. A incerteza padrão de medição foi determinada de acordo com a publicação EA-4/02. Os resultados apresentados referem-se exclusivamente ao instrumento calibrado. Este documento não pode ser reproduzido sem a aprovação do laboratório, exceto se reproduzido na íntegra.								
DATA DE CALIBRAÇÃO: 07/03/2022			RESPONSÁVEL			DATA DE EMISSÃO: 07/03/2022		

 NÚCLEO DE ESTUDOS EM ESCOAMENTO E MEDIÇÃO DE ÓLEO E GÁS CERTIFICADO DE CALIBRAÇÃO NÚMERO 0032.2863.21									
TAG: PIT-09	MODELO: LD301								
NÚMERO DE SÉRIE: 365118-2020	FABRICANTE: Smar								
FAIXA DE SAÍDA ESCALONADA De 4.0000 a 20.0000 mA (Sinal) De 0.000 a 10.000 bar (Escala)	ERRO MÁXIMO = 0.5% SPAN(SPAN = 10 bar)								
FAIXA DE ENTRADA: 0 a 10 bar (Pressure)	SETOR: circuito multifásico								
PADRÃO:									
<i>FABRICANTE</i>	<i>NÚM. SÉRIE</i>	<i>MODELO</i>	<i>PROX. CAL.</i>	<i>NÚM. CERTIFICADO</i>					
Presys	060.10.15	MCS-XV	01/09/2022	R4756.09.21					
Presys	060.10.15	MCS-XV	01/09/2022	R4758.09.21					
Calibração preliminar realizada por: Ulisses Reis CONDIÇÕES DE CALIBRAÇÃO: UMIDADE: 50,00 % TEMPERATURA: 25,00 °C DATA 27/10/2021									
Calibração (bar)	Referência (bar)	Cal. Corr. (bar)	Ref. Corr. (bar)	Leitura 1 (bar)	Leitura 2 (bar)	Média (bar)	Erro (bar)	U (bar)	k
0,00	0,000	0,00	0,000	-0,001	-0,001	-0,001	-0,001	0,002	2,291
3,33	3,333	3,33	3,331	3,322	3,317	3,320	-0,011	0,033	12,805
6,67	6,667	6,67	6,670	6,653	6,649	6,651	-0,019	0,026	11,915
10,00	10,000	10,00	10,000	9,973	9,977	9,975	-0,025	0,019	7,971
0,00	0,000	0,00	0,000	-0,001	-0,001	-0,001	-0,001	0,002	2,291
3,33	3,333	3,33	3,331	3,322	3,317	3,320	-0,011	0,033	12,805
6,67	6,667	6,67	6,670	6,653	6,649	6,651	-0,019	0,026	11,915
10,00	10,000	10,00	10,000	9,973	9,977	9,975	-0,025	0,019	7,971
OBSERVAÇÕES: O campo Ref. Corr. corresponde ao Valor Convencional. O campo Média corresponde à Indicação. A incerteza de medida U está associada à Indicação. A incerteza expandida foi calculada para uma probabilidade de abrangência de 95,45%. A incerteza padrão de medição foi determinada de acordo com a publicação EA-402. Os resultados apresentados referem-se exclusivamente ao instrumento calibrado. Este documento não pode ser reproduzido sem a aprovação do laboratório, exceto se reproduzido na íntegra.									
DATA DE CALIBRAÇÃO: 27/10/2021			RESPONSÁVEL				DATA DE EMISSÃO: 27/10/2021		

APPENDIX C

ZÜRICH[®] LABORATÓRIO ZÜRICH DE CALIBRAÇÃO

PRESSÃO & TEMPERATURA

Laboratório ZÜRICH de calibração - REDE BRASILEIRA DE LABORATÓRIOS DE CALIBRAÇÃO (RBC).
Laboratório de Calibração acreditado pela Cgcre de acordo com a ABNT NBR ISO/IEC 17025, sob o número CAL 0561.



CERTIFICADO DE CALIBRAÇÃO N°: LT - 7165 / 2020

CLIENTE: FUNDAÇÃO ESPIRITO SANTENS E DE TECNOLOGIA - FEST

ENDEREÇO: AV.FERNANDO FERRARI,CAMPUS UNIV.845 - VITORIA - ES

SOLICITANTE: O MESMO

DESCRIÇÃO DO INSTRUMENTO:

INSTRUMENTO: Medidor de Temperatura com Sensor Termorresistivo - Transmissor de Temperatura
FABRICANTE: ZÜRICH
ORDEM DE SERVIÇO: 2056 / 2020

MODELO: T.420.1 12N
N° SÉRIE: ID:TH / 2186 / 06 / 2020
IDENTIFICAÇÃO: TT-1

FAIXA DO INSTRUMENTO: 0 a 100 °C // 4 a 20 mA
FAIXA CALIBRADA: 10 a 90 °C
SENSOR: PT 100

COMPRIMENTO HASTE: 38 mm
DIAMETRO HASTE: 6 mm
LIGAÇÃO: 3 fios

CONDIÇÕES AMBIENTAIS:

TEMPERATURA: 20° C ± 2 ° C
UMIDADE RELATIVA: 50 % ± 20 %
PRESSÃO ATMOSFÉRICA: 926,8 mbar

PADRÃO(ÕES) UTILIZADO(S) NA CALIBRAÇÃO:

IDENTIFICAÇÃO	DESCRIÇÃO	Nº CERTIFICADO	VALIDADE
TRP-01+CTB-01	Termômetro de Resistência (Fluke 5609) com Forno de Calibração (FLUKE 9142)	A 0093/2020	fevereiro-22
MUT-03	Muúltimetro Digital	RI 1120 / 19	março-21

RESUMO DO PROCEDIMENTO DE CALIBRAÇÃO:

A calibração foi realizada em três ciclos de medição pelo método da comparação direta a um padrão de referência em um meio térmico com homogeneidade conhecida, conforme procedimento: PL 7.2-04 Rev.01

As medições foram realizadas após a estabilização, confirmada pelas leituras do padrão e do instrumento em calibração em 3 séries de medições, com intervalos de 1 minuto.

RESULTADOS DA CALIBRAÇÃO:

Profundidade de Imersão (mm)	PADRÃO (° C)	Instrumento sob Calibração		Erro de Indicação (° C)	Incerteza de Medição (° C)	Fator de Abrangência (k)	Grau de Liberdade Efetivos (ν_{eff})
		(mA)	(° C)				
38	10,00	5,601	10,01	0,01	0,12	2,00	∞
38	50,01	11,967	49,79	-0,22	0,12	2,00	∞
38	90,01	18,371	89,82	-0,19	0,12	2,00	∞
----	----	----	----	----	----	----	----
----	----	----	----	----	----	----	----

OBSERVAÇÕES:

- Os valores de temperatura estão em conformidade com a Escala Internacional de Temperatura ITS - 90.
- A incerteza expandida de medição relatada é declarada como incerteza padrão da medição multiplicada pelo fator de abrangência (k), o qual para uma distribuição t com ν_{eff} graus de liberdade efetivos correspondente a uma probabilidade de abrangência de aproximadamente 95%. A incerteza de medição foi determinada de acordo com a publicação do EA-4/02.
- Os resultados deste certificado referem-se exclusivamente ao instrumento submetido à calibração, nas condições específicas, não sendo extensivo a quaisquer lotes. Esta calibração não isenta o instrumento do controle metrológico estabelecido na regulamentação metrológica. A reprodução deste certificado só poderá ser total.

Data da Calibração: 8 Junho 2020

Data da Emissão: 8 Junho 2020

Técnico Executante: Edenilson

Gerente Técnico: Edenilson L. Cunha

Este Certificado atende aos requisitos de acreditação da Cgcre, que avaliou a competência do laboratório e comprovou sua rastreabilidade a padrões nacionais de medida (ou ao sistema internacional de unidades - SI).

Página 1 de 1.

ZÜRICH INDÚSTRIA E COMÉRCIO LTDA

Rua Serra da Piedade, 183 - Vila Prudente - São Paulo - SP - Brasil / CEP 03131-080

Tel: 55 (11) 2020-8080 / Fax: 55 (11) 2965-9202 / Site: www.zurichpt.com.br / e-mail: laboratorio@zurichpt.com.br